The Philosophical Magazine

FIRST PUBLISHED IN 1798

A Journal of Theoretical Experimental and Applied Physics

Vol. 5 May 1960 No. 53
Eighth Series

25s. 0d., plus postage
Annual Subscription £13 10s. 0d., payable in advance

Printed and Published by
TAYLOR & FRANCIS LTD
RED LION COURT, FLEET STREET, LONDON, E.C.4

THE PHILOSOPHICAL MAGAZINE

AUTHORS wishing to submit papers for publication in the Journal should send manuscripts directly to the Publishers.

Manuscripts should be typed in *double* spacing on one side of quarto (8×10 in.) paper, and authors are urged to aim at absolute clarity of meaning and an attractive presentation of their texts.

References should be listed at the end in alphabetical order of authors and should be cited in the text in terms of author's name and date. Diagrams should normally be in Indian ink on white card, with lettering in soft pencil, the captions being typed on a separate sheet.

A leaflet giving detailed instructions to authors on the preparation of papers is available on request from the Publishers.

Authors are entitled to receive 25 offprints of a paper in the Journal free of charge, and additional offprints can be obtained from the Publishers.

The *Philosophical Magazine* and its companion journal, *Advances in Physics*, will accept papers for publication in experimental and theoretical physics. The *Philosophical Magazine* publishes contributions describing new results, letters to the editor and book reviews. *Advances in Physics* publishes articles surveying the present state of knowledge in any branch of the science in which recent progress has been made. The editors welcome contributions from overseas as well as from the United Kingdom, and papers may be published in English, French and German.

Some Effects of Vibration on the Internal Friction of Sodium Chloride†

By R. W. Whitworth‡
Department of Physical Metallurgy, University of Birmingham

[Received December 23, 1959]

Abstract

The room temperature internal friction of single crystals of NaCl vibrating at a frequency of 90 kc/s has been measured at strain amplitudes up to $2{\cdot}7 \times 10^{-4}$. The damping of plastically deformed crystals increased with increasing strain amplitude, and can be attributed to the motion of the dislocations introduced by the deformation. Vibration of specimens at high amplitudes changed their internal friction in three distinct ways.

(*a*) When deformed specimens were annealed at 100 to 200°c the internal friction was reduced, but subsequent vibration at high amplitudes caused the damping to rise towards its value before annealing.

(*b*) While lightly deformed crystals were being driven at very high amplitudes the damping was observed to decrease; the value at lower amplitudes was afterwards found to be less than that determined before this vibration.

(*c*) At the highest amplitudes attained in these experiments new dislocations were produced in the crystals, and their presence has been shown by etching experiments; an increase in the damping was associated with the introduction of these dislocations.

These observations are discussed in terms of current theories.

§ 1. Introduction

The internal friction of metals and ionic crystals in vibration at frequencies of 10–100 kc/s has been studied by many workers, and has been reviewed by Nowick (1953). The damping is normally found to rise with increasing strain amplitude in the specimen, and following the suggestion of Read (1940), a considerable amount of evidence has been produced to show that in many cases this internal friction is due to the motion of dislocations. Various theories, such as those of Granato and Lücke (1956), Nowick (1954) and Weertman (1955), have been proposed to explain how the dislocations give rise to damping, but the details of this subject are not yet fully understood.

One effect which is often reported in experiments on this type of damping is a change in the internal friction produced by driving the specimens at

† Communicated by the Author.

‡ Now at Department of Metallurgy, Imperial College, London, S.W.7.

sufficiently high strain amplitudes. Most of these observations fall into one of the following categories of behaviour.

I. After vibrating the specimen at a strain amplitude in the amplitude-dependent region the internal friction at lower amplitudes is increased above its original value (e.g. Swift and Richardson (1947) in Zn, and Beshers (1959) in Cu).

II. The internal friction is reproducible in the amplitude-dependent region until the strain amplitude is raised above some high critical value; the damping then rises very steeply with amplitude, and is subsequently found to have increased at all lower amplitudes (e.g. Mason (1956) in Pb).

III. As the driving force applied to the specimen is increased the amplitude of resonance rises to a maximum value and then starts to fall, resulting in a double valued decrement *vs.* strain amplitude curve (e.g. Frankl (1953) in NaCl, and Birnbaum (1955) in Ag and Al).

IV. The internal friction rises with increasing strain amplitude, but when the amplitude is subsequently reduced the damping continues to rise (e.g. Hiki (1958) in Pb).

V. In some fatigue tests on specimens vibrating at 100–1000 c/s the internal friction is found to decrease with time during the early part of the test (e.g. Wadsworth (1957) in Cu, Al and Cd, and Broom and Ham (1959) in Cu).

The present paper reports a series of experiments on the internal friction of single crystals of sodium chloride, in which vibration of the specimens at high amplitudes has been observed to change the damping in three quite distinct ways. An increase in the damping of type I has been observed in deformed crystals which had been lightly annealed, and this effect is attributed to the motion of dislocations which were pinned during the anneal. Increases of type II have also been observed, and are shown to be due to the creation of new dislocations. The third effect is a decrease in the damping of lightly deformed crystals vibrating at sufficiently high amplitudes, and this may be similar to the changes of type V previously observed only at lower frequencies. This classification of effects is purely phenomenological, and is not intended to imply that the explanations are necessarily the same in all materials.

Before describing these changes of damping in detail it is necessary to consider the internal friction of sodium chloride observed under conditions where it is not changed by vibration. This is done in § 3, where results of measurements over a wide range of strain amplitudes are reported and discussed in terms of existing theories. The changes in this internal friction which can be produced by vibration are then described in § 4, and some possible interpretations of these effects are considered in § 5.

Previous experiments on the internal friction of sodium chloride have been reported in detail by Frankl (1953), who observed some increases in damping as a result of vibration, and also by Gordon and Nowick (1956), though they did not use high enough strain amplitudes to produce any changes in the damping. Birnbaum (1955) has presented some complicated results on one specimen with a high impurity content.

§ 2. Experimental Details

All the internal friction measurements described here were made on specimens vibrating in their fundamental longitudinal mode at frequencies of about 90 kc/s and at temperatures between 18 and 25°C. The apparatus used was a three-component piezoelectric resonator similar to that described by Marx (1951). It consists of two $-18{\cdot}5°$ X-cut quartz bars and the sodium chloride specimen, all cut to have the same longitudinal resonant frequency, cemented end to end, and suspended *in vacuo*. This resonator is driven by applying a variable frequency a.c. potential difference, V_d, to plating on the X faces of the central quartz crystal, and the potential difference developed across plating on the centre of the X faces of the other quartz crystal is measured with a high impedance valve voltmeter. This p.d. is proportional to the amplitude of vibration of the resonator, and reaches a maximum value, V_g, when the frequency of the driving voltage equals the resonant frequency of the system. The value of V_d/V_g is then proportional to the decrement of the resonator, and from it the decrement, δ, of the specimen can be calculated, after allowing for the damping of the quartz bars, which is equivalent to a specimen decrement of 9×10^{-5}. In order to obtain absolute values of δ and the maximum strain amplitude in the specimen, ϵ, the resonator was calibrated in an a.c. bridge as indicated by Marx; however, there may be errors in this calibration which could lead to systematic errors of about 40% in all the values of δ and ϵ. Nevertheless, the relative accuracy of individual damping measurements should be about $\pm 2\%$, except at the lowest values of δ, where it is difficult to keep the frequency on resonance and the damping of the quartz bars is larger than that of the specimen. The frequency control of the oscillator was only sensitive enough to measure modulus changes in heavily deformed crystals.

As the results obtained sometimes depended on the time for which a crystal was vibrated, the following procedure was adopted unless otherwise stated. At some definite time a predetermined a.c. voltage between 0·001 and 100 v was applied to the driver crystal from a low impedance source. During the following minute the frequency was adjusted in order to find the maximum p.d. across the gauge crystal, and if this changed appreciably during the minute the change was recorded. At the end of the minute the driving voltage was turned off, and one minute later the next larger driving voltage was applied. This procedure was repeated until the highest amplitude to be used was reached.

All quantitative results quoted in this paper were obtained using specimens cleaved from one large single crystal grown in this laboratory by the Kyropoulos method. The crystal was pulled from a melt of Analar grade sodium chloride contained in a silica vessel, and it seems probable that the total impurity concentration in the specimens was less than about 0·01%. Qualitatively similar results have also been obtained on the damping of specimens taken from three other crystals including one from the Harshaw Chemical Company. The specimens had {100} faces, and measured about $0{\cdot}5 \times 0{\cdot}5 \times 2{\cdot}52$ cm in size, the length being chosen to

give the correct resonant frequency to within 0·3% when the crystal was mounted on the resonator. After cleavage the specimens were annealed for about 1 hour at 650°C to remove the internal stresses produced by the cleavage damage, and then cooled to room temperature over a period of two days.

The joints between the specimens and the quartz bar were made with beeswax, melted at about 70°C in a stream of hot air; using great care joints can be made in this manner with very little associated plastic deformation of the specimens. The joints contributed only a small amount to the damping of the resonator, but, as this contribution is not known, little reliance can be placed on the measured values of the amplitude-independent decrement of the crystals at low strain amplitudes. The joints do not appear to give rise to any significant amplitude-dependent damping.

§ 3. The Internal Friction of Sodium Chloride

3.1. *Experimental Results*

The internal friction of specimens annealed at 650°C and slowly cooled was found to be very low, that of a typical crystal being 10^{-5} at low amplitudes, and rising to about 10^{-4} at $\epsilon = 4 \times 10^{-5}$. However, using even great care it was impossible to avoid deforming the crystal very slightly during mounting, and it is known that deformation gives rise to amplitude-dependent damping. This difficulty can be overcome in slightly impure crystals, which are less easily deformed, and in such crystals the damping was found to be independent of amplitude in this region. It therefore seems probable that the damping of a truly undeformed 'pure' crystal would also be amplitude-independent and so small as to be insignificantly different from zero when measured with the present apparatus.

Plastic deformation of such a pure annealed crystal increases its internal friction. This is shown by fig. 1, in which the decrement δ is given as a function of the strain amplitude ϵ for three typical specimens deformed in compression along their long axes. For convenience δ is plotted on a linear scale and ϵ on a logarithmic one. The plastic strain in each specimen is given below the figure, together with the stress required to produce this deformation and the actual magnitude of δ_0, the amplitude-independent decrement at the lowest amplitudes; δ_0 may however include an uncertain contribution from the beeswax joint. The measurements were made within 2 hours of the deformation of the specimens, and, after mounting, each specimen was vibrated at the highest amplitude to be used and then allowed to rest for 20 min before its damping was measured. This driving at high amplitude was found to produce an increase in δ_0, which disappeared in about 20 min, and measurements made over a period of a few hours after this treatment were reproducible to within a few per cent. On leaving the crystal to stand at room temperatures for several hours or days the value of δ was found to decrease at all amplitudes. A number of measurements were made on crystals other than those shown in fig. 1, and for the

same amount of deformation the values of δ were found to be the same as those shown within a factor of about 2. There does not seem to be any simple connection between the value of δ_0 and the rate of rise of δ at the higher amplitudes.

Fig. 1

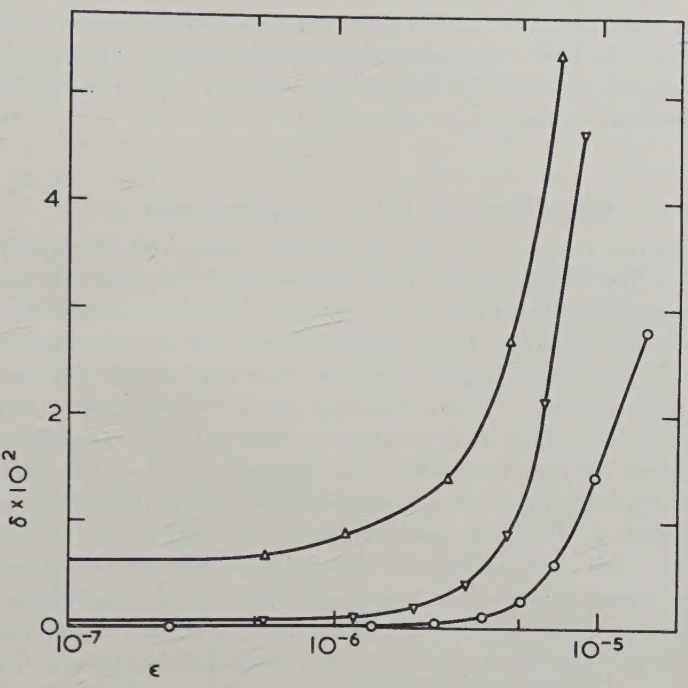

The internal friction of deformed crystals.

Symbol	Deformation %	Stress required g/mm²	δ_0
○	0·2	62	9×10^{-5}
▽	1·1	87	$5{\cdot}4 \times 10^{-4}$
△	6·7	400	$6{\cdot}2 \times 10^{-3}$

The effect of annealing a deformed crystal is to reduce its internal friction. The reduction occurs only very slowly at room temperature, but large effects can be obtained by annealing for an hour at 100 to 200°C. The magnitude of the reduction obtained by a given anneal varies between specimens cleaved from different melt grown crystals, and this suggests that the effect depends in some way on the impurities present. Similar decreases in damping are produced by irradiation with x-rays.

The motion of the dislocations which is believed to give rise to the internal friction observed in these experiments would also be expected to give rise to a decrease in the elastic modulus of the specimen, and this

would produce a change in its resonant frequency. While the apparatus was not primarily designed to measure such frequency changes, it was found possible to make a few rough measurements of the way in which the resonant frequency varied with strain amplitude. These measurements show that when δ is greater than δ_0 the value of Young's modulus, E, is reduced by an amount ΔE below its value observed at the lowest amplitudes. For four specimens deformed between 4 and 7% the ratio $(\delta-\delta_0)/(\Delta E/E)$ was fairly constant, and took values between 1·0 and 2·2 for values of ϵ from 2×10^{-6} to 10^{-5}. For specimens deformed 1% and less the results are less reliable, but $(\delta-\delta_0)/(\Delta E/E)$ was found to lie between 2 and 6 in the two crystals where it was measured.

3.2. *Discussion of the Damping Mechanism*

The internal friction of sodium chloride measured in experiments of this type is due to the motion of those dislocations which are introduced into the specimen after it has been annealed. This conclusion was reached by Gordon and Nowick (1956), and is confirmed by the present results, which show that deformation increases the very small internal friction of an annealed crystal. This damping can be subsequently reduced by annealing the specimen or irradiating it with x-rays. The effect of such treatments on the ease with which the dislocations move has been studied by R. W. Davidge (private communication), using an etching technique similar to that of Johnston and Gilman (1959, § III E). His results show that dislocations present before annealing do not move under a static or 90 kc/s stress, while those introduced after annealing move even on gentle handling of the specimen. The motion of these 'fresh' dislocations under an applied stress can be prevented by those annealing or irradiation treatments which also produce a considerable decrease in the internal friction.

Before considering the mechanism by which moving dislocations give rise to internal friction it is of interest to make a rough calculation of the distances through which the dislocations move in the vibrating crystal. In the Appendix it is shown that, when there is a total length of dislocation line Λ per unit volume which is capable of moving under the applied stress, the average amplitude of motion of the dislocations, x, at a strain amplitude ϵ, must satisfy the inequality

$$x \gtrsim \frac{2}{\pi}\frac{\epsilon\delta}{\Lambda b},$$

where b is the Burgers vector of the dislocations. Internal friction measurements have been made on two lightly deformed crystals which were subsequently etched in order to estimate Λ. In one of these crystals (for which further results will later be given in fig. 3) Λ was of the order of $2\times10^4\,\mathrm{cm}^{-2}$, and it was found that $\delta=2{\cdot}4\times10^{-3}$ at $\epsilon=1{\cdot}5\times10^{-5}$; this gives a value of $x\gtrsim800b$. In the other crystal Λ was of the order of $4\times10^5\,\mathrm{cm}^{-2}$, and, again at $\epsilon=1{\cdot}5\times10^{-5}$, x was estimated to be $\gtrsim160b$.

These results indicate that the model which must be used for the amplitude-dependent damping of these specimens is one in which dislocations can move large distances through the lattice. For this motion to be obtained by the bowing of loops against their line tension, loops of length at least $10^4 b$ would have to be able to move freely over the slip plane. It is difficult to estimate dislocation densities in the more heavily deformed specimens, but it seems probable that x is smaller in a heavily deformed crystal than in a lightly deformed one tested at the same strain amplitude.

No satisfactory empirical equation has been found which relates the internal friction determined in these experiments to the strain amplitude. However, it has been observed that for $\epsilon < 10^{-5}$, $(\delta - \delta_0)$ varies roughly as ϵ^n, with n varying from specimen to specimen between about 1·7 and 2·3. Coupled with the fact that $(\delta - \delta_0)/(\Delta E/E)$ lies between 1 and 6, this result is rather similar to that given by the simple phenomenological hysteresis model of Nowick (1950).

Various authors have proposed more detailed models to describe the internal friction of solids due to the motion of dislocations. The theory which has been studied in most detail is that of Granato and Lücke (1956), who consider the motion of dislocation loops which are pinned firmly at their ends and more weakly at points along their length. When a large-enough stress is applied some of these loops break away from their pinning points and move freely through the lattice, returning to their pinned positions when the stress falls to zero. Granato and Lücke have calculated the form of the variation of δ with ϵ to be expected on this model, and comparison of the present measurements with their theory shows that their equation is far from being satisfied in the amplitude-dependent region. This suggests that their model is not applicable to sodium chloride. Such a conclusion is to be expected when it is realized that the fresh dislocations probably lie on the slip planes in long loops rather than in a network in which loops are strongly pinned at their ends (cf. Gilman and Johnston 1957).

Nowick (1954) suggested that the internal friction of annealed and lightly deformed metals is due to the hysteresis in the motion of dislocation lines which is caused by their interaction with obstacles such as impurity atoms lying on the slip plane. Weertman (1955) has discussed this model in the case where the interaction between the dislocations and impurities is due to the long range elastic stresses around them, but rough calculations suggest that this elastic interaction is too small to account for the flow stress and damping of sodium chloride. However, a hysteresis model of the type considered by Nowick may be applicable in this case if the dislocations have a strong short range interaction with impurities, point defects, clusters, etc. distributed over the slip plane. The interaction is likely to be of a predominantly short range character if the binding energy arises mainly from electrostatic forces at the dislocation core, as has been shown to be the case for vacancies by Bassani and Thomson (1956).

In this model the defects which cause the pinning are assumed to be fairly immobile, and we will consider a long dislocation line lying in its

slip plane at a position where it is pinned at a number of points along its length. When a stress is applied to the crystal the dislocation bows out between the pinning points, and may break away from some of them with or without the aid of thermal activation. However, it cannot move far before it reaches a defect on the slip plane, where it will probably become pinned; this will happen because the time period of atomic vibrations is much less than the time the dislocation takes to cross the defect (unless it is moving at a velocity near that of sound). Subsequently the dislocation may break away at this or at other pinning points, and so move through the lattice in a series of jumps. When the stress is reversed the dislocation will move in the reverse direction, but in general there is no reason why it should follow a path given by the reversed sequence of forward jumps, nor why it should return exactly to its original position. This motion of the dislocation line will give rise to hysteresis in the stress–strain curve in vibration and so to internal friction. Higher applied stresses will cause larger lengths of dislocation line to move, and the damping produced by this mechanism should therefore be amplitude-dependent. Provided the impurities etc. present are not too strongly clustered this model seems not unreasonable in comparison with the distances moved by the dislocations calculated above.

§ 4. Changes in Internal Friction produced by Vibration

4.1. *Changes of Type I: Increases in the Damping of Annealed Crystals*

As has already been stated, the effect of annealing a deformed crystal is to decrease its internal friction. After annealing at a sufficiently high temperature the damping is reduced almost to zero, but after a low temperature anneal the damping may still be fairly large and amplitude-dependent. Many such lightly annealed crystals have been vibrated on the resonator at amplitudes in the amplitude-dependent region, and it has been found that after such treatment the damping at lower amplitudes is greater than that observed immediately after the anneal. This is an effect similar to type I referred to in the Introduction.

Figure 2 (*a*, *b*, *c* and *d*) shows the results of measurements made to study this effect on four specimens which were annealed at different temperatures between 100 and 170°C. Each specimen was first deformed by 0·2%, mounted on the resonator, and vibrated at the highest amplitude attainable. After an interval of 20 min, δ was measured as a function of ϵ, and the results are shown in the upper curve on the appropriate figure. The crystal was then removed from the resonator, heated to its annealing temperature, held there for 1 hour, furnace cooled in 1 to 2 hours, and carefully remounted. Internal friction measurements were then made as a function of increasing ϵ, and gave the results shown by the lowest curve for each specimen. These curves show that the damping was reduced by the annealing, and also that it rose abnormally rapidly at high amplitudes; in some cases it was even observed to rise with time during measurements at a constant driving voltage. 20 min after taking these readings

the damping was again measured, and the results were found to lie between those obtained before and after annealing. They are shown by the middle curves on the figure, and, provided the amplitude was not increased above its value at the end of the previous series of measurements, these curves were fairly reproducible. However, if the amplitude was raised above that used previously, the damping at all lower amplitudes was once more increased. This is shown in fig. 2 (*b*). After annealing this specimen, its damping was measured, and the results are shown by the points △. These

Fig. 2

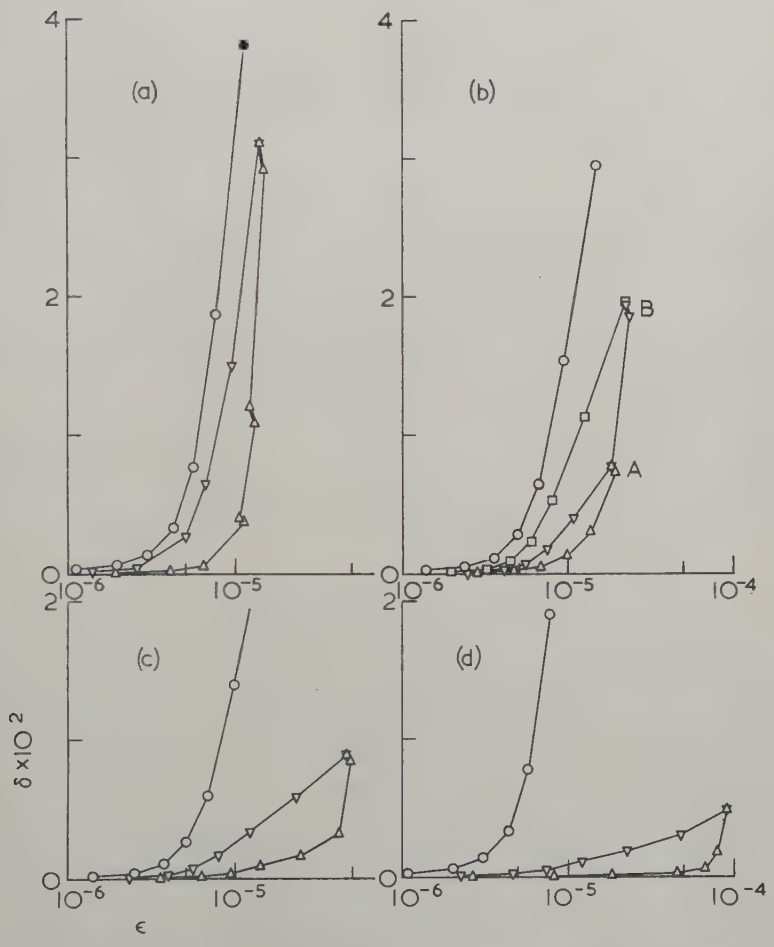

The internal friction of specimens deformed 0·2%, annealed and vibrated on the resonator. ○, before anneal; △, after 1 hour anneal at temperature stated below; ▽, repeat measurements; □, (only) second repeat.

Annealing temperatures: (*a*) 102°c, (*b*) 127°c, (*c*) 146°c, (*d*) 167°c.

Thick lines with negative slope indicate changes of δ during measurements at fixed V_d.

measurements were stopped at the point marked A, and the next series of readings gave the points ▽. In this series the crystal was driven to the point B where the amplitude is higher than at A, and this further increased the damping so that subsequent measurements yielded the points □.

Several specimens were tested in addition to those shown in fig. 2. One of these was deformed 0·2% and annealed for 1 hour at 198°C, after which the damping in the first series of measurements only exceeded 10^{-4} at values of ϵ greater than 10^{-4}. Another crystal was annealed for 20 hours at 123°C, and gave results fairly similar to those obtained after a 1 hour anneal at 146°C. Experiments were also performed on specimens deformed 1·1% and 4·3% and then annealed; these too showed an increase in the damping produced by vibration.

The damping of a deformed crystal can be reduced by x-irradiation as well as by annealing, and to study this a deformed crystal was lightly irradiated, bleached and tested on the resonator. When this specimen was vibrated at a high-enough amplitude, its damping was increased in just the same manner as that of an annealed crystal. This effect in x-irradiated crystals has previously been observed by Frankl (1953).

In the above experiments increases in damping produced by vibration have only been observed in crystals in which the damping had previously been reduced in some way; moreover the damping was never increased above that found in the specimen immediately after deformation. It will be recalled, however, that all measurements reported on such freshly deformed crystals were made after the specimen had been driven at the highest amplitude to be used. This was done because there is a small increase in the damping on first testing the specimen after mounting,and this may amount to a change in δ of up to 20%. Subsidiary experiments suggest that this increase in δ occurs as a consequence of the slight anneal given to the crystal in mounting it at about 70°C.

4.2. *Changes of Type V: Decreases in Damping at High Amplitudes*

This section describes some decreases in the damping of freshly deformed crystals, which have been observed to occur when specimens are vibrated at very high amplitudes. The strain amplitude at which measurements can be made in a deformed crystal is limited by the magnitude of its internal friction, and so it has only been possible to observe these decreases in specimens in which the density of fresh dislocations was fairly low. Figure 3 shows some results obtained on one such specimen. It was deformed longitudinally in compression under a stress of 26 g/mm², when slip occurred in some 50 slip bands, and etching showed that the density of dislocations introduced was of the order of 2×10^4 cm^{-2}. After mounting, the damping was measured as a function of increasing ϵ, giving the results shown in the upper curve. At amplitudes higher than 3×10^{-5} the value of ϵ rose at constant driving voltage, corresponding to a decrease in δ during the measurements; these decreases are shown on the figure by

thick lines against which the time taken for the change is marked. Points linked by thin lines correspond to changes in the driving voltage, but there may be some decrease in δ before a reading can be made. Where it is felt that an appreciable decrease has occurred the line is shown broken. The rate of fall of δ has not been studied in detail. However, it was noticed that at constant driving voltage ϵ rose slowly to a value of about $1{\cdot}3 \times 10^{-4}$, and then at an increasing rate until it reached about $2{\cdot}7 \times 10^{-4}$; after this little further change occurred. When this point had been reached a new series of measurements was made as a function of increasing ϵ. These are plotted as the lower curve in fig. 3, and show that the damping has been reduced by a large amount as a result of driving the specimen at high amplitudes.

Fig. 3

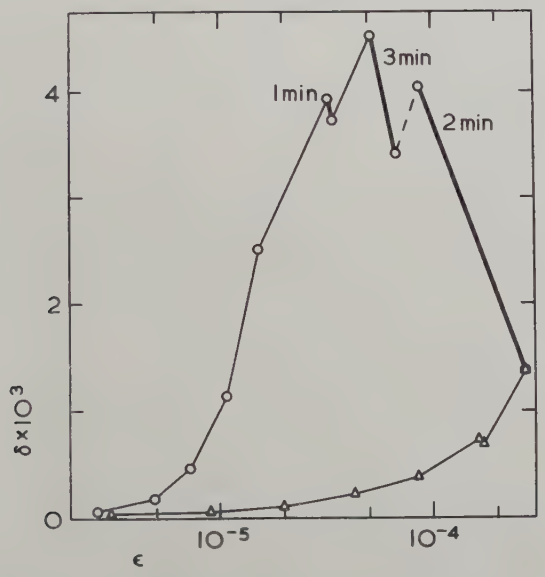

The internal friction at high amplitudes of a specimen lightly deformed in compression. ○, first series of measurements; △, subsequent measurements.

This reduction in damping has been observed in many specimens, including both lightly deformed crystals and crystals which were heavily deformed over a small region. The results of a more detailed series of measurements on a specimen of the latter type are shown in fig. 4. This specimen was locally deformed by dropping a 5 mm diameter steel ball on to the centre of one face from a height of 9·5 cm. It was then mounted on the resonator, and five series of damping measurements were made as a function of increasing ϵ, each series being taken to a higher final amplitude than the previous one. The first series stopped at the point A, and the

results of the second series show that a small type I increase in damping occurred during the first measurements. The second series extended to the point B, where the hardening process was interrupted; this left the crystal in a state where its damping was given by the third curve, which joins the second at B. An increase in the driving voltage at B produced very rapid hardening to the point C, and the fourth series of readings then gave the lowest values of δ observed in this specimen. A further increase in the driving voltage at C produced very little change in ϵ, the value of δ rising to that at D. A corresponding increase was then found in all values of δ determined in the fifth and final series of measurements.

Fig. 4

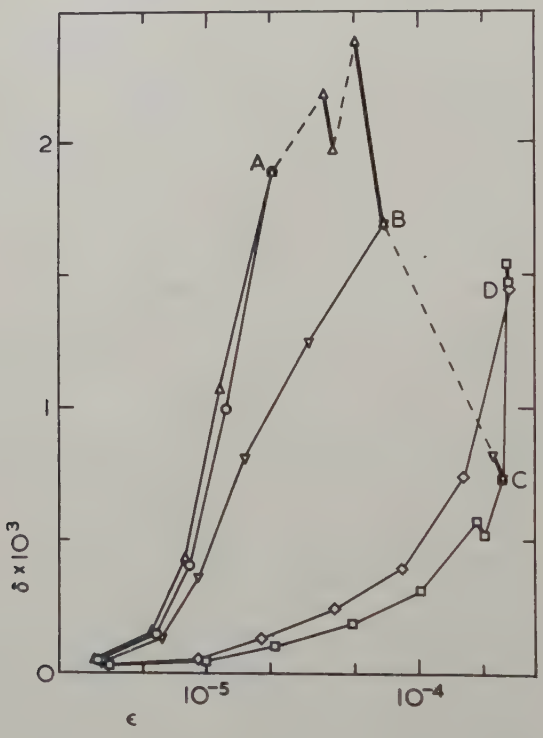

Five series of damping measurements on a locally deformed crystal. ○, 1st series to A, △, 2nd series to B, ▽, 3rd series to C, □, 4th series to D, ◇, 5th series to D,

4.3. *Changes of Type II: Increase in Damping and Creation of New Dislocations at the Highest Amplitudes*

Whenever a specimen was driven at a strain amplitude of about $2{\cdot}7 \times 10^{-4}$ its internal friction was increased at that and all lower amplitudes. A typical example of this is the rise of damping observed between points C

and D in fig. 4, which has just been described. The effect has also been observed in specimens which were not given any deformation before testing, and in all cases the stress amplitude ($\sim 1100\,g/mm^2$) at which the increase occurred was constant to within a few per cent. This increase in damping is similar to the type II effects mentioned in the Introduction.

Some simple etching experiments have been performed which show that these increases in damping are associated with the creation of new dislocations in the crystals. The specimens were etched using a method developed by R. W. Davidge (private communication), which is believed to reveal all the dislocations in the crystal; the interpretation of the observations is in many ways similar to that of Gilman and Johnston (1957). Fully annealed specimens were carefully mounted on the resonator and etched; they were then vibrated at a high amplitude and re-etched. After this treatment a large pyramidal etch pit indicates the position of a dislocation present in the same place before and after vibration; a large flat-bottomed pit represents the original position of a dislocation which has moved during the vibration, and a small pyramidal pit represents a dislocation not present at that position prior to vibration. Only very rarely has an apparently annealed-in dislocation been seen to move during vibration. However, dislocations introduced by handling, which occur on slip planes, move very easily even as a result of moving the resonator assembly about. After vibration at strain amplitudes up to $2{\cdot}0 \times 10^{-4}$, very few new dislocations were seen which could not be accounted for by the movement or multiplication of dislocations produced by handling before the first etch. However, when the specimens had been vibrated at an amplitude of $2{\cdot}7 \times 10^{-4}$ so that their damping was considerably increased, the appearance of the central part of the etched crystal was quite different, containing a large number of new etch pits lying on slip planes. These new pits were not apparently related to fresh dislocations present before vibration. Figure 5 (*a*) (Pl. 44) shows a typical region from such a specimen, the new dislocations being seen as small pits lying in straight lines. Figure 5 (*b*) shows an interesting but rather unusual region of the same specimen in which a large number of dislocations seem to have originated at a sub-grain boundary.

§ 5. Discussion

5.1. *Increases in the Damping of Annealed Crystals*

As has already been explained, the internal friction of a deformed crystal is reduced by annealing or x-irradiation. Comparison with etching experiments suggests very strongly that this reduction is due to the pinning of dislocations, presumably by point defects or impurity atoms. As described in § 4.1 vibration of such a crystal at high amplitudes gives rise to a type I increase in its internal friction. It is very unlikely that this increase is due to the creation of new dislocations, because that effect has been observed at much higher amplitudes and gives rise to a type II increase in damping. The only alternative explanation of the type I

increase in sodium chloride seems to be that the existing dislocations are unpinned by the vibration, and a simple account of this process can be given in terms of the model of damping considered at the end of § 3.2.

After annealing, the dislocations in the crystal will all be pinned at rather more points than previously, and therefore fewer dislocations will move from their initial positions at any given stress. However, after one of these dislocations has been broken away from its pinned position by the applied stress, it will move on its slip plane in the manner already described. If the interaction with its pinning points is of a short range character, there is in general no reason why it should return to the precise position where it will once more be fully pinned, and high amplitude vibration will therefore lead to a permanent increase in the damping of the specimen. On the basis of the theory of Granato and Lücke (1956), however, this effect would not be expected to occur, because in their model the dislocations return to their pinned positions after every half cycle of the stress.

5.2. *Decreases in Damping at High Amplitudes*

No satisfactory explanation has yet been found for the decreases in damping which are produced by vibration at high amplitudes, but two possibilities require brief consideration. In the Introduction attention was drawn to a similar effect (type V) observed in the fatigue of metals at lower frequencies, and Broom and Ham (1959) have attributed this effect to the production of vacancies by the motion of dislocations under the alternating stress. Subsequent experiments by Davidge *et al.* (1959) have shown that vacancies are produced by fatigue in sodium chloride crystals deformed more than 2%. In all these fatigue experiments the amplitude of motion of the dislocations is almost certainly great enough to produce many interactions between dislocations on intersecting slip planes, and it is probably these interactions which lead to the generation of vacancies. It is possible that the decrease in damping observed in the present experiments is also due to the production of vacancies or of jogs on dislocations. However, it is uncertain whether the number of dislocation interactions which can occur is sufficient to explain the observations. This can be seen from the fact that the average amplitude of motion of the dislocations at the stress where the damping begins to decrease in the specimen of fig. 3 is probably $\gtrsim 3000b$, while the separation of annealed-in dislocations other than those in sub-grain boundaries may be ten to a hundred times larger than this.

An alternative explanation of the decrease in damping can be given in terms of the model of internal friction considered above, in which the dislocations move from one pinned position to another in a series of jumps. As the amplitude is raised each dislocation will move over an increasingly large area of the slip plane, and may by chance come to lie in a configuration where the density of pinning points along its length is so high that the applied stress cannot break it away. It will then play no further part in

the damping, and if a growing number of dislocations become trapped in this way, the damping of the crystal will decrease.

In both of these models the dislocations have to move a considerable distance across their slip planes at the stress where the damping starts to decrease, and this stress may therefore be related to the static stress necessary to move a dislocation. In this connection it is interesting to note that the stress amplitude at which the decrease starts is about $130\,g/mm^2$, while C. W. A. Newey (private communication) has shown that the static flow stress of a similar crystal is about $300\,g/mm^2$ at 78°K and $54\,g/mm^2$ at room temperature.

5.3. *The Creation of New Dislocations by Vibration*

The production of new dislocations by vibration described in § 4.3 occurs at a fairly well-defined stress amplitude of $1100\,g/mm^2$. This is higher than the value of the flow stress extrapolated to absolute zero, and much lower than the stress required theoretically to nucleate new dislocations in a perfect lattice ($\sim 2\mu/100 \simeq 4 \times 10^4\,g/mm^2$). The etching experiments show that the new dislocations do not appear to be created by the movement of dislocations already present, and it seems probable that they are in fact nucleated at precipitates or other defects in the lattice; this has been shown to be the case in lithium fluoride by Gilman (1959). In this connection it is interesting to note the apparent nucleation at a sub-grain boundary shown in fig. 5 (*b*).

The fact that the dislocations are formed only at a stress higher than the flow stress can be understood when it is realized that the process requires the nucleation of a small loop, which then expands under the applied stress. If this stress is oscillatory the loop must expand so far during the first half cycle that it reaches a position from which it is not collapsed by the combined line tension and reverse stress in the second half cycle. In order to expand the loop sufficiently rapidly in the first half cycle a high stress is required, and the stress required to form new dislocations in vibration may be governed more by the stress needed to move the dislocation than by that required to nucleate the loop initially. Figure 5 shows that when new dislocations are created they move relatively large distances ($\sim 0{\cdot}01$ cm) from their point of formation, as might be expected from the above considerations.

Acknowledgments

This work was carried out during the tenure of a University Research Fellowship at Birmingham University, and the author wishes to thank Professor G. V. Raynor, F.R.S. for providing research facilities in the Department of Physical Metallurgy; Dr. P. L. Pratt for suggesting the project and for his continued encouragement and advice; Mr. R. W. Davidge for making available his etching technique and giving invaluable assistance with the experiments; and many other members of the department for valuable discussions.

APPENDIX

Calculation of the Amplitude of Motion of Dislocations in a Vibrating Specimen

If the alternating stress is assumed to be uniform and represented by $\sigma = \sigma_0 \exp(i\omega t)$, the corresponding compressive strain $\epsilon_0 \exp(i\omega t)$ can be divided into two parts; an elastic part $\epsilon' = \epsilon_1' \exp(i\omega t)$, and a non-elastic part due to the motion of the dislocations $\epsilon'' = (\epsilon_1'' - i\epsilon_2'') \exp(i\omega t)$. It can then be shown (Nowick 1953) that

$$\delta = \pi \epsilon_2''/\epsilon_1' \quad \text{and} \quad \Delta E/E = \epsilon_1''/\epsilon_1'.$$

The strain amplitude due to the motion of the dislocations, ϵ_d, is then given by

$$\epsilon_d = (\epsilon_1''^2 + \epsilon_2''^2)^{1/2} = \epsilon_1' [(\Delta E/E)^2 + (\delta/\pi)^2]^{1/2}.$$

The present results on heavily deformed crystals show that $\Delta E/E \sim \delta/\pi$, so that $\epsilon_d \sim \epsilon_1' \delta/\pi$; however, even if this is not the case in lightly deformed crystals the inequality $\epsilon_d \gtrsim \epsilon_0 \delta/\pi$ must be satisfied.

This dislocation strain can be considered as due to a total length of dislocation line Λ per unit volume moving a distance x on {110} planes, and it follows that $\epsilon_d = \frac{1}{2}\Lambda b x$, where b is the Burgers vector of the dislocations. Equating these values of ϵ_d, we find that

$$x \gtrsim \frac{2}{\pi} \frac{\epsilon_0 \delta}{\Lambda b}.$$

References

Bassani, F., and Thomson, R., 1956, *Phys. Rev.*, **102,** 1264.
Beshers, D. N., 1959, *J. appl. Phys.*, **30,** 252.
Birnbaum, H. K., 1955, *Acta Met.*, **3,** 297.
Broom, T., and Ham, R. K., 1959, *Proc. roy. Soc.* A, **251,** 186.
Davidge, R. W., Silverstone, C. E., and Pratt, P. L., 1959, *Phil. Mag.*, **4,** 985.
Frankl, D. R., 1953, *Phys. Rev.*, **92,** 573.
Gilman, J. J., 1959, *J. appl. Phys.*, **30,** 1584.
Gilman, J. J., and Johnston, W. G., 1957, *Dislocations and Mechanical Properties of Crystals* (New York: Wiley), p. 116.
Gordon, R. D., and Nowick, A. S., 1956, *Acta Met.*, **4,** 514.
Granato, A., and Lücke, K., 1956, *J. appl. Phys.*, **27,** 583 and 789.
Johnston, W. G., and Gilman, J. J., 1959, *J. appl. Phys.*, **30,** 129.
Hiki, Y., 1958, *J. phys. Soc., Japan*, **13,** 1138.
Marx, J., 1951, *Rev. sci. Instrum.*, **22,** 503.
Mason, W. P., 1956, *J. acoust. Soc. Amer.*, **28,** 1207.
Nowick, A. S., 1950, *Phys. Rev.*, **80,** 249; 1953, *Prog. Metal Physics*, **4,** 1; 1954, *J. appl. Phys.*, **25,** 1129.
Read, T. A., 1940, *Phys. Rev.*, **58,** 371.
Swift, I. H., and Richardson, J. E., 1947, *J. appl. Phys.*, **18,** 417.
Wadsworth, N. J., 1957, *Dislocations and Mechanical Properties of Crystals* (New York: Wiley), p. 479.
Weertman, J., 1955, *J. appl. Phys.*, **26,** 202.

Reverse Bending of Crystals of Silver Chloride†

By M. T. Sprackling
H. H. Wills Physics Laboratory, University of Bristol

[Received November 12, 1959]

Abstract

The reverse bending of single crystal bars of silver chloride that have already been singly bent has been studied by using the photoelastic effect. There is no indication of the preferential deformation at a certain place on the bar found when annealed crystals are bent. This is also true if the crystals are first heated at temperatures between room temperature and 375°c, but if they are heated at higher temperatures and as a result all detectable long-range stresses are removed from the crystal the sharp yield point of the first bending is recovered. The results are considered in terms of a simple dislocation model.

§ 1. Introduction

In a previous paper (Nye *et al.* 1957) an account was given of some photoelastic observations on the deformation of single crystal bars of silver chloride. These indicate the existence of a sharp yield point in the bending test, which is manifested by plastic deformation starting at a particular place and the propagation of plasticity longitudinally down the bar rather than transversely. The latter is the conventional view.

The observations were interpreted by means of a simple dislocation model (Read 1957) in which σ_c is the stress necessary to generate dislocations and σ_0 is the stress necessary to move them through the crystal. (We interpret σ_c not literally as the stress needed to generate dislocations but as the stress necessary to create a mobile dislocation (that is, one which can move under a stress σ_0) or to "cause a dislocation to break away from a locked position"). On this model the curve of bending moment versus curvature goes through a sharp maximum at the elastic limit if σ_0/σ_c is less than 0·6. We should then expect instability in a bending test; when deformation started at a certain place it would continue there preferentially. Thus the non-uniform deformation of the silver chloride bars can be interpreted to mean that in this crystal σ_0/σ_c is less than about 0·6.

In this paper we describe the effect of applying reversed bending couples to bars that have already been plastically bent.

§ 2. Experiments on Reverse Bending

When an annealed single crystal of silver chloride is deformed plastically in bending along its complete length (Nye *et al.* 1957), so that

† Communicated by the Author.

its upper side is convex, after the deforming couples have been removed the appearance between crossed nicols is shown in fig. 1†. The distribution of longitudinal stress σ, inferred from birefringence measurements, is shown at the side of fig. 1.

When a bar that has been bent plastically along its complete length is subject to reverse bending couples the photoelastic pattern changes as the couple increases as shown in figs. 2, 3, 4 and 5 respectively. The corresponding distributions of longitudinal stress are shown at the sides of the figures. It can be seen that the two broad outer dark bands move towards the narrow dark band which represents the neutral plane of bending. This process continues as the reversed load is increased and the three bands finally coalesce to form one narrow central band.

In this deformation there is no indication of a sharp yield point. The two broad dark bands remain parallel to the narrow central band along the complete length of the bar during reverse bending; there is no tendency for the bar to deform preferentially at any place. This is in complete contrast to the behaviour of an annealed bar.

An annealed bar can be bent so that only part of the bar deforms plastically (Nye *et al.* 1957). When such an elastic–plastic bar is subject to reverse bending couples the two dark broad bands in the plastic region move towards the narrow central band with increasing load. but they do not remain parallel to this band. They are always slightly closer to the central band in the part of the plastic region nearest the elastic–plastic junction. The ultimate coalescence is first achieved at the elastic–plastic junction. During the whole of this process the initially elastically bent region of the bar remains elastic and deforms plastically only when the three bands in the plastic region have coalesced. Hence, while the reverse bending of the plastic region is taking place, the maximum stress in the elastic region of the bar is always less than the stress σ_c needed to generate dislocations in the annealed material.

Figures 2–5 show that as the reverse couples are increased two well-defined regions of approximately constant stress σ_R appear, close to the edges of the bar at first, but spreading towards the middle of the bar as the deformation continues, until a stage is reached when the stress is uniform over almost the whole of the bar.

The 'discontinuity' in stress on crossing the neutral plane of bending found in singly-bent bars seems to become gradually smaller with increasing reverse loading, and finally disappears, to be replaced by a new discontinuity of opposite sign.

In the first bending we observed a uniform longitudinal stress σ_P over most of the plastic region which was identified with the σ_0 of Read's model. Measurements of σ_P resulting from the first bending and σ_R resulting from the reverse bending have been made and the results for σ_R/σ_P in six different specimens are 1·11, 1·03, 1·02, 1·10, 1·04, 1·18; mean = 1·08.

† All figures are shown as plates.

§ 3. Effect of Heating

A number of singly-bent crystals were tested in reverse bending after being heated. Temperatures ranging from about 375°C to room temperature were used (m.p. of silver chloride = 455°C).

Specimens that were not heated were left at room temperature for three weeks before retesting and those that received heat treatment were heated for eight hours followed by furnace cooling. In none of these cases was there complete annealing as judged from the photoelastic pattern. This was reduced in intensity but the main features were unchanged, indicating that there was no large-scale redistribution of stress. None of these specimens recovered the sharp yield point and associated inhomogeneous deformation of the first testing: their behaviour under reversed couples was similar to that of specimens that were untreated.

After heating for twelve hours at 400°C some specimens annealed completely (i.e. they contained no detectable long-range internal stresses) while others still showed the photoelastic pattern, but greatly reduced in intensity.

The crystals that appeared to be fully annealed, and these only, showed a yield point when tested in reverse bending and their behaviour was similar to that in the first bending: plastic yielding started at a certain place on the bar and the plastic region progressed longitudinally down the bar.

§ 4. Conclusions

The experiments on the reverse bending of bars already plastically bent show that the sharp yield point appears only in the first bending. When the bar is bent under reverse couples it behaves in the conventional manner, with no indication of preferential deformation at any place.

We may interpret this in terms of Read's (1957) dislocation model of bending. On this model, the absence of any instability in the deformation means that the ratio of the stress needed to propagate dislocations through the material to the stress needed to generate them lies between about 0·67 and 1. We may identify the uniform stress σ_R with the theoretical stress needed to propagate dislocations through the singly-bent material. Thus if σ_c' is the stress needed to generate dislocations in the singly-bent material we have $0{\cdot}67 \leqslant \sigma_R/\sigma_c' \leqslant 1$. Experimentally, σ_R is only slightly (about 8%) greater than σ_P, the stress needed to move dislocations in the annealed material. The model therefore gives two extreme possibilities: either $\sigma_c \doteq \sigma_c'$ and the slight difference between σ_R and σ_P is sufficient to raise the ratio σ_R/σ_c' above the critical value of 0·67, or alternatively, σ_c' is appreciably less than σ_c. The latter explanation seems more likely.

The experiments on heating show that in bending tests the crystals fail to recover the yield point unless they are fully annealed, that is, all long-range internal stresses are removed. Incomplete annealing by heating over a range of temperatures to within 50°C of the melting point does not produce recovery of the yield point.

If the yield point of the first bending is determined by the stress needed to break away from locking atmospheres of impurity atoms (Cottrell 1948) or vacancies, then our experiments show that these atmospheres do not form below about 400°C.

An alternative suggestion is that the yield point is determined by the stress needed to break-up stable (low-energy) arrays of dislocations, with no associated long-range stresses, within the crystal. Following deformation, the dislocations would only collect into arrays of this type after complete annealing of the crystal.

Acknowledgments

I should like to thank Dr. J. F. Nye for his encouragement in the course of the work and his comments on the manuscript of this paper. The work was carried out during the tenure of a maintenance grant from the Department of Scientific and Industrial Research.

References

Cottrell, A. H., 1948, *Report on Strength of Solids* (London: The Physical Society).

Nye, J. F., Spence, R. D., and Sprackling, M. T., 1957, *Phil. Mag.*, **2**, 772.

Read, W. J., Jr., 1957, *Acta Met.*, **5**, 83.

The Generation of Dislocation Loops at the Surfaces of Crystals of Silver Bromide†

By J. T. Bartlett and J. W. Mitchell‡
H. H. Wills Physics Laboratory, University of Bristol

[Received January 18, 1960]

Abstract

A method for preparing chemically sensitized, dislocation-free, silver bromide single crystals is described in this paper. When these crystals are strained beyond the elastic limit and exposed to light, both the dislocation loops which are generated at the surfaces, and the surface terraces which may be associated with them, are made visible by the separation of particles of silver. The glide planes of the dislocations may then be determined from microscopic measurements and the Burgers vectors of the dislocations may be inferred if the stress distribution responsible for the deformation is at least qualitatively known. This provides a powerful method for studying dislocation interactions and the fundamental processes of plastic deformation.

§ 1. Introduction

During the course of the experimental work on dislocations in crystals of silver halides, which has been carried out at Bristol (Mitchell 1957 a, 1958 b), it has been observed from time to time that both dislocation loops generated at the surfaces of crystals, and surface terraces associated with them, can be made visible by the separation of particles of silver (see, for example, Jones 1959). It soon became clear, however, that a particularly favourable state of chemical sensitization had to be established before particles of photolytic silver would separate preferentially along the surface terraces during illumination. Until recently, we have not been able to define the conditions under which the required state of sensitization could be reproducibly achieved and an account of this work has consequently not previously been published. Our systematic investigations have now resulted in the development of a technique for sensitization which leads to reliable decoration of both dislocation loops and surface terraces when plastically deformed crystals are exposed to light.

The purpose of this paper is to describe the method which has been used for the production of dislocation-free, chemically sensitized crystals of silver bromide and some of the observations which have been made with them. The normal mode of plastic deformation involves the generation of dislocation loops at the surfaces as shown in the figures accompanying this paper. Observations on interactions between dislocations in silver bromide crystals will be presented in subsequent papers.

† Communicated by the Authors.

‡ Now at the Department of Physics, University of Virginia, Charlottesville, Virginia.

§ 2. Experimental Methods

Globules of high purity silver bromide were first prepared and sheets with a thickness of 400 microns and optically flat, plane-parallel surfaces were then made and cut into strips of convenient width (about 5 mm). The methods employed up to this point have already been described in detail by Clark and Mitchell (1956). It was known from previous work that the required sensitization was associated with the presence of traces of silver iodide in the crystals but it proved impossible to prepare satisfactory sheet crystals from globules of silver bromo-iodide. The sensitization was therefore carried out by annealing the strips for eight hours at 380°c in a sealed tube containing sections of crystals of silver bromide with 5 mol % silver iodide, bromine and oxygen. The pressure of bromine was about 700 mm Hg at 380°c and the pressure of oxygen, between 1 and 10 mm Hg, the precise value within this range being unimportant. The sealed tubes were allowed to cool slowly to room temperature. The crystals were then removed, strained, and the dislocations and associated surface terraces made visible by exposing them to radiation from a medium pressure mercury vapour lamp with a glass envelope. For microscopic examination, the crystals were mounted in Canada balsam on 3 in. × 1 in. glass slides and protected with a thin cover-glass. The orientations of the surfaces of the crystals were determined from back-reflection Laue x-ray diffraction photographs. The glide planes of the dislocations were established from measurements made with a calibrated micrometer eyepiece used in conjunction with the calibrated fine focusing knob of the microscope. The depth measurements had, of course, to be corrected for the refractive index of the silver halide. The points of intersection of dislocations with the surfaces of the crystals could also be made visible by etching with a 3 to 7 N solution of sodium thiosulphate for the shortest possible time and then examining them with the phase contrast microscope (Jones and Mitchell 1957).

§ 3. Experimental Observations

The etching method is a convenient one for following the process of recrystallization during annealing. The dislocations are made visible on {100} and {111} but not on {110} surfaces (Jones and Mitchell 1957, Mitchell 1958 b, Jones 1959, Parasnis 1959). In the present work we found that large areas around the edges of the strips which had been cut with the razor blade recrystallized during annealing. Compared with any remaining polygonized areas in the centres of the sheets, there was always a low density of dislocations in the recrystallized areas. The majority of the residual dislocations in these areas were edge dislocations running normal to the surfaces from one side of the crystal to the other and arranged in small angle tilt sub-boundaries with the axis of tilt also normal to the surface. These sub-boundaries were not eliminated by long periods of annealing (see Mitchell 1958 b). Our observations show that small areas

which are free from dislocations appear at the heavily deformed cut edges of the crystals during the early stages of the annealing process. The interface between these areas and the central area, where there is always a high density of dislocations, then advances into the crystals, and large areas are swept free from dislocations under favourable circumstances. The lattice disorder is of the Frenkel type so that dislocation loops will not be formed by the condensation of lattice defects during cooling as might occur in crystals of alkali halides. All the studies on the generation of dislocations at the surfaces of crystals and on interactions between dislocations which will be described in this and subsequent papers have been made in recrystallized areas of the annealed crystals.

Microscopic observations and quantitative measurements have now been made on many dislocation loops generated at the surfaces of silver bromide crystals under the influence of applied stresses. It has been established by direct observation that the glide planes frequently do not coincide with low index crystallographic planes but that they always contain a ⟨110⟩ direction. This is consistent with the conclusion of Nye (1948a, b, 1949) that the silver halides deform plastically by pencil glide and with the observations of Jones and Mitchell (1958) on prismatic slip. For a given ⟨110⟩ Burgers vector, we have, however, found that slip occurs on planes with poles between the poles of the {111} and {110} planes with far higher probability than on planes with poles between {110} and {100}. No glide planes with poles near those of the {100} planes have ever been observed. This is a little surprising in view of the circular contours of the stress-generated prismatic and helical prismatic dislocations studied by Jones and Mitchell (1958, see also, Mitchell 1958b).

Fig. 2

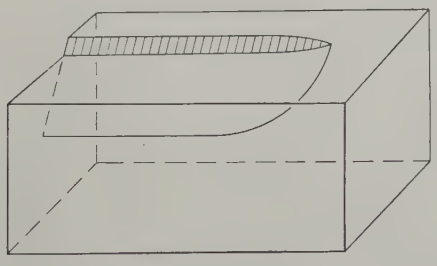

Diagram showing a dislocation loop of the type illustrated in fig. 1 (*a*), (*b*) and (*c*) (Pl. 48).

The most interesting observations have been made on crystals with surfaces parallel to (001) crystallographic planes. When these crystals are stressed along the [010] direction, dislocation loops may be nucleated at the surface on either the $(0\bar{1}1)$ and (011) or the (110) and $(\bar{1}10)$ planes. In the first case, the dislocation loops lie on planes making angles of 45° with the surface of the crystal. They meet the surface in the screw orientation and their two points of intersection with the surface are joined

by a length of surface terrace with a height determined by the resolved component of the Burgers vector normal to the surface. The dislocation line is in the edge orientation where the loop is parallel to the surface. This case, which represents the usual mode of deformation under the conditions of our experiments, is illustrated in fig. 1 (*a*), (*b*) and (*c*) (Pl. 48), and fig. 2. In the second case, the dislocation loops lie on the (110) or ($\bar{1}$10) planes which are normal to the surface of the crystal but make angles of 45° with the direction of the applied stress. The dislocation loops which are generated at the surface on these planes meet the surface in the edge orientation and are in the screw orientation when they are parallel to the surface. This case is illustrated in fig. 3 (Pl. 48). The reason why dislocation loops of the first type are nucleated with higher frequency than those of the second may be that the attractive interaction between screw components at the surface will be less than that between edge components (see Eshelby and Stroh 1951) so that the first type should be generated in a dislocation free crystal by the application of a lower stress than the second.

The formation of these two types of dislocation loop can also be inferred, as in the earlier experiments of Gilman and Johnston (1956, 1957) on lithium fluoride crystals, by etching the strained silver bromide crystals with a 3 to 7 N solution of sodium thiosulphate which produces localized depressions where the dislocations meet the surface. In the case of silver halide crystals, this is, however, a less satisfactory technique. The etch pits coalesce at quite low dislocation densities and the resolution is lower than that which can be achieved by the separation of silver during exposure to light, quite apart from the substantial advantage that this allows the observation of surface terraces and of dislocation loops on glide planes below the surfaces of the crystals. The surface dislocation loops on glide planes in lithium fluoride crystals have recently also been observed directly by x-ray extinction contrast in the experiments of Newkirk (1959).

Two dislocation loops which were generated by straining a crystal to a very small extent are illustrated in fig. 1 (*a*), (*b*) and (*c*). Only a section of each loop is included in the photomicrograph. In fig. 1 (*a*), the microscope is focused on the surface of the specimen and it can be seen that specks of silver have been formed preferentially during exposure along the edges of the surface terraces associated with the dislocation loops. The effect of the surface terrace is clearly to increase the probability for the formation of nuclei of silver by the combination of conduction electrons and silver ions during exposure (Mitchell 1957 b, 1958 a). The surface density of particles of silver is greater along the edges of the terraces, and the size of the particles correspondingly smaller, than elsewhere on the sensitized surface. The microscope is focused 3 microns below the surface in fig. 1 (*b*) and the focal plane intercepts the dislocation loops in a position where they are essentially in the screw orientation. In fig. 1 (*c*), the microscope is focused on the dislocation lines 6 microns below the surface where they are parallel to the surface and in the edge orientation. One such dislocation loop is illustrated diagrammatically in fig. 2 which is based on

the standard illustrations which appear in monographs on dislocations (see, for example, Read 1953, pp. 2, 15 and 18) but has been redrawn to correspond to the loops in fig. 1. The glide plane of the dislocation is defined by the surface terrace and the dislocation line below the surface. It may be determined by microscopic observations after the orientation of the crystal has been established from a Laue back-reflection x-ray diffraction photograph. In the case of the specimen of fig. 1, the surface was almost parallel to the (001) crystallographic planes and the glide planes of the two dislocations in the photomicrographs were very close to (011) planes which contain $\frac{1}{2}[0\bar{1}1]$ Burgers vectors. Neither the two surface terraces nor the two dislocations where they are in the edge orientation are parallel to each other from which it is evident that the glide planes do not coincide precisely with the low index (011) planes. These dislocation loops usually expand by the outward motion of the screw components which is frequently accompanied by extensive cross-slipping. Regular successions of parallel dislocation loops of this kind lying on the same glide plane are not observed.

Such successions are typical of the second mode of deformation which is illustrated in fig. 3. The glide plane is here the (110) plane and the dislocations have a Burgers vector $\frac{1}{2}[\bar{1}10]$. The leading sections of the dislocation loops are in the edge orientation and therefore cannot cross-slip as they glide outwards. Well-defined slip planes now appear but there are no surface terraces associated with the individual dislocation loops which are in the screw orientation and very feebly decorated where they are parallel to the surface.

The heavy decoration of the dislocation loops near the surface in fig. 1 (*b*), where they are in the screw orientation, is probably due to cross-slipping on a microscale which would introduce a high linear density of jogs and edge components. Such cross-slipping and jogging will be much less likely to occur in the case shown in fig. 3; here the dislocation lines will tend to minimize their length where they are in the screw orientation by remaining on the glide planes.

It is surprising that the monatomic steps which are associated with dislocation loops of the type illustrated in fig. 1 can be revealed by the preferential separation of surface particles of photolytic silver, as there must be a high density of such steps or terraces on crystal surfaces which do not coincide accurately with crystallographic planes. The situation must be that surface nuclei for the separation of silver are formed during the exposure of the sensitized crystals with higher probability along the newly formed surface terraces where, on account of the cross-slip on a microscale which has just been discussed, there may be a relatively high density of kink sites (Mitchell 1957 b, 1958 a).

Acknowledgments

This work was carried out during the tenure of a Research Studentship awarded by the Department of Scientific and Industrial Research to

J. T. Bartlett. The photomicrographs were taken with equipment purchased with a special grant from the Department of Scientific and Industrial Research. This assistance is gratefully acknowledged. We are also grateful to Kodak, Ltd., for financial support and to J. H. Burrow and G. D. Freke for much valuable assistance.

References

Clark, P. V. McD., and Mitchell, J. W., 1956, *J. photogr. Sci.*, **4,** 1.

Eshelby, J. D., and Stroh, A. N., 1951, *Phil. Mag.*, **42,** 1401.

Gilman, J. J., and Johnston, W. G., 1956, *J. appl. Phys.*, **27,** 1018; 1957, *Dislocations and the Mechanical Properties of Crystals* (New York: John Wiley), p. 116.

Jones, D. A., 1959, Ph.D. Thesis, University of Bristol.

Jones, D. A., and Mitchell, J. W., 1957, *Phil. Mag.*, **2,** 1047 ; 1958, *Ibid.*, **3,** 1.

Mitchell, J. W., 1957 a, *Dislocations and the Mechanical Properties of Crystals* (New York : John Wiley), p. 69 ; 1957 b, *Rep. Progr. Phys.* (London : Physical Society), **20,** 433 ; 1958 a, *J. photogr. Sci.*, **6,** 57 ; 1958 b, *Growth and Perfection of Crystals* (New York : John Wiley), p. 386.

Newkirk, J. B., 1959, *Trans. Amer. Inst. min. (metall.) Engrs*, **215,** 483.

Nye, J. F., 1948 a, *Nature, Lond.*, **161,** 367 ; 1948 b, *Ibid.*, **162,** 299 ; 1949, *Proc. roy. Soc.* A, **198,** 190.

Parasnis, A. S., 1959, Ph.D. Thesis, University of Bristol.

Read, W. T., Jr., 1953, *Dislocations in Crystals* (New York: McGraw-Hill).

The Electrical Resistance of Iron–Aluminium Alloys and its Dependence on Crystallographic Order†

By R. W. Cahn and R. Feder‡
Department of Physical Metallurgy, University of Birmingham

[Received January 18, 1960]

Abstract

The electrical resistance of two iron–aluminium alloys, bordering on the composition Fe_3Al, was measured at room and liquid nitrogen temperatures after inducing various states of order. By means of an analysis based on values of residual resistivity and of the temperature coefficient of resistivity, the influence of order on electronic factors in the conductivity, and on the perturbations of the lattice that produce scattering, were separately estimated. The freedom of conduction electrons diminishes as the order increases, and the decrease in low temperature resistivity associated with increasing order is due to the greatly reduced scattering potential. These conclusions permitted a qualitative interpretation of the form of the anomalous resistance/temperature relation at high temperatures.

§ 1. Introduction

The present study arose from the wish to interpret the anomalous form of the resistance–temperature curves for a number of iron–aluminium alloys, first published by Bennett (1952). An example of such a curve, for nearly stoichiometric Fe_3Al, is shown in fig. 1, which is based upon measurements by the present authors. On this graph, θ_c represents the ferromagnetic Curie temperature and T_c the temperature at which crystallographic ordering sets in (Bradley and Jay 1932, Taylor and Jones 1958, McQueen and Kuczynski 1959). Bennett attributed the resistance hump just below T_c to the influence of antiphase domain boundaries, which can scatter conduction electrons and thus increase resistivity§. This, however, seemed improbable since a curve such as that in fig. 1 can be traced reversibly, whereas a structure of small antiphase domains is unstable; the domains quickly grow at high temperatures, and the resistance hump would be expected progressively to disappear if it were associated with the presence of domain boundaries.

The present experiments were designed to disentangle the various factors that determine the electrical resistance so as to achieve an understanding of the resistance at high temperatures.

---

† Communicated by the Authors.

‡ Now at Frankford Arsenal, Philadelphia, Pennsylvania.

§ Other, non-stoichiometric alloys show more pronounced humps on the resistance/temperature curves.

Fig. 1

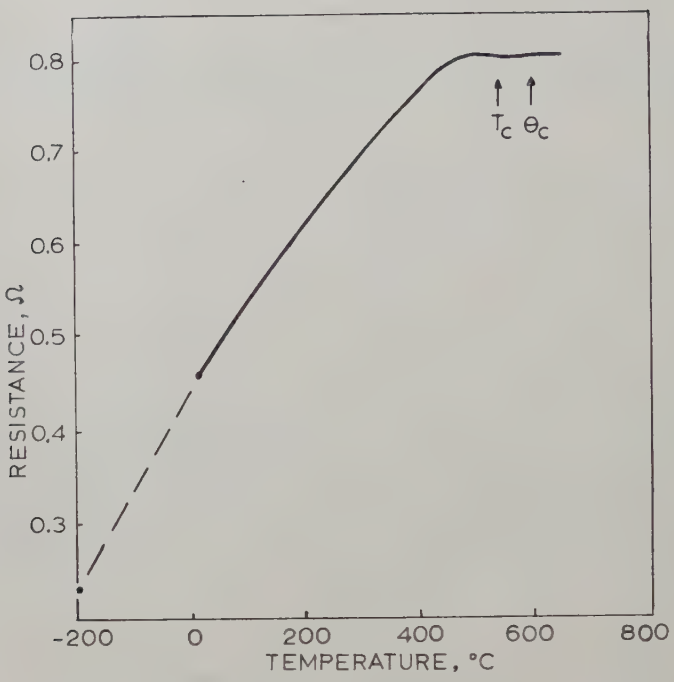

Equilibrium resistance-temperature curve of alloy containing 24·8 at. % aluminium.

§ 2. Analysis of the Electrical Resistance of an Iron-base Ordering Alloy

Since it is necessary to take into account the ferromagnetic resistivity component, an appropriate framework for analysis is provided by Coles' (1958) theory of spin–disorder terms in the resistivity. According to the quantum mechanical model for iron recently advanced by Mott and Stevens (1957), two 3*d* electrons with unpaired spins are located on each atom in body-centred cubic iron. These electrons do not themselves take part in conduction but, interacting by exchange with conduction electrons, they scatter these and contribute to the electrical resistivity. Their scattering power diminishes progressively as the spins become aligned, i.e. as the saturation magnetic moment increases with falling temperature. It is therefore possible, as a crude approximation, to express the total resistivity at a given temperature in the form

$$\rho = F \times (P_A + P_S + P_T). \quad . \quad . \quad . \quad . \quad . \quad . \quad . \quad (1)$$

Here P_S and P_T represent the scattering perturbations due to *spin* disorder (*non*-alignment of spins) and *thermal* disorder, respectively, while P_A represents scattering due to *atomic* (i.e. crystallographic) disorder.

The factor F expresses the freedom of the conduction electrons†; it depends on the concentration, effective masses, etc. of conduction electrons, and hence on the Brillouin zone structure. When the electrons responsible for the magnetic moment are bound to individual atoms and do not enter energy bands, then neither the zone structure nor the freedom of conduction electrons will be affected by alignment of their spins, (i.e. onset of ferromagnetism) and therefore F will remain unaffected. Coles showed that this separation of resistivity into terms provided a self-consistent analysis of the resistance of iron itself, and also of iron–ruthenium solid solutions.

2.1. *Influence of Crystallographic Order*

Not only P_A, but also F will vary when the state of order changes, because any change in lattice periodicity will influence the Brillouin zone structure. To apply eqn. (1) to our alloys, therefore, it is necessary to find how P_A and F vary with order below the critical temperature T_c. We can get an approximate idea of this by obtaining data on resistivity, at room temperature and below, of alloys quenched from different temperatures and which are, consequently, in different states of order. The specimen remains in the state of order corresponding to the quenching temperature, and retains corresponding values of P_A and F, since the rate of diffusion is vanishingly small at room temperature. We have

(i) $$\rho_0^{QT} = F^{QT} P_A^{QT}. \quad . \quad . \quad . \quad . \quad . \quad . \quad . \quad . \quad . \quad (2)$$

Here the suffix 0 indicates the residual resistivity (at 0°K) while the superfix QT denotes the fact that the quantities refer to an alloy quenched from temperature T. The terms in P_S and P_T disappear because zero point thermal energy and residual spin disorder at absolute zero are small enough to be neglected in comparison with P_A. (The state of *spin* disorder characteristic of the quenching temperature is, of course, not frozen in by quenching.)

(ii) The temperature coefficient $\partial\rho/\partial T$, at or below room temperature, of an alloy quenched from temperature T is given by

$$\left(\frac{\partial\rho}{\partial T}\right)^{QT} = F^{QT}\frac{\partial}{\partial T}(P_S^{QT} + P_T^{QT} + P_A^{QT}). \quad . \quad . \quad . \quad . \quad (3)$$

P_S will vary somewhat with temperature below room temperature, but the observed variation of the saturation magnetic moment with temperature is slight below 20°c (Taylor and Jones 1958), and this implies that the alignment of spins is already far advanced at this temperature. P_S will therefore be small throughout the range of temperatures in question. Moreover, this remains true for *all states of order*, since in Fe_3Al the saturation magnetic moment at room temperature varies by less than 10% between complete disorder and full order (Masumoto and Saito 1952, Rode

† A large value of F implies a low degree of freedom.

1957). At or below room temperature, we therefore have $\partial P_S/\partial T \approx 0$, irrespective of quenching temperature; and to an even better approximation, $\partial P_S/\partial T$ is small and constant for all quenching temperatures.

$\partial P_T/\partial T$ is also taken to be virtually independent of the state of order. The thermal perturbation P_T due to lattice vibrations is closely correlated with elastic properties, and we can estimate how much P_T varies with order by noting to what extent an elastic modulus changes with order. Yamamoto and Taniguchi (1956) showed that the change, due to ordering, of the *intrinsic* Young's modulus at room temperature (i.e. corrected for the irrelevant ferromagnetic ΔE-effect) is only 1–3% for alloys near the composition Fe_3Al. (By way of comparison, the corresponding change for Cu_3Au is about 50% (Lord 1953).) From this we can conclude that the thermal perturbation is virtually independent of order, and hence $\partial P_T/\partial T$ is independent of quenching temperature for Fe_3Al†.

P_A is determined by the quenching temperature; it does not vary with temperature below 20°C, and therefore $\partial P_A/\partial T = 0$.

From the foregoing, it follows that

$$\alpha^{QT} = \left(\frac{\partial \rho}{\partial T}\right)^{QT} \approx F^{QT} . \left(\frac{\partial P_T}{\partial T}\right)^{QT} \approx K . F^{QT} \quad . \quad . \quad . \quad . \quad (4)$$

where K is a constant.

If we take into account the small but appreciable term in $\partial P_S/\partial T$ then we have (since $\partial P_S/\partial T$ is, as argued above, nearly independent of the state of order) that

$$\alpha^{QT} = F^{QT} \left\{ \left(\frac{\partial P_T}{\partial T}\right)^{QT} + \left(\frac{\partial P_S}{\partial T}\right)^{QT} \right\} \approx K' . F^{QT}$$

where K' is another constant.

2.2. *Principle of Present Experiments*

Relations (2) and (4) permit independent estimates to be obtained of F^{QT} and ${P_A}^{QT}$ for alloys quenched from different temperatures, by measuring resistance at room temperature and in liquid nitrogen, extrapolating to 0°K to obtain an approximate value of ${\rho_0}^T$‡, and obtaining a mean value of α^{QT} from the resistance values at 293°K and 77°K. These values of F^{QT} and ${P_A}^{QT}$ can then be used to estimate a set of values of resistance at high temperatures, for comparison with observation. This has been done.

2.3. *The Alloy Fe_3Al*

Some remarks are in order concerning the applicability of eqns. (1)–(4) to the case of Fe_3Al. In the first place, there is some doubt about the quantum mechanical state of the electrons responsible for the atomic magnetic moments. The hypothesis that in iron (and iron alloys) they are in non-conducting states is largely based upon the x-ray diffraction data

† The Debye temperature of Fe_3Al was also found to be unaffected by ordering (Nemnonov and Finkel'shtein, 1959).

‡ It would have been better to make measurements at several temperatures, down to 20°K or below, but the necessary equipment was not available.

due to Weiss and de Marco (1958) and Weiss and Freeman (1959), and these have recently been challenged by Batterman (1959). Coles' analysis of various resistivity data does provide clear-cut support for the hypothesis; however, the present analysis stands or falls by its correctness.

The formulation of eqn. (1) is open to the criticism that the P_A and P_S terms are not entirely independent, since at high temperatures the spins are disordered in both distribution and orientation. P_S at moderate temperatures is almost independent of the state of order, so that this objection is not too serious†; however, at temperatures near T_c the spin disorder does depend appreciably on the state of atomic order, and this will limit the accuracy with which the above analysis can be used to interpret the high temperature resistivity.

Nathans *et al.* (1958) have direct experimental evidence, from neutron diffraction, about the distribution of spins on different iron sites in fully ordered Fe_3Al, and find that iron atoms in crystallographically distinct sites have slightly different moments; this cannot be the case in the disordered alloy. This variation of the atomic magnetic moments with order must again limit the accuracy of the analysis.

In view of the foregoing, the conclusions reached from the present experiments should be regarded as semi-quantitative at best.

§ 3. Experimental Methods

Two alloys containing 24·8 at. % and 25·5 at. % aluminium, balance iron, were vacuum melted and chill cast *in vacuo*, using constituents of 99·99% purity. The more dilute alloy also contained about 0·03% carbon owing to the use of graphite as deoxidiser; the carbon content of the other was negligible. The ingots were hot rolled to strip 1 mm thick, and resistance specimens of the form shown in fig. 2 were milled from the strip. The resistance was roughly 0·5 Ω at room temperature. This form of specimen was compact and could readily be heated to a uniform temperature and quenched.

Current and potential leads were brazed to the specimen, as illustrated. For resistance measurements at high temperatures (to obtain data such as those of fig. 1), the specimens were placed, together with a mica insulation, into a block which ensured temperature uniformity within ± 2°C. Smooth heating and cooling rates of 1–2°C/min were obtained by means of a motor-driven rheostat, and such a rate was known (Lawley *et al.* 1960) to be sufficiently slow to maintain equilibrium order down to about 350°C. Measurements were taken up to 600°C; at this temperature oxidation was negligible. All specimens were 'wiped clear' before use by means of a vacuum anneal at 800°C followed by a quench into silicone oil. X-ray studies had

† Formally, a scattering potential arising from the distributional disorder of spins is concealed in P_A; at moderate temperatures the magnetic moment per iron atom is almost independent of order, and there is therefore no point in trying to separate out the concealed term, which will be a constant fraction of P_A.

shown that this treatment expunges any effects caused by preceding heat-treatments.

To achieve different states of order, each specimen was first heated to 670°C in air and brine quenched, and its resistance measured at 293°K and 77°K. The specimen was then reheated to 650°C, quenched and remeasured. Successive equilibrations were carried out at temperature intervals of about 20°C; the times required to equilibrate the specimen at each temperature were estimated from kinetic data (Feder and Cahn 1960) and from X-ray kinetic studies (Lawley *et al.* 1960).

Fig. 2

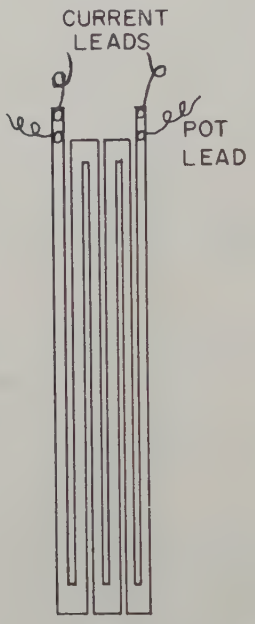

Form of resistance specimens.

The resistance was measured by the double potentiometer method, using a standard resistor in series with the specimen; a reversible circuit was used to correct for spurious e.m.f.'s of thermoelectric origins. No attempt was made to express results in terms of absolute resistivities, in view of the complex shape of the specimens.

§ 4. Experimental Results

In fig. 1 the equilibrium ρ versus T curves for the two alloys are reproduced. The influence of various thermal pretreatments in producing deviations from this curve was also studied and will be reported separately.

In fig. 3 are plotted the results of resistance measurements at 293°K and 77°K of specimens quenched from successively lower temperatures. For comparison, the graph also shows the resistance of the same alloys *at* the temperatures from which they were quenched.

The dashed curves in fig. 3 refer to repeat measurements on the same specimens, made after a preliminary 40-hour anneal at 530°C. This was intended to find whether the initial state of order, which had been found to affect ordering kinetics (Feder and Cahn 1960) also affected the *equilibrium* value of the resistance. The asymptotic final values of resistance found in Feder and Cahn's isothermal anneals by experiments are also included in fig. 3 and it will be seen that these fell on, or close to, the corresponding curves.

Fig. 3

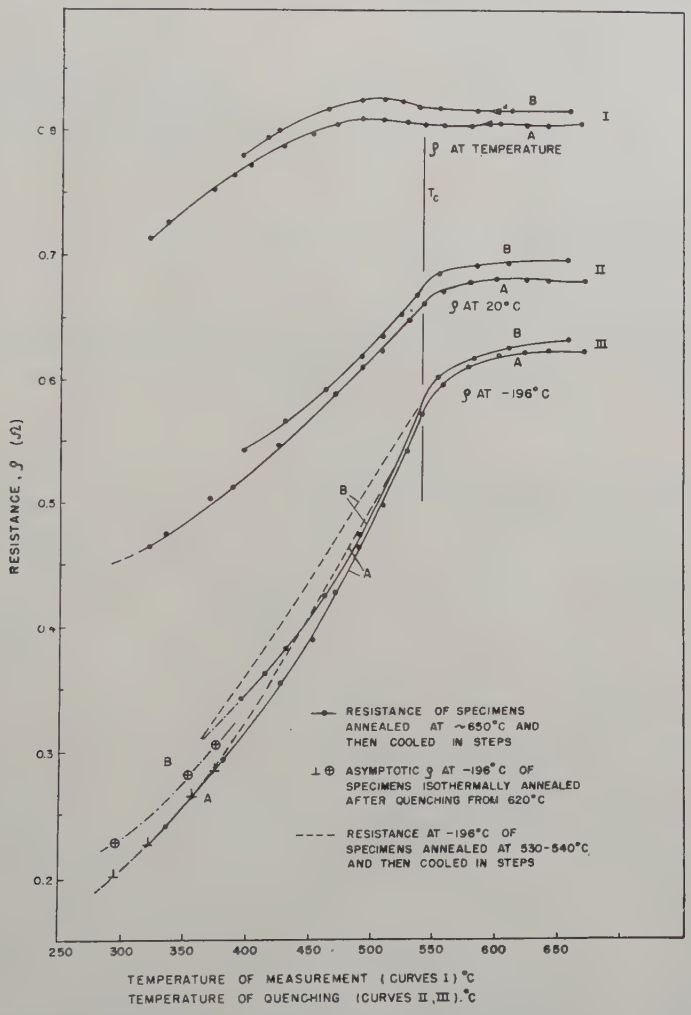

Resistance at temperature, and at 293°K and 77°K, of alloys A (24·8 at. % aluminium) and B (25·5 at. % aluminium), quenched from successively lower temperatures. Asymptotic resistance values from isothermal annealing experiments are included for comparison.

Fig. 4

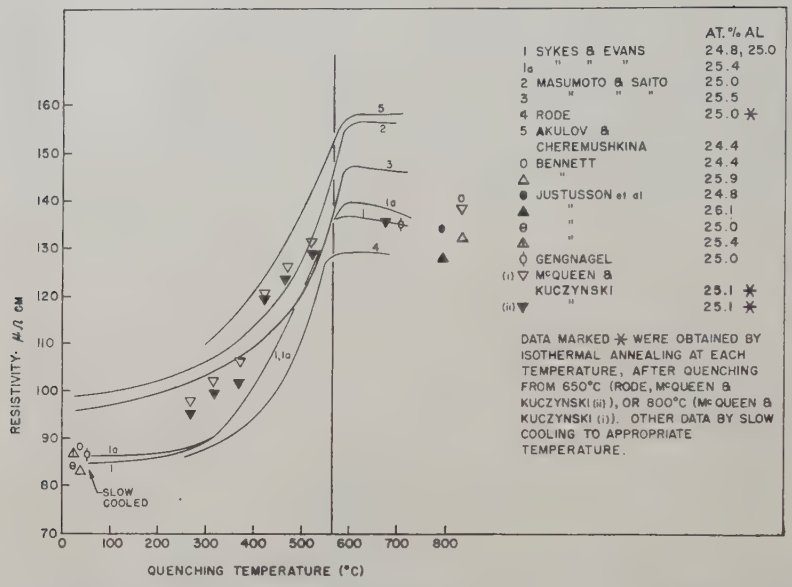

Published data on room temperature resistivity of Fe_3Al quenched from different temperatures. Exact alloy composition is listed for each set of data.

Fig. 5

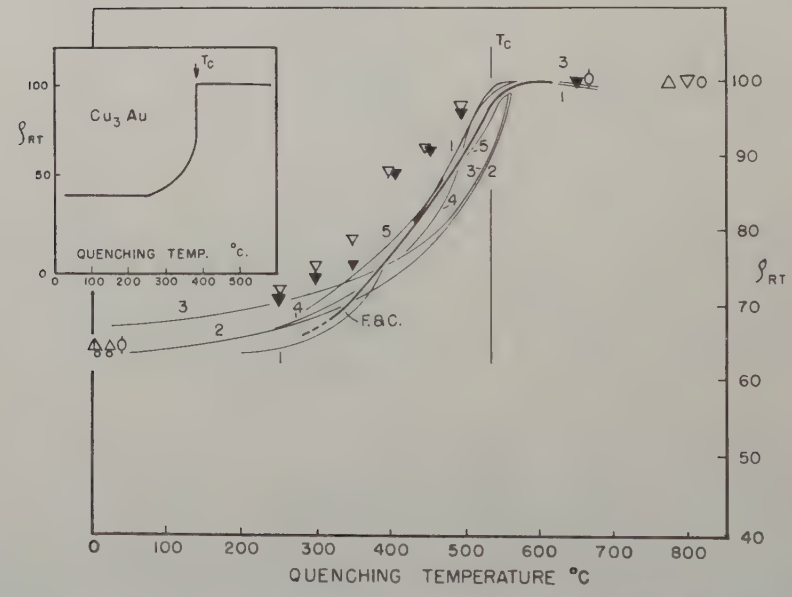

Data of fig. 4, normalized at 600°c. Inset : Data for Cu_3Au after Wright and Thomas (1958).

For comparison with these data, other published data on the room temperature resistivities are shown in fig. 4. The corresponding references will be found at the end of the paper. These data have been replotted in fig. 5, together with the present results, after normalizing the resistivity of all alloys at 600°c. Except for the recent isothermal data of McQueen and Kuczynski (1959) and those of Masumoto and Saito (1957), the various normalized plots are in fair agreement. Our own results agree best with Sykes and Evans' (1935) classical data.

A curve for Cu_3Au (Wright and Thomas 1958) has been included in fig. 5 to emphasize the difference between this alloy, in which there is a brusque discontinuity of order at T_c, and Fe_3Al, in which order appears gradually.

§ 5. Interpretation of Results

In fig. 6, the data for the 24·8 at. % alloy are replotted in a different form. Straight-line extrapolation was used to obtain estimated residual restivities

Fig. 6

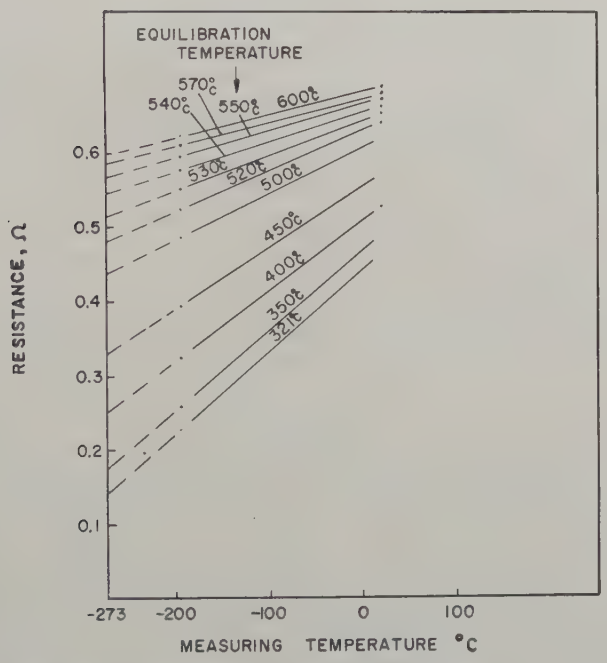

Resistance of alloy containing 24·8 at. % aluminium, quenched from different temperatures, and measured at 77°K and 293°K.

ρ_0^{QT}: for the degree of reliability of the proposed analysis, this form of extrapolation was considered adequate. From this plot values of the mean temperature coefficients of resistance were also obtained.

According to eqns. (2) and (4),

$$F_T^{QT} \propto \left(\frac{d\rho}{dT}\right)^{QT} \quad \text{and} \quad F_T^{QT} . P_A^{QT} \approx \rho_0^{QT}$$

Hence,

$$P_A{}^{QT} \propto \left\{ \rho_0{}^T \Big/ \left(\frac{d\rho}{dT} \right)^{QT} \right\},$$

Plots of these three quantities against quenching temperature are shown in fig. 7. Corresponding plots for the other alloy are very similar.

Fig. 7

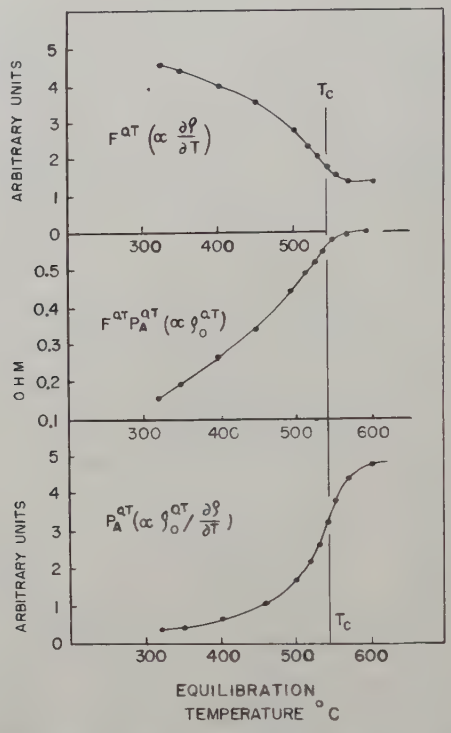

Resistivity parameters F^{QT}, (F^{QT} . $P_A{}^{QT}$) and $P_A{}^{QT}$ (alloy containing 24·8 at. % aluminium) as function of quenching temperature.

The implication of these curves is that the decrease of resistance of quenched alloys with increasing order takes place *in spite of* a decreased freedom of conduction electrons, since F increases by a factor of almost 4. This increase in F is overcompensated by the very sharp decrease of P_A as atomic order builds up.

This is exactly what Coles (1958) has proposed for the case of Cu_3Au. The postulated increase of F when Cu_3Au orders, which is supported by the observed change of the Hall coefficient, is explained by the creation of new Brillouin zones corresponding to the superlattice (Slater 1951), as a result of which the Fermi level is brought closer to a plane of energy discontinuity and the electron mobility correspondingly diminished. Coles reports that preliminary experimental results on Cu_3Au show F to increase by a factor

of nearly 2 on ordering. Fe_3Al has the advantages over Cu_3Au, as an experimental material, that all degrees of order can be obtained, and that the thermal perturbations hardly depend on order; however, Cu_3Au is free of the complications arising from spin disorder, and lends itself better to an interpretation of the results in terms of Brillouin zones.

In fig. 7, the slight variation of F^{QT} and $\rho_0{}^{QT}$, and rather greater variation of $P_A{}^{QT}$, for quenching temperatures *above* T_c, is due partly to the finite rate of quenching which allows some increase of order during the quench, and partly to a very imperfect type of order which persists in the range 540–740°c (Taylor and Jones 1958, McQueen and Kuczynski 1959). This order however is so slight that it has little influence on physical properties, and is here ignored.

Note that, as the quenching temperature diminishes, P_A appears to approach asymptotically a value distinctly above zero. This implies that order never becomes perfect. This indeed is the conclusion from x-ray data (Lawley *et al.* 1960) and also from neutron diffraction (Nathans *et al.* 1958). The maximum value of the Bragg–Williams order parameter S appears to be roughly 0·8. Because of the experimental uncertainties in the experimental x-ray determination of S as a function of temperature, and the complication arising from slight order above T_c, no useful purpose would be served by seeking an exact correlation of S with P_A and F. Very roughly, P_A and F appear to be linear functions of S. ρ_0 and S^2 approximate to a linear relationship, as required by Muto's (1936) theory.

5.1. *Analysis of Resistance–Temperature Curves*

The present experiments have established that the slight humps in the ρ/T curves just below T_c are not due to the presence of small antiphase domains of order, as had been proposed by Bennett (1952). The following reasons can be adduced:

Exactly the same ρ/T curve was traced out on heating and cooling, starting with initially ordered and initially disordered alloy, respectively.

The plot of room temperature resistance as a function of quenching temperature exhibits no hump (fig. 3). Yet data on Cu_3Au (Burns and Quimby 1955, Wright and Thomas 1958) show that such a plot should possess a slight hump if small domains are present. (Such a hump is, however, restricted to quenching temperatures very close to T_c.)

X-ray studies (Lawley *et al.* 1960) show that slowly cooled Fe_3Al has a large domain size.

Some other interpretation of the form of the curves near T_c is therefore required, and this can be attempted by making use of the values of P_A and F which have been determined for various states of order. However, the complications of estimating the high-temperature resistance are such that only a semi-quantitative treatment is possible.

At a particular temperature T, the resistance is expressed by

$$\rho^T = F'^T(P_A{}^T + P_S{}^T + P_T{}^T). \quad . \quad . \quad . \quad . \quad . \quad (5)$$

Here, the superfix T represents the value of the corresponding term *at* temperature T; $P_A{}^T$ is the atomic disorder scattering potential, which is purely configurational and can be taken direct from the graph of $P_A{}^{QT}$ as a function of equilibration temperature, fig. 7. The meaning of the dash in F'^T is explained below. The spin disorder scattering potential $P_S{}^T$ will be left aside for the moment. The thermal vibration scattering potential $P_T{}^T$ depends upon the mean square displacement of the vibrating atoms, and a quite general treatment (Mott and Jones 1936, p. 243) shows that at 'high' temperatures (i.e. near and above the Debye characteristic temperature), $\partial P_T/\partial T$ remains constant. For present purposes, therefore, $\partial P_T/\partial T$ is independent of temperature above 100°C.

The 'electrical freedom', F^{QT}, as plotted in fig. 7 for various equilibration temperatures, cannot be used direct in eqn. (5), because, *even for a fixed configuration of the alloy*, F must decrease with rise of temperature. This is a consequence of the quantum theory of the electrical resistance of transition metals (Mott and Jones 1936, p. 268). Much of the resistance arises from s–d and p–d scattering transitions. The transition probability, and F, depends on the number of energy states in the d band within an energy range of about kT at the Fermi surface. When the d band is nearly full, $N(E)$ is a steeply falling function of E and therefore the number of available states does not increase proportionately to T. The resistance of a pure transition metal therefore does not rise proportionately to T. In terms of the present formalism, this implies that for iron *or* for an iron alloy, the 'electronic freedom' F falls with rising temperature. We will reserve the symbol F for the configurationally determined value, determined from measurements at 20°C and 196°C of a quenched alloy as plotted in fig. 7. The true value, at any higher temperature, will be termed F' and is lower than F for the same state of order.

In fig. 8, curve 1 represents the observed ρ^T versus T data for the 24·8 at. % alloy. Curve 2 represents the predicted resistance, omitting the spin disorder term and using the configurational (temperature-invariant) values of F^{QT}. This curve has been computed from the data of fig. 6 by simply extrapolating each line to the corresponding temperature†. It was then arbitrarily assumed that over the limited temperature range 300–600°C, $(F-F')$ for a given configuration varies proportionately to absolute temperature and that $F'/F=\frac{2}{3}$ at 600°C. In spite of the arbitrariness of this correction, the corrected curve, 3, is expected to give the right general form of the configurational and thermal terms in the resistance.

The difference between this computed curve and the observed curve corresponds to the spin disorder term $F'P_S$. P_S will presumably rise increasingly rapidly with temperature as the temperature approaches the Curie point θ_c (except for a short plateau near T_c on which the spontaneous

† This simple extrapolation procedure is justified since $F^T=F^{QT}$ and is *ex hypothesi* independent of temperature for a given state of order, and $\partial P_T/\partial T$, which together with F_T determines the slope of the lines of fig. 6, is also approximately independent of temperature.

magnetization is almost constant with temperature†). This is borne out by the curve 4 of fig. 8, which represents the difference ($\approx F'P_S$) between curves 1 and 3, and by curve 5, in which P_S (derived from curve 4) is plotted against T. The general shape of curves 4 and 5, which will not depend sensitively on the exact value of the correction factors F'/F used to construct curve 3, is similar to that of the plot of spontaneous magnetization against temperature.

Fig. 8

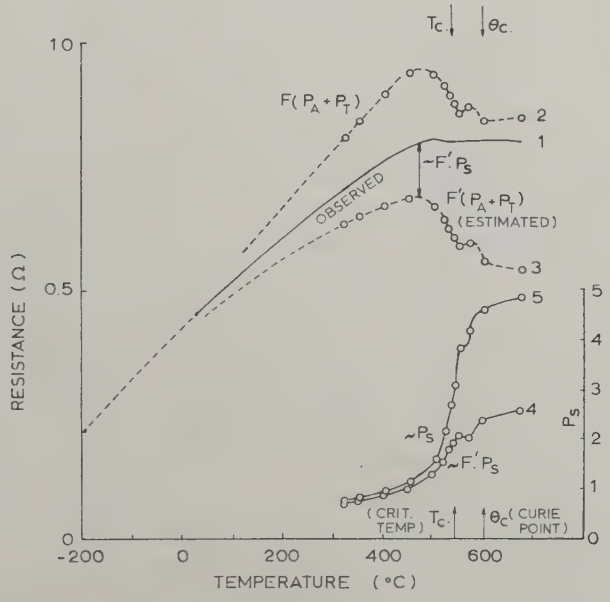

Observed and computed high-temperature resistivity values for alloy containing 24·8 at. % aluminium.

The foregoing analysis, in spite of the inevitable assumptions and approximations, is adequate for interpreting the general shape of the observed ρ^T versus T curve, and in particular the slight hump and the level part of the curve. In fact, if it were not for the counteracting influence of the spin disorder term, there would be a much more pronounced hump, as in curve 3. The hump, then, is due to the effect of atomic ordering on the various terms that determine the electrical resistance.

§ 6. Discussion and Conclusions

The present experimental data have some bearing on the proposal advanced by Haworth (1938) that, in alloys not readily amenable to study by x-ray diffraction, the thermal coefficient of resistivity α might be taken

† This plateau is deduced from magnetic data by Crangle (private communication) and Ivanovsky and Denisov (1957).

as a criterion of the existence of order. If suitable heat treatment causes a substantial increase in this coefficient, then this, it was argued, should be regarded as evidence of order, and various known alloys were adduced in evidence. On this criterion, Ni_3Fe was at that time stated to be incapable of ordering, since α *decreases* slightly on slow cooling. Yet it is known by evidence from x-ray (Wakelin and Yates 1953) and neutron diffraction (Lyaschenko *et al.* 1957) that this alloy can in fact acquire long range order. The present analysis shows that the decrease in α may be due to a reduction in $\partial P_T/\partial T$ resulting from an altered Debye temperature, or from a fall in $\partial P_S/\partial T$ due to an altered Curie temperature, and these may outweigh any change in F that occurs. Evidently, α is not a good criterion; a decrease of the residual resistivity ρ_0 is a much safer criterion for the presence of atomic order, since this depends on P_A, which is highly sensitive to the state of order. Even here, however, a large increase of F due to ordering might lead to mistaken conclusions.

It should be possible to apply the present analysis to some other alloys which show interesting resistance anomalies. A promising candidate is the alloy U_2Mo. This is based on the body-centred cubic γ-uranium lattice, with partial long range-order of the C 11b ($MoSi_2$) type. The degree of order depends on temperature. The resistivity is almost constant over a wide range of temperature (Bostrom and Halteman 1957), and the low-temperature ρ/T curves of an alloy of somewhat different composition, quenched from various temperatures (Loasby 1959), bear a marked resemblance to the data of our fig. 2. If measurements of this type could be correlated with high temperature measurements on the stoichiometric alloy, interesting conclusions might emerge as to the electronic structure of metallic uranium.

In résumé, we list the conclusions of the present study:

(1) As the alloy Fe_3Al is progressively ordered, the freedom of conduction electrons (F) decreases considerably, but the reduction of the electron scattering (P_A) associated with atomic disorder is more than enough to compensate for this; in consequence, the residual resistivity falls sharply with increasing order.

(2) The slight maximum in resistance at about 500°C in the resistance–temperature curve of Fe_3Al has been rationalized without recourse to the discredited notion that antiphase domain boundaries are implicated. An analysis based on Coles' theory of resistivity of iron alloys, in conjunction with present experimental results on quenched alloys, shows that the maximum is due to the way in which F and P_A change with order. Moreover, the form of the entire resistance–temperature curve has been satisfactorily interpreted.

The fact that this interpretation proved feasible can be taken as presumptive evidence in favour of Mott and Stevens' model of the electronic structure of body-centred cubic iron.

Acknowledgments

We are grateful to Professor G. V. Raynor, F.R.S., for his support and the provision of laboratory facilities. Thanks are due to Professor J. D. Fast of Eindhoven, who kindly arranged the casting of one of the alloys, and the British Iron and Steel Research Association who presented specially pure iron for casting the other. We are much indebted to Dr. B. R. Coles, Professor G. V. Raynor, Professor A. D. McQuillan and Dr. J. Friedel for their comments on the paper. One of us (R. F.) is indebted to the Secretary of the U.S. Army for a Fellowship.

References

Akulov, N. S., and Cheremushkina, A. V., 1955, *C.R. Acad. Sci. U.R.S.S.*, **102,** 45.
Batterman, B. V., 1959, *J. appl. Phys.*, **30,** 508.
Bennett, W. D., 1952, *J. Iron St. Inst.*, **171,** 372.
Bostrom, W. A., and Halteman, E. K., 1957, *Proc. 2nd Nuclear Engineering and Science Conference*, (ASME).
Bradley, A. K., and Jay, A. H., 1932, *Proc. roy. Soc.* A, **136,** 210.
Burns, F. P., and Quimby, S. L., 1955, *Phys. Rev.*, **97,** 1597.
Coles, B. R., 1958, *Advanc. Phys.*, **7,** 40.
Feder, R., and Cahn, R. W., 1960, *Phil. Mag.*, **5,** 343.
Gengnagel, W., 1958, *Naturwissenschaften*, **45,** 81.
Haworth, F. E., 1938, *Phys. Rev.*, **54,** 693.
Ivanovsky, V. I., and Denisov, P. P., 1957, *Fizika Metallov i Metallovedenie*, **4,** 550.
Justusson, W., Zackay, V. F., and Morgan, E. R., 1957, *Trans. Amer. Soc. Metals*, **49,** 905.
Lawley, A., Davies, R. G., and Cahn, R. W., 1960 (submitted to *Acta Met.*).
Loasby, R. G., 1959, *Proc. phys. Soc. Lond.*, **72,** 470.
Lord, N. W., 1953, *J. chem. Phys.*, **21,** 692.
Lyaschenko, B. G., Litvin, D. F., Puzey, I. M., and Abov, U. G., 1957, *Kristallografiya*, **2,** 64.
Masumoto, H., and Saito, H., 1952, *Sci. Rep. Res. Inst. Tohoku Univ.* A, **4,** 321 ; 1957, *Ibid.* A, **9,** 338.
McQueen, H. J., and Kuczynski, G. C., 1959, *Trans. Met. Soc. Amer. Inst. min. (metall.) Engrs*, **215,** 619.
Mott, N. F., and Jones, H., 1936, *The Theory of the Properties of Metals and Alloys* (Oxford : University Press).
Mott, N. F., and Stevens, K. W. H., 1957, *Phil. Mag.*, **2,** 1364.
Muto, T., 1936, *Sci. Pap. Inst. phys. chem. Res. Tokyo*, **30,** 99.
Nathans, R., Piggott, M. T., and Shull, C. G., 1958, *J. Phys. Chem. Solids*, **6,** 38.
Nemnonov, S. A., and Finkel'shtein, L. D., 1959, *Fizika Metallov i Metallovedenie*, **7,** 944.
Rode, V. E., 1957, *Bull. Acad. Sci. U.S.S.R., Phys. Ser.*, **21,** 1234.
Slater, J. C., 1951, *Phys. Rev.*, **84,** 179.
Sykes, C., and Evans, H., 1935, *J. Iron St. Inst.*, **131,** 225.
Taylor, A., and Jones, R. M., 1958, *J. Phys. Chem. Solids*, **6,** 16.
Wakelin, R. J., and Yates, E. L., 1953, *Proc. phys. Soc. Lond.* B, **66,** 221.
Weiss, R. J., and de Marco, J. J., 1958, *Rev. mod. Phys.*, **30,** 59.
Weiss, R. J., and Freeman, A. J., 1959, *J. Phys. Chem. Solids*, **10,** 147.
Wright, P., and Thomas, K., 1958, *Brit. J. appl. Phys.*, **9,** 330.
Yamamoto, M., and Taniguchi, S., 1956, *Sci. Rep. Res. Inst. Tohoku Univ.* A, **8,** 193.

Nuclear Magnetic Resonance in Lithium and Dilute Lithium–Magnesium Alloys†

By D. G. Hughes‡
Division of Pure Physics, National Research Council, Ottawa

[Received December 12, 1959]

Abstract

The Knight shift and line-width of the ^{7}Li resonance in dilute Li–Mg alloys has been investigated. The observed rapid fall in Knight shift with alloying concentration is interpreted using Drain's theory. Linewidth measurements show that the activation energy of self-diffusion of the ^{7}Li atoms increases from $13{\cdot}1 \pm 0{\cdot}2$ kcal/mole for pure lithium to $14{\cdot}5 \pm 0{\cdot}3$ kcal/mole for the 10 at. % magnesium alloy.

§ 1. Knight Shift Measurements

A study has been made of the ^{7}Li nuclear magnetic resonance signal in lithium and some dilute lithium–magnesium alloys (up to 10 at. % Mg). The experiments were carried out using a marginal-oscillator spectrometer and a fixed magnetic field of 6750 gauss.

Figure 1 shows the observed variation of Knight shift with alloying concentration. All these Knight shift measurements were taken at about 75°C where the nuclear dipole–dipole contributions to line-widths are negligible because of rapid thermal diffusion of the lithium atoms (Gutowsky and McGarvey 1952). The line-widths of the 2·1%, 4·4% and 10% magnesium alloys and of pure (99·9%) lithium were approximately 100 c/s (0·06 gauss), determined mainly by magnetic field inhomogeneity and modulation frequency broadening (Cagnac *et al.* 1955). The narrow lines obtained from these samples indicate that no appreciable contamination had occurred and that the alloys were quite homogeneous. However, the 0·2% and 0·8% magnesium alloys showed line-widths of 240 c/s (0·15 gauss) and 190 c/s (0·12 gauss) respectively. The lines were nevertheless fairly symmetrical and it is felt that the line centres were not appreciably perturbed by the broadening. It may also be mentioned that our value for the Knight shift of pure lithium of $0{\cdot}0263 \pm 0{\cdot}0001\%$ is in agreement with the value of $0{\cdot}0261 \pm 0{\cdot}0002\%$ reported by Gutowsky and McGarvey (1952). There is however an unexplained discrepancy between the value reported here and Knight's value of 0·0249% (Knight 1956). (In our work and in Knight's measurements the Knight shift

† Communicated by the Author.
‡ National Research Council Postdoctorate Fellow.

was measured relative to an aqueous solution of LiCl.) The decrease in lattice parameter which occurs when magnesium is introduced into lithium (Levinson 1955) is expected to have an explicit effect on the Knight shift (Benedek and Kushida 1958) but this is negligible compared to the magnitudes involved here. It can be concluded from the results that the Knight shift falls almost linearly with increasing concentration of magnesium.

Fig. 1

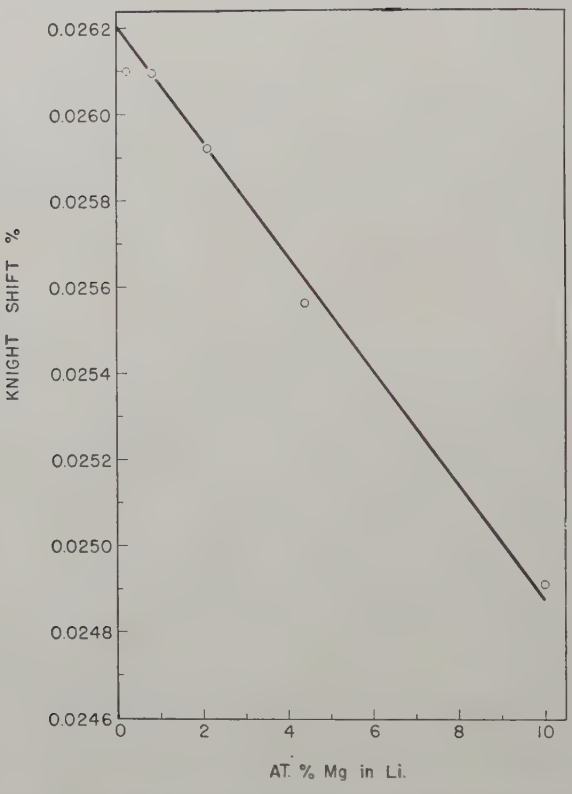

Variation of the ^{7}Li Knight shift with alloying concentration for the Li–Mg system.

It is interesting to compare the present results with those obtained by Drain (1959) for the silver–cadmium system: in both cases the introduction of a divalent metal reduces the Knight shift of a monovalent metal. Moreover, the theory given by Drain is relevant to the present system. In his theory Drain relates the density of states $N(\zeta)$ of an alloy to the density of states, $N_A(\zeta)$ and $N_B(\zeta)$, of the pure constituents by the following formula:

$$N(\zeta)=(1-c)\frac{N_A(\zeta)(\Delta H/H)_A}{(\Delta H/H)_{AA}}+c\frac{N_B(\zeta)(\Delta H/H)_B}{(\Delta H/H)_{BB}}.$$

Here c is the atomic concentration of constituent B in A, $(\Delta H/H)_{AA}$ and $(\Delta H/H)_{BB}$ are the Knight shifts in the pure metals, and $(\Delta H/H)_A$ and $(\Delta H/H)_B$ are the Knight shifts of the A and B nuclei in the alloy. In the present case:

$(\Delta H/H)_{AA} = 0{\cdot}0263\%$ for pure lithium,
$(\Delta H/H)_{BB} = 0{\cdot}28\%$ for pure magnesium (predicted value, see Knight 1956),
$N_A(\zeta) = 0{\cdot}37$ levels/atom ev (from specific heat data, Roberts 1957) for pure lithium†, and
$N_B(\zeta) = 0{\cdot}29$ levels/atom ev (from specific heat data, Estermann *et al.* 1952) for pure magnesium.

However, $(\Delta H/H)_B$ (the Knight shift of magnesium in small quantities in lithium) has not been measured and may well be difficult to measure since ^{25}Mg, the only stable magnesium isotope with non-zero nuclear spin, is only about 10% abundant and its spin number of $\frac{5}{2}$ is expected to give rise to serious quadrupole broadening. We therefore make some estimate of this quantity. If we assume an unusually high value of 0·56% for $(\Delta H/H)_B$, then $N(\zeta) = 0{\cdot}37$ levels/atom ev for the 10 at. % Mg alloy, i.e. the density of states in this alloy is the same as in pure lithium. If however we assume that $(\Delta H/H)_B = 0{\cdot}28\%$ (the same as in pure magnesium) then $N(\zeta) = 0{\cdot}34$ levels/atom ev and the density of states has fallen by nearly 10%. This means that unless the Knight shift of magnesium in lithium is greater than about 0·56% (which we feel is rather unlikely), Drain's theory suggests a fall in the density of states with increasing electron/atom ratio.

Such a fall is consistent with the predictions of the rigid band model (for references see Cohen and Heine 1958) assuming contact of the Fermi surface with the first Brillouin zone. If instead of accepting the rigid band model, we apply the ideas of Cohen and Heine (1958) then we find that the introduction of magnesium into lithium is expected to reduce the distortion of the Fermi surface. Any such ' sphericalizing ' of the Fermi surface will reduce contact, *increase* the density of states and make the conduction electron wave functions more *s*-like in character. But we have already seen that the present results when interpreted on the basis of Drain's assumptions indicate that the density of states if anything *decreases* on alloying. This is therefore not in accord with Cohen and Heine's theory and it would seem that the rigid band model is adequate to explain the results reported here. It must however be emphasized that the conclusions drawn are highly tentative in view of the lack of direct experimental evidence on the Knight shift of ^{25}Mg in both magnesium and lithium.

---

† There is some uncertainty in this value due to the martensitic transformation which occurs in lithium at low temperatures. However, this uncertainty is not expected to exceed about 10% (Dugdale and Gugan 1960).

§ 2. Line-width Measurements

The ^{7}Li line-width has been investigated for various Li–Mg alloys (up to 10 at. % Mg) between room temperature and 200°c. No evidence of any appreciable quadrupolar broadening was found. The dipolar broadening observed above room temperature in these alloys suggested that the activation energy of self-diffusion of the lithium atoms increases with increasing concentration of magnesium. Measurements of the ^{7}Li line-width have thus been made on pure lithium and a 10 at. % Mg alloy in the temperature range where line narrowing by self-diffusion occurs. Figure 2 shows these line-width data. The rigid lattice value of the line-width of about 10·3 kc/s (6·2 gauss) for pure lithium and about 9·8 kc/s (5·9 gauss) for the 10% alloy can be explained on the basis of nuclear dipole–dipole interactions alone.

Fig. 2

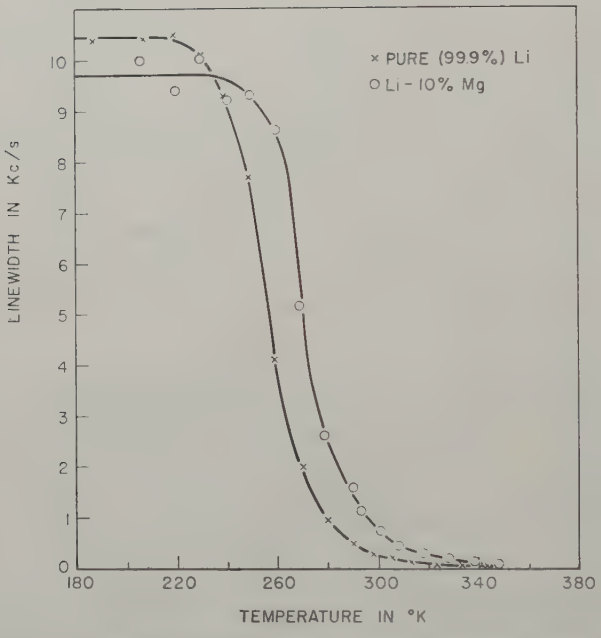

Variation of the ^{7}Li line-width with temperature for pure Li and Li–10% Mg.

From the line-width data, the activation energy of self-diffusion for ^{7}Li nuclei was calculated for both samples using the method given by Holcolm and Norberg (1955). From the region where the line-width shows an exponential dependence on temperature the following activation energies were determined: for pure lithium: $13{\cdot}1 \pm 0{\cdot}2$ kcal/mole; for the 10 at. % Mg alloy: $14{\cdot}5 \pm 0{\cdot}3$ kcal/mole. The error limits are estimated from the experimental scatter observed in the plots. The former value is in agreement with the value for pure lithium obtained by Holcolm and Norberg (1955) using pulse techniques.

The observed increase in activation energy is consistent with a picture of the alloy as more closely packed than pure lithium. Despite the larger size of the magnesium atom and ion the lattice parameter decreases with increasing magnesium concentration (Levinson 1955). Again, the van Liempt relation (van Liempt 1935), which might be expected to hold for a dilute alloy, predicts an increase in the activation energy of self-diffusion of the lithium atoms since the melting point (solidus and liquidus curves) rises with increasing concentration of magnesium.

In conclusion it may be mentioned that no line broadening arising from a dependence of Knight shift on nuclear environment has been observed for the Li–Mg system. This is in contrast to Drain's results on Ag–Cd alloys. However, such a broadening would not be expected at high temperatures due to rapid thermal diffusion and at low temperatures it is probably too small in the case of the Li–Mg alloys to be seen against the nuclear dipole–dipole broadening. The anomalous line broadening (referred to earlier) found in the 0·2% and 0·8% alloys is virtually temperature independent even in the liquid state. Its temperature independence rules out quadrupolar interactions and the type of broadening observed by Drain. It may however be related to the unexplained broadening observed in lithium samples by Holcolm and Norberg (1955). Further experiments are in progress to determine whether the effect is genuine or whether it is caused by simple contamination.

Acknowledgments

I wish to thank Dr. J. S. Dugdale and Dr. D. K. C. MacDonald for their interest and stimulating discussions, and Dr. Drain for correspondence.

I am also indebted to the National Research Council for the award of a Postdoctorate Fellowship.

References

Benedek, G. B., and Kushida, T., 1958, *J. Phys. Chem. Solids*, **5**, 241.

Cagnac, B., Manus, C., Béné, G., and Extermann, R., 1955, *Helv. Phys. Acta.*, **28**, 626.

Cohen, M. H., and Heine, V., 1958, *Advanc. Phys.*, **7**, 395.

Drain, L. E., 1959, *Phil. Mag.*, **4**, 484.

Dugdale, J. S., and Gugan, D., 1960 (to be published).

Estermann, I., Friedberg, S. A., and Goldman, J. E., 1952, *Phys. Rev.*, **87**, 582.

Gutowsky, H. S., and McGarvey, B. R., 1952, *J. chem. Phys.*, **20**, 1472.

Holcolm, D. F., and Norberg, R. E., 1955, *Phys. Rev.*, **98**, 1074.

Knight, W. D., 1956, *Solid State Physics*, Vol. 2 (New York: Academic Press Inc.).

Levinson, D. W., 1955, *Acta Met.*, **3**, 294.

Roberts, L. M., 1957, *Proc. phys. Soc. Lond.* B, **70**, 744.

van Liempt, J., 1935, *Z. Phys.*, **96**, 534.

On the Growth of Cadmium Crystals from the Vapour†

By P. B. Price‡
H. H. Wills Physical Laboratory, University of Bristol

[Received February 18, 1960]

Abstract

Crystals of cadmium were grown from the vapour on a quartz fibre in an argon diffusion cell designed so that the temperature, T, could be measured and the supersaturation, σ, calculated at every point. A critical σ of $\sim 0{\cdot}4$ for nucleation was observed below which no crystals grew and above which the density of crystals increased with σ. For $\sigma \lesssim 2$, crystals grew as whiskers and thin platelets independently of σ and T; for $2 \lesssim \sigma \lesssim 10^2$ the end products were thick hexagonal plates; for $\sigma \gtrsim 10^2$ and $T \lesssim 250°$C spike and leaf dendrites appeared and grew to large dimensions. The observed dependence of whisker growth rates on σ and whisker radius showed that growth was probably controlled by the diffusion of cadmium vapour through argon. Evidence for both tip growth and non-tip growth of whiskers is presented.

§ 1. Introduction

At the present time a great deal of effort is being directed to studies of the unusual properties of single crystal whiskers of various materials (Doremus *et al.* 1958). However, with the exceptions of the work of Gomer (1958) on mercury whiskers and the work of Price *et al.* (1958) on electro-deposited silver whiskers, very little experimental work is being devoted to studies of the growth of whiskers under carefully controlled conditions. Because of the interesting results which studies of the mechanical properties of vapour-grown zinc and cadmium whiskers have yielded (Cabrera and Price 1958, Coleman *et al.* 1957), it was felt that a careful investigation of the kinetics of growth of these whiskers would be worthwhile.

This paper describes the results of a study of the growth rates and habits of whiskers and other small crystals of cadmium which were grown from the vapour in an atmosphere of argon under the simplest possible conditions, in which all the variables were fixed except the temperature, which was measured, and the supersaturation, which was calculated. The crystals were grown and observed in a closed cell in which convection was eliminated and the impurity content was very low. The geometry of the cell was such that the isothermals were plane, horizontal surfaces and the temperature varied linearly from top to bottom. The supersaturation was then a function of the temperatures of the top and bottom and of vertical position in the cell. The crystals grew on a quartz fibre so thin that cadmium atoms were removed from the diffusing vapour at a very low rate. As long as the density of crystals on the fibre was low, each crystal could be

† Communicated by J. W. Mitchell, F.R.S.

‡ Fulbright Fellow, 1958–59. Present address: Cavendish Laboratory, University of Cambridge.

considered to act as an independent sink for the cadmium, which simplified the analysis of the observed growth rates.

A study of this nature is of importance because of the lack of quantitative information on the kinetics of crystal growth when diffusion of the material through a gas is the rate-controlling process. The main interest in diffusion-controlled growth in the past has been in the radical habit changes undergone by ice crystals falling through air at different temperatures. Reynolds (1952) and Mason (1953) have made rough measurements of rates of mass increase of ice crystals falling through a supercooled water cloud, but individual crystals were not followed during growth, so that there was considerable scatter in their data. Hallett and Mason (1958) have designed a diffusion cloud chamber in which the temperature and supersaturation can be controlled during the growth of ice crystals but, being interested mainly in crystal habit, they have not made growth rate measurements.

The cadmium vapour–argon system seems to be ideally suited for studies of growth rates and crystal habit. Both gases are monatomic, which simplifies the analysis, and cadmium has a high triple point pressure ($\sim 10^{-1}$ mm), does not react with glass, and is a stable solid at room temperature, so that crystals can be studied microscopically after growth.

§ 2. Experimental Details

2.1. *The Diffusion Cell*

The growth cell, shown in fig. 1, was designed to facilitate the interpretation of the results. Two Pyrex discs were sealed to the ends of a Pyrex cylinder 7 cm in diameter and 3·5 cm in length. Then a portion of the curved cell wall was ground away and replaced by an optically flat observation window about 3·5 cm by 3 cm. To the bottom of the cell was attached a small Pyrex tube containing a thin quartz fibre ending in a quartz sheath. An iron slug was sealed into the sheath so that the fibre could be raised to various positions along the axis of the cell by means of a small, d.c.-operated solenoid.

The top and bottom surfaces of the cell were maintained at fixed temperatures by pairs of aluminium discs heated internally by soldering iron elements. Temperature measurement to about 1 °C was achieved with the use of two low heat capacity chromel–alumel thermocouples passing through small holes in the discs and making contact with the glass surfaces. The sides of the cell were also heated by a widely spaced wire coil wound on a cylindrical Pyrex frame which just fitted over the cell. The front portion of this frame was optically flat, so that crystals could be viewed and photographed through the frame and cell during growth.

Temperature profiles along the axis of the cell were measured for various voltages on the disc and ' cage ' heaters by inserting a thermocouple into the cell through the tube which normally contained the fibre. These measurements were made in air; it was then assumed that the temperature distribution under the same conditions was the same when the cell was

filled with argon and cadmium and sealed off. By proper adjustment of the relative voltages on the heaters, the temperature could be made to decrease linearly from the top to the bottom of the cell with any gradient desired and with plane, horizontal isothermals except near the cell walls. To obtain a very steep gradient it was necessary to replace the bottom disc heater by a water-cooled copper block whose temperature was varied by varying the rate of flow of the water.

Fig. 1

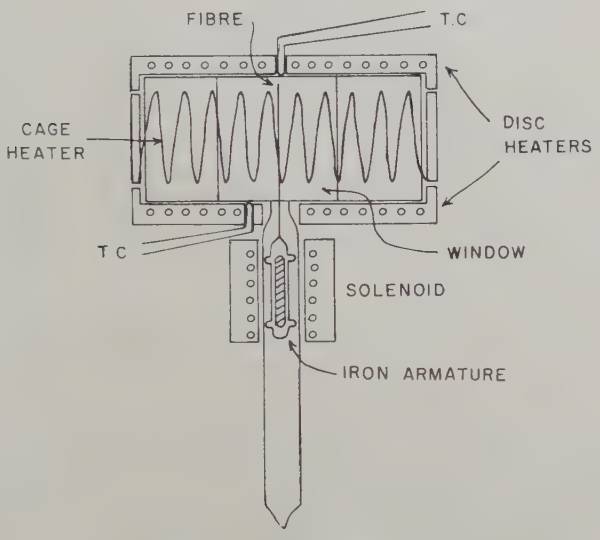

Diffusion cell for crystal growth.

A diffusion cell was prepared for crystal growth experiments by joining the small tube containing the fibre and iron slug through a constriction to a high vacuum system and to a three-stage distillation train containing high-purity cadmium (99·999%)†. The cell and connecting tubing were baked out at 500°C for 24 hours. The cadmium was then further purified by successive distillations and finally a small quantity was condensed into a layer on the top and a layer on the bottom of the cell. Then high-purity argon at a pressure of 600 mm of Hg at 20°C was introduced from a Pyrex flask by means of a break-seal arrangement and the cell sealed off.

2.2. *Experimental Procedure*

During an experiment cadmium vapour diffuses from the hot top surface through an atmosphere of argon along vertical flow lines to the bottom cooler surface. The presence of the argon, whose temperature varies linearly down the cell, causes the partial pressure and the temperature of the cadmium vapour also to vary linearly. A knowledge of the temperatures of the top and the bottom of the cell thus allows one to calculate the

† Kindly supplied by the Imperial Smelting Corporation Ltd.

supersaturation of cadmium vapour as a function of position in the cell. This is done in the Appendix.

Let us now consider the effect of raising a fibre into the cell. If the fibre is very thin, so that it removes cadmium atoms from the diffusing vapour at a very low rate, the flow lines of the vapour will not be appreciably affected by the few crystals which can grow on the fibre except in the immediate vicinity of a crystal. This means that the interaction between neighbouring crystals and the reduction in cadmium vapour pressure near the fibre can be neglected in calculations of the supersaturation. This is a tremendous advantage over the usual whisker growth arrangement (cf. Cabrera and Price 1958), in which vapour flows through a long tube, depositing on the walls in the form of crystals as it goes and gradually decreasing in pressure until it reaches the end of the tube.

Crystals were grown in a series of temperature gradients, with the top surface of the cell usually held at the melting point of cadmium, about 320°C. The crystals grew at various temperatures and at calculated supersaturations varying from about 10^{-1} to 10^{4}. In this paper the supersaturation is defined as $\sigma=(p-p_{\mathrm{eq}})/p_{\mathrm{eq}}$, where p and p_{eq} are the actual and equilibrium partial pressures of cadmium vapour.

The procedure was to allow the temperature distribution in the cell to reach a steady state, then to torch the tube containing the fibre in order to evaporate any cadmium which might have diffused down from the cell and to heat the fibre above the temperature of the cell, and then quickly to raise it into position in the cell by means of the solenoid. In this way the experiment was started with the vapour phase in the immediate vicinity of the fibre in a temporarily undersaturated condition. Without the preheating, the vapour near the cold fibre would have initially been in a highly supersaturated condition, making nucleation of crystals easier.

Crystals were observed and photographed at magnifications of $\times 12{\cdot}5$ and $\times 35$, both by reflected light and by transmitted light. A stereoscopic microscope was mounted as a cathetometer so that the position of a given crystal on the fibre could be determined to $\pm 0{\cdot}05$ mm. Growth rates were determined by measuring the dimensions of the crystals with a micrometer eyepiece as a function of time, the sensitivity being 1 division $= 2{\cdot}7$ microns at $\times 35$. Only those crystals were selected for measurements which were extending in directions nearly perpendicular to the axis of the microscope. The radii of thick whiskers were measured with the eyepiece; the radii of very thin whiskers were estimated to an accuracy of about $\pm 25\%$ by observing the amounts by which they sagged under their own weight.

§ 3. Observations

3.1. *Crystal Habit*

3.1.1. *Low supersaturations*

It is shown in the Appendix that the supersaturation varies from zero at the top of the cell, through a maximum value, $\sigma_{\max}$, at some point $z_{\max}$

along the axis, then back to zero at the bottom. It was experimentally observed that no deposition occurred when σ_{max} was less than about 0·4. As σ_{max} was increased above this critical value, the number of crystals increased from only one or a few, located near the calculated value of z_{max} on the fibre, to a very large quantity at high supersaturation. Once nucleated, crystals continued to increase in size, even if σ was reduced to values as low as 0·12. This suggests that there is a large free energy barrier to nucleation but only a small one to the continued growth of these crystals.

At low supersaturations ($\sigma \lesssim 2$) the predominant habits were found to be whiskers and thin platelets. Figure 2† shows a typical group of crystals after 75 min of growth in a cell in which σ_{max} was $\sim 0{\cdot}95$. In the region included in the picture, the temperature, T, was decreasing downward from 295°C to 290°C and σ was increasing from 0·65 to 0·75.

Observations of many crystals which grew at low σ showed that there was no systematic variation of habit with either σ or T. The crystal habit seemed to be determined at a very early stage in the growth process, even before the crystal was observable in the microscope. This is suggested by fig. 3, which shows a random distribution of whiskers and platelets 5 min after the beginning of growth, when σ_{max} was $\sim 1{\cdot}4$.

3.1.2. *Intermediate supersaturations*

For $\sigma \gtrsim 2$ the density of crystals was rather high, and most of the whiskers and thin platelets eventually disappeared, both by growing into neighbouring crystals and by fairly rapid thickening. Under these conditions thick hexagonal plates occurred as end products. In fig. 4 ($\sigma_{max} \simeq 3$), for example, only one whisker is left after a period of growth of a few hours. Figure 5 shows the appearance of a fibre after one day of growth at $\sigma_{max} \simeq 8$.

3.1.3. *High supersaturations*

The higher the supersaturation the smaller was the average plate size, since the closely spaced crystals grew into each other and competed for cadmium atoms. When σ_{max} approached or exceeded about 10^2 and when T was less than ~ 250°C, a few large crystals with very interesting dendritic habits appeared in the deposit. Figure 6 shows a portion of a fibre at z_{max} when the bottom was water-cooled to produce a maximum supersaturation of ~ 110 at a temperature of ~ 180°C. Near the centre are four leaf-shaped crystals, only one of which is in focus, and toward the top of the picture are two polycrystalline, spike-shaped dendrites which, instead of having smooth sides as the whiskers do, are covered with overgrowth in the form of tiny hexagonal plates and irregular microscopic crystals. Figure 7 shows a cadmium 'snowflake', which also grew at high supersaturation. The morphology and growth mechanism of the leaf dendrites are discussed in detail in another paper (Price 1959).

† Figures 2 to 7 are shown as plates.

3.2. *Whisker Growth Rates*

Because of the absence of distinguishing marks on most of the whiskers, it was impossible to decide on the basis of observations where material was added to them during growth. It was occasionally observed, however,

Fig. 8

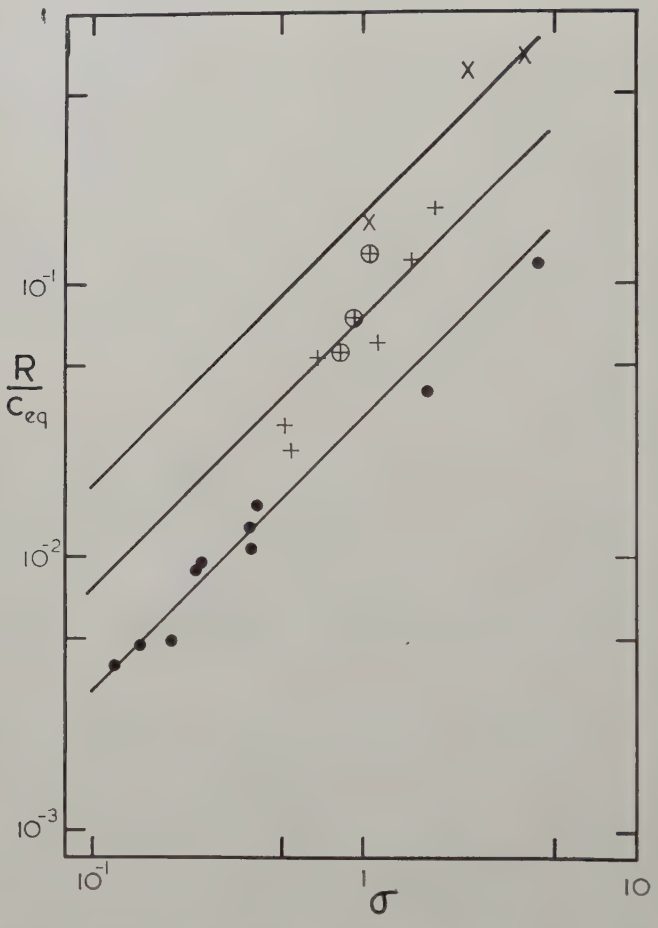

Growth rates of cadmium whiskers. Whisker radii are indicated by • for $r_w = 2\,\mu$, + for $r_w = 1\,\mu$, and × for $r_w = \frac{1}{2}\,\mu$. ⊕ denotes non-tip growth for whiskers with $r_w = 1\,\mu$. The units for R/c_{eq} are $\mu^4\,\mathrm{min}^{-1}$.

that two adjacent whiskers crossed each other during growth and formed a figure X whose acute angles were gradually filled in with cadmium. The fact that these joined whiskers continued to grow in length beyond the joint and that the sections below the joint remained straight was evidence

for tip growth. On the other hand, it was observed several times, particularly at rather high supersaturations ($\sigma \gtrsim 0{\cdot}8$), that a whisker would grow with a speck of cadmium at its tip. The speck remained the same size and stayed at the tip as the whisker lengthened. This seemed to indicate that material was not being added at the tip.

Some preliminary measurements were made of the axial growth rates of whiskers with no distinguishing marks and whiskers with observable specks at their tips, as a function of σ and whisker radius, r. Rates varied from a few tenths of a micron per minute to as much as 160 μ/min. The results are displayed in fig. 8, with $\log(R/c_{eq})$ plotted as a function of $\log\sigma$ and with individual points labelled according to the estimated values of r. R is the observed growth rate in μ/min, $c_{eq} = (p_{eq}\, kT)$ is the equilibrium density of cadmium vapour in atoms per μ^3, and r is in microns.

Fig. 9

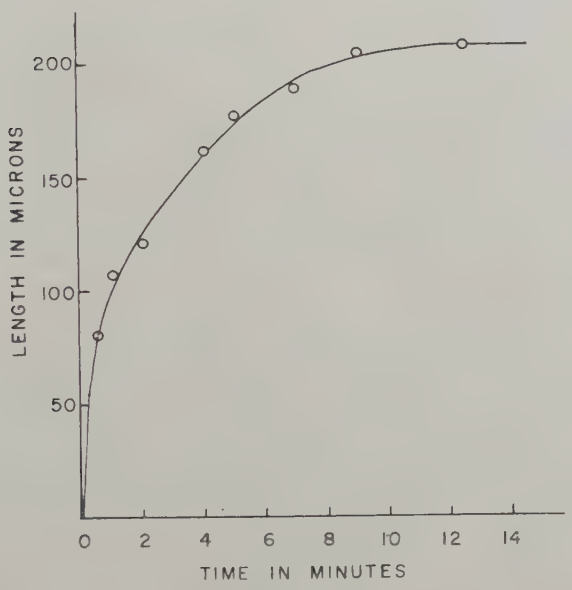

Growth rate curve of a whisker which thickens during growth at $\sigma \simeq 2{\cdot}4$.

Usually the curve of whisker length as a function of time was linear over the entire period of observation, and the whisker appeared to grow at constant radius. At high supersaturation, however ($\sigma \gtrsim 1$), a whisker was often observed to extend itself axially at a decreasing rate and radially at an increasing rate until the two rates were about the same. It then gradually grew into a bulk crystal. Figure 9 shows the change in axial growth rate for a typical whisker when σ was $\sim 2{\cdot}4$.

§ 4. Interpretation of the Results

4.1. *Crystal Habit*

The observation that whiskers and thin platelets are stable growth forms only when $\sigma \lesssim 2$ is very significant and is probably connected with the onset of surface nucleation. In fact, this is not an unreasonable value for the critical σ at which the rate of surface nucleation becomes appreciable.

This implies that at low supersaturation whiskers grow axially and thin platelets grow laterally by a dislocation mechanism. Subsequent thickening at higher supersaturation is then due to nucleation of new layers, probably where the crystal is attached to the substrate.

Since there seems to be no systematic variation of habit with either σ or T in the region of low supersaturation, and since it appears always to be determined at a submicroscopic stage of development, the dislocation configuration is probably introduced at or soon after nucleation and is responsible for the habit.

Cabrera and Price (1958) found that vapour-deposited cadmium whiskers generally grew in a $\langle 11\bar{2}0\rangle$ or a $\langle 11\bar{2}3\rangle$ direction, and that all cadmium platelets were basally oriented. It will be assumed that the crystals described above have the same orientations. Then it is proposed that a whisker develops from a nucleus containing a pure screw dislocation with a Burgers vector of $\frac{1}{3}\langle 11\bar{2}0\rangle$ or $\frac{1}{3}\langle 11\bar{2}3\rangle$ and that a platelet can develop when the nucleus has a system of one, two, or perhaps three $\langle 11\bar{2}0\rangle$ dislocations. Experiments on the plastic deformation of whiskers and platelets of zinc (Price 1960) confirm the existence of dislocations of both types.

4.2. *Whisker Growth Rates*

Although the measurements of axial growth rates of whiskers are only preliminary, it is possible from a study of fig. 8 to draw some general conclusions about the functional relationship between R, σ and r. It will be noticed that the points corresponding to whiskers of radii $\frac{1}{2}$, 1 and $2\,\mu$ fall into three groups which lie roughly along straight lines of unit slope. The equation

$$R = \frac{\alpha\sigma c_{\mathrm{eq}}}{r^{\beta}} \quad . \quad . \quad . \quad . \quad . \quad . \quad . \quad . \quad . \quad (1)$$

can therefore be used to describe the relationship empirically, with α and β adjustable constants. For the three lines drawn in fig. 8, which were chosen to give the best fit to the data, the relation is

$$R = \frac{0{\cdot}076\sigma c_{\mathrm{eq}}}{r^{1{\cdot}2}}\ \mu\,\mathrm{min}^{-1}. \quad . \quad . \quad . \quad . \quad . \quad . \quad (2)$$

This equation is also valid for the growth rates of whiskers with observable specks at their tips (indicated in fig. 8 by circles). Furthermore, it is in agreement with the qualitative observation that thickening whiskers grow at decreasing rates.

If diffusion of cadmium vapour through the argon is the rate-controlling process, and if it is assumed that there is a spherical diffusion field around the tip of each growing whisker, than it can be shown that the growth rate is given by

$$R = \frac{4D\Omega\sigma c_{eq}}{r} \quad . \quad . \quad . \quad . \quad . \quad . \quad . \quad (3)$$

where D is the diffusion coefficient of cadmium in argon and Ω is the atomic volume. For $D \simeq 0{\cdot}2\,\mathrm{cm}^2/\mathrm{sec}$, the equation becomes

$$R = \frac{0{\cdot}1\sigma c_{eq}}{r}\,\mu\,\mathrm{min}^{-1} \quad . \quad . \quad . \quad . \quad . \quad . \quad (4)$$

which, although it differs from eqn. (2) in the value of the exponent of r, gives order of magnitude agreement with all the observed growth rates.

Because of the limited range of values of r for which data were obtained, and because of uncertainty in the measurements of r, it is impossible to decide exactly how R depends on r. It seems fairly certain, however, from the correspondence between (2) and (4), that R is determined by the rate of diffusion of material through the inert gas, both for the tip growing and the non-tip growing whiskers.

Let us now consider briefly how a whisker might grow by the addition of atoms at points other than the tip. One possible mechanism could operate if the whisker had a pure screw dislocation along the axis which suddenly became a pure edge dislocation and ran out to the lateral surface. If the temperature were sufficiently high, the edge dislocation would maintain the equilibrium concentration of vacancies around it. At the surface, on the other hand, there would be an understaturation in surface vacancies corresponding with the supersaturation in adsorbed surface atoms. A concentration gradient would therefore be established in which vacancies would diffuse to the surface from the edge dislocation and thus cause it to climb. Every rotation of the edge dislocation around the axis would incorporate a new plane of atoms so that the whisker would be continuously lengthened. This is one possible mechanism, similar to the one suggested by Frank (1953) to explain the growth of tin whiskers on plated surfaces. Other mechanisms for the non-tip growth of whiskers may be envisaged but it seems desirable to defer further speculation until more observations and quantitative measurements are available.

§ 5. Summary

Cadmium crystals were grown from the vapour on a quartz fibre in an argon diffusion cell which was designed so that the temperature could be measured and the supersaturation calculated at every point. Crystal habits and growth rates were studied as a function of σ and T. A critical σ of $\sim 0{\cdot}4$ for nucleation was observed below which no crystals grew and above which the density of crystals increased with σ.

At low supersaturations ($\sigma \lesssim 2$) the crystal habit appeared to be determined at a very early stage in growth and was independent of σ and T,

consisting mainly of whiskers and thin platelets. For $\sigma \gtrsim 2$ the frequency of two-dimensional nucleation was so high and the density of crystals on the fibre so great that whiskers and thin platelets thickened and grew into each other, leaving as the stable growth forms mainly thick hexagonal plates. The average plate dimensions decreased as the density increased, because of increased competition for the vapour. At very high supersaturations ($\sigma \gtrsim 10^2$) crystals with dendritic habits grew to large dimensions from the deposit.

Axial growth rates of whiskers were measured as a function of σ and r and found to give fair agreement with rates derived assuming growth to be controlled by the diffusion of cadmium vapour through argon. Growth rates were accurately linear except at high supersaturations ($\sigma \gtrsim 1$), in which case the rates decreased as the whiskers thickened.

Some whiskers were observed to grow with observable specks of cadmium at their tips, which was interpreted as evidence for non-tip growth.

Acknowledgments

It was a pleasure to work under the direction of Dr. J. W. Mitchell and Professor F. C. Frank, to whom I am indebted for many valuable discussions. The growth cells were constructed by J. H. Burrow, who was to a large extent responsible for the success of the experiments. The photomicrographs were taken with equipment purchased with the assistance of a grant from the Department of Scientific and Industrial Research. The work was carried out during the tenure of a Fulbright grant from the U.S. Government and was a continuation of research begun at the University of Virginia with Professor N. Cabrera, to whom I am grateful for reviewing the manuscript.

APPENDIX

Determination of Supersaturation in the Cell

The top and bottom surfaces of the cell may be regarded as two infinite parallel plane layers of cadmium held at fixed temperatures T_a and T_{-a} at the vertical position coordinates a and $-a$. Assuming a steady state with the vapour being transported downwards by diffusion through the gas, and assuming the diffusion constant to be independent of temperature, the diffusion equation predicts a linear variation of the vapour density of cadmium between the two layers. Using the boundary conditions that the partial vapour pressures of cadmium at a and $-a$ will be the equilibrium vapour pressures at T_a and T_{-a}, the actual values of the partial vapour pressure p at any level are determined. Since p_{eq} varies exponentially with temperature, whereas p varies linearly, it is obvious that the gas will be supersaturated with cadmium vapour at every point in the cell except at the top and bottom.

The supersaturation curve can be obtained graphically from a table of p_{eq} as a function of T (Honig 1957) for any values of T_a and T_{-a}, but it is interesting to get an analytic expression for the supersaturation as a function of temperature and position in the cell. For convenience the saturation ratio, defined by $\alpha=\sigma+1=(p/p_{eq})$, will be used. Assuming that $\Delta T/T_0$ is small, where

$$\Delta T=T_a-T_{-a} \quad \text{and} \quad T_0=\frac{T_a+T_a}{2},$$

the result is

$$\alpha\simeq\cosh\beta a[1+(z/a)\tanh\beta a]\exp(-\beta z), \qquad (1)$$

where $\beta=q\Delta T/2akT_0^2$, with q=latent heat of condensation and k=Boltzmann's constant. This expression is accurate to within 6% for $\Delta T/T_0\lesssim 0{\cdot}1$. For temperature differences greater than this it is better to solve for α graphically.

Fig. 10

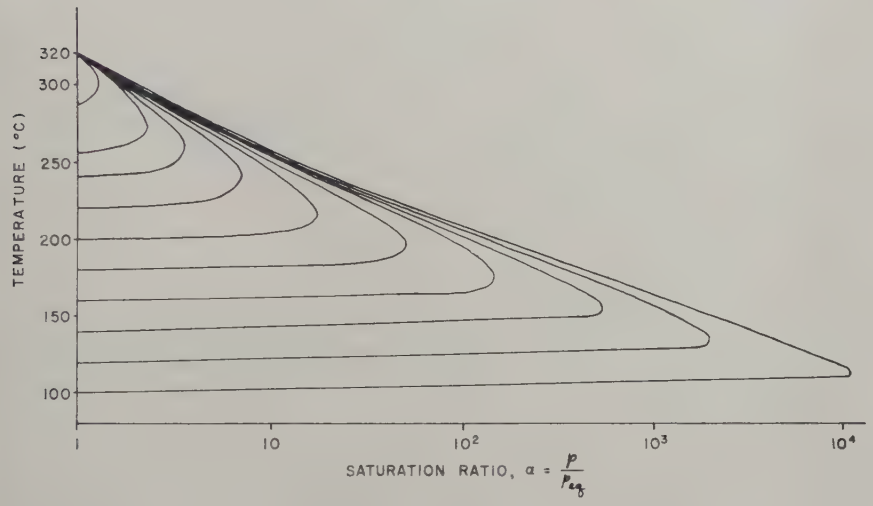

α-curves for different values of T_a and T_{-a}.

The saturation ratio varies from one at the top of the cell, through some maximum value α_{max} at the position z_{max}, to one at the bottom. Differentiation of (1) gives

$$\alpha_{max}=(1/\beta a)\sinh\beta a\exp(\beta a\coth\beta a-1), \quad . \quad . \quad . \quad . \quad (2)$$

$$z_{max}=(1/\beta)-a\coth\beta a. \quad . \quad . \quad . \quad . \quad . \quad . \quad . \quad . \quad (3)$$

Since $\coth\beta a$ is always greater than βa, z_{max} is always below the middle of the cell, and as βa increases (i.e. ΔT increasing), α_{max} increases and z_{max} approaches $-a$.

It is seen from (1) that α is a function only of z/a and $\Delta T/T_0^2$, so that there is no point in using cells of different dimensions. The only way to vary α and T independently is to vary T_0, which means varying the fixed

temperatures of the top and bottom of the cell. This is of limited usefulness, because for low values of T_a growth proceeds only very slowly due to the low vapour pressure of the source, whereas for high values of T_a part of the fibre is above the melting point of cadmium. There are thus certain practical limitations on the values of the growth parameters which can be achieved independently.

Figure 10 shows a series of α curves plotted on the same graph, with the saturation ratio as the abscissa on a logarithmic scale, with T_a for each curve fixed at the melting point of cadmium, about 320°C, and with T_{-a} varying from 300° to 100°C in 20° intervals along the ordinate axis. The curves give an idea of the behaviour of α for different values of ΔT ranging from 20° to 220°, showing qualitatively the behaviour of $\alpha_{\max}$ and $z_{\max}$. It is to be noted that, since the temperature varies linearly with cell height, the ordinate can also be taken as a measure of position in the cell, with the top of the cell at 320° for each curve but with the bottom of the cell at a point on the ordinate determined by the value of ΔT for a particular curve.

References

Cabrera, N., and Price, P. B., 1958, *Growth and Perfection of Crystals* (New York: Wiley), p. 204.

Coleman, R. V., Price, P. B., and Cabrera, N., 1957, *J. appl. Phys.*, **28,** 1360.

Doremus, R. H., Roberts, B. W., and Turnbull, D., 1958, editors of *Growth and Perfection of Crystals* (New York: Wiley).

Frank, F. C., 1953, *Phil. Mag.*, **44,** 854.

Gomer, R., 1958, *J. chem. Phys.*, **28,** 457.

Hallett, J., and Mason, B. J., 1958, *Proc. roy. Soc.* A, **247,** 440.

Honig, R. E., 1957, *R. C. A. Rev.*, **18,** 195.

Mason, B. J., 1953, *Quart. J. R. met. Soc.*, **79,** 104.

Price, P. B., 1959, *Phil. Mag.*, **4,** 1229; 1960, *Phil. Mag.* (in the press).

Price, P. B., Vermilyea, D. A., and Webb, M. B., 1958, *Acta Met.*, **6,** 524.

Reynolds, S. E., 1952, *J. Met.*, **9,** 36.

The Dislocation Distribution, Flow Stress, and Stored Energy in Cold-worked Polycrystalline Silver†

By J. E. Bailey and P. B. Hirsch
Crystallographic Laboratory, Cavendish Laboratory, Cambridge

[Received January 5, 1960]

Abstract

Distribution and densities of dislocations, determined by electron transmission microscopy, flow stress and stored energy measurements (by microcalorimetry) on cold-worked polycrystalline silver are correlated with each other. The dislocations are arranged in dense networks forming the boundaries of an otherwise relatively dislocation-free cell structure. The flow stress is explained quantitatively in terms of the forest intersection mechanism at the boundaries. The stored energy after recovery is of the same order as the total self-energy of the dislocation arrangement, so that the long-range stresses must be largely relaxed. The considerable energy release during the recovery stage produces no observable change in dislocation distribution. This recovery stage is thought to be due to the relief of long-range stresses or to the removal of point defects.

While the values of flow stress and stored energy can be accounted for in terms of the observed non-uniform distribution of dislocations (cell structure), they are not compatible with each other on a model based on a uniform distribution of pile-ups; nor are pile-ups observed on the electron micrographs.

§ 1. Introduction

Theories of flow stress and work hardening depend on the particular dislocation distributions assumed in the model of a cold-worked metal (Seeger 1957, Friedel 1955, Hirsch 1958). The present paper describes a direct correlation between the experimentally determined distribution and density of dislocations, the flow stress and the stored energy in cold-worked polycrystalline silver. The distribution and density of dislocations are determined by means of the transmission electron microscope technique (Hirsch *et al.* 1956), the flow stress is measured on a conventional straining machine, and the stored energy using an isothermal calorimeter (Bailey 1959).

§ 2. Flow Stress and Stored Energy Measurements

The silver for all the experiments was supplied by the Sheffield Smelting Company; the purity is 99·99%, the major part of the impurity being copper together with traces of silicon, magnesium and iron.

The calorimetry experiments were carried out using specimens of about 13 mm diameter cut from tensile specimens. The grain size of the specimens was $\sim 12\,\mu$. The specimens were extended at a rate of $\sim 10^{-2}$/min; fig. 1 shows the stress–strain data of the tensile specimens. It was found

† Communicated by the Authors.

Fig. 1

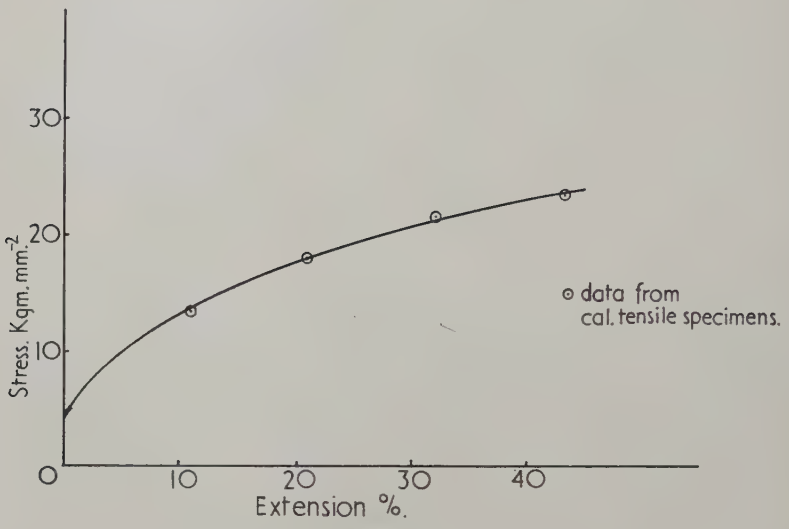

Stress–strain curves of the silver foils (full curve) and calorimetry tensile specimens (points).

Fig. 2

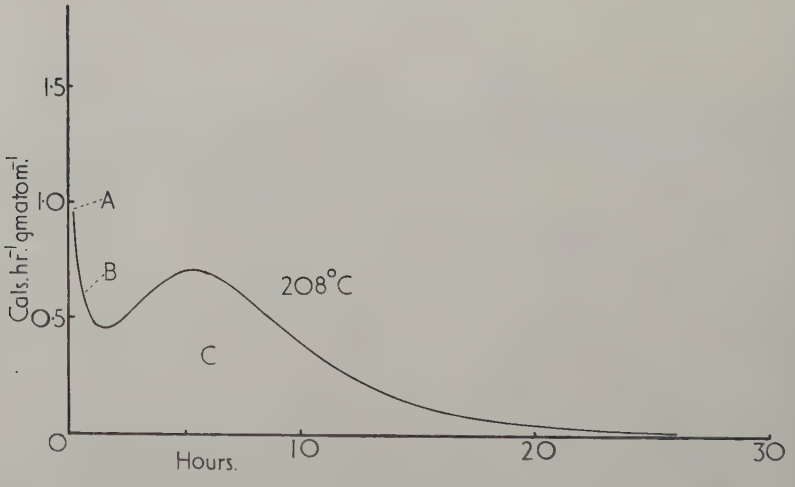

Energy release curve for silver deformed 43% in tension and annealed at 208°c, showing the recovery stage B and recrystallization stage C. Measurements cannot be made over the first fifteen minutes (region A).

impracticable to prepare electron microscope specimens from those used for calorimetry because of their large size. To overcome this difficulty a calorimeter specimen was rolled into sheet 0·005 in. thick. After suitable

annealing treatments the silver foil had a grain size of $\sim 20\,\mu$. These foils were extended at a rate of $1{\cdot}5 \times 10^{-4}$/min; fig. 1 shows a stress–strain curve. It is clear from fig. 1 that the stress–strain curves of both types of specimen are almost identical. It is reasonable to assume therefore that the dislocation distributions are closely similar in both types of specimen for a given degree of deformation.

Table 1. Values of E_P, E_R, E_T and E^* at different temperatures for a given deformation

Deformation (% extension)	Temperature (°C)	E_T (cals/g atom)	E_P (cals/g atom)	E_R (cals/g atom)	E^* (cals/g atom)
32	253	8·10	3·34	4·76	7·60
32	245	7·75	2·91	4·84	7·25
32	229	7·54	2·78	4·76	7·14
32	209·5	7·60	2·44	5·16	7·40

Table 2. Average values of the total stored energy, E_T, and the energies evolved during recovery, E_P, and recrystallization, E_R

Deformation (% extension)	E_T (cals/g atom)	E_R (cals/g atom)	E_P (cals/g atom)
11	2·70	1·25	1·45
21	5·10	2·83	2·27
32	7·75	4·9	2·85
43	7·27	6·03	1·24

The stored energy was determined by measuring the heat evolved as a function of time in an isothermal calorimeter. A typical heat release curve is shown in fig. 2. The energy released in region A, corresponding to the first 15 min, could not be measured; this is the time interval in which the specimen reaches the equilibrium temperature of the calorimeter. Region B corresponds to a recovery stage, and region C is accompanied by recrystallization (checked by x-ray diffraction methods). The composite curves can always be analysed in terms of two overlapping components; one of these (C) has the usual recrystallization kinetics (Burke and Turnbull 1952), while region B can be fitted to a law $dQ/dt = A/(t+t_0)$, where dQ/dt is the rate of release energy, A and t_0 are constants depending on temperature and prior deformation. The total stored energy is obtained by integrating the area under the curve; the energy is in two parts, one released during recovery, E_P, and the other during recrystallization, E_R. The part released during recrystallization is usually accurate

to $\sim 5\%$. In order to determine the energy released during recovery, curve B is extrapolated to zero time using the above law. Table 1 gives values of E_P, E_R, the total stored energy E_T $(=E_P+E_R)$ and the energy released after the first 15 min E^*, at different temperatures for a given deformation. It is clear from the agreement between the results obtained at the different temperatures that the values of E_T are accurate to about 10%. Similar results have been obtained for specimens deformed by different amounts; however, for the smallest deformation studied (11% extension) the errors are somewhat larger (Bailey 1959). The energy released during the first 15 min does not usually exceed about 20% of the total energy, except again for the specimens with the smallest deformation. The general agreement between values obtained at different temperatures suggests that the extrapolation technique used is satisfactory.

Table 2 shows the average values of E_P, E_R and E_T for each deformation.

§ 3. Electron Microscope Observations

Electron microscope specimens were prepared by electropolishing the silver sheet of thickness 0·005 in. mentioned above, after various deformations. A polishing bath recommended for gold by Jacquet (1956) was found to be suitable. Its constituents are, per litre: 67·5 g potassium cyanide; 15 g Rochelle salt; 19·5 cm^3 orthophosphoric acid; 2·5 cm^3 ammonia; 15 g potassium ferrocyanide. The voltage required across the cell is about 4 v; a stainless-steel cathode is used and the specimen is agitated slightly to avoid etching. The specimen is removed rapidly after polishing, washed in distilled water and stored in absolute alcohol until required.

Typical areas of specimens deformed 10, 20 and 30% in tension are shown in fig. 3 (*a*), (*b*) and (*c*) (Pl. 52). The dislocations are arranged mainly in complex bands separating relatively dislocation-free areas. This cell structure becomes more pronounced with increasing deformation; i.e. at low deformation the dislocation density is rather more uniform, while at the higher deformation there is clearer distinction between the cell walls containing a high density of dislocations, and the relatively dislocation-free interior. After 30% deformation the diameter of the cells is $\sim 1\,\mu$. It is difficult to decide from the micrographs whether there is a significant decrease in cell size with increasing deformation over the range of extensions investigated, i.e. 10–30%. The cell boundaries appear to be regions of complex 3-dimensional networks; they are not single plane low angle boundaries. Figure 4 (Pl. 53) shows the nature of the cell boundaries at high magnification. The dislocation density in the cell walls increases with increasing deformation. It is not clear however whether there is any significant change in the thickness of the cell walls with increasing deformation.

The misorientations across the boundaries are less than 1°; this is evident from diffraction patterns, an example of which, from an area

of $\frac{4}{3}\mu$ in diameter of a specimen extended 30%, is shown in fig. 3(*d*). Similar single crystal patterns are obtained also from specimens deformed 10 or 20 %; areas completely within one grain were chosen for these experiments. A study of the orientation of the cell boundaries failed to reveal any tendency for them to follow any particularly simple crystallographic directions. There is no evidence on the micrographs for groups of piled-up dislocations.

The original grain boundaries are still clearly visible after deformation. No large discontinuities or steps were observed. With increasing deformation, however, there appears to be a tendency to roughening of the boundaries on a scale of about 100 Å.

Table 3. Dislocation densities in silver foil deformed in tension

Extension (%)	Dislocation density (cm/cm³)	Mean dislocation density (cm/cm³)
32	$6{\cdot}0\times10^{10}$ $8{\cdot}0\times10^{10}$ $7{\cdot}5\times10^{10}$ $5{\cdot}2\times10^{10}$ $7{\cdot}8\times10^{10}$ $7{\cdot}0\times10^{10}$ $7{\cdot}0\times10^{10}$	$6{\cdot}8\times10^{10}$
21	$5{\cdot}5\times10^{10}$ $4{\cdot}0\times10^{10}$ $6{\cdot}2\times10^{10}$ $5{\cdot}0\times10^{10}$	$5{\cdot}2\times10^{10}$
11	$2{\cdot}0\times10^{10}$ $2{\cdot}0\times10^{10}$ $2{\cdot}5\times10^{10}$ $2{\cdot}5\times10^{10}$	$2{\cdot}2\times10^{10}$

Dislocation densities were estimated by measuring the total projected length of dislocation line in a given area on a micrograph. A typical area was selected in the electron microscope, a micrograph and diffraction pattern taken, and the electron beam was then increased to allow some dislocations to move to produce slip traces. Since the orientation of the foil is known from the diffraction pattern, the particular (111) plane corresponding to a given slip trace can be determined. From the widths of the slip trace and the orientation of this (111) plane, the local thickness of the specimen can be calculated. In this way the total projected length of dislocation line in a given volume of specimen is determined. Assuming that the dislocation segments are randomly orientated, the mean length of dislocation line, R, can be derived from the mean projected length, R_P, by using the relation $R=(4/\pi)R_P$.

An important source of error arises from the difficulty of resolving individual dislocations in regions of very high dislocation density. Such areas are interpreted as bands of high dislocation density inclined almost perpendicularly to the foil surface, so that the dislocations overlap in projection. This effect was allowed for by assuming that the denstiy in these bands is similar to that in bands lying more parallel to the surface, in which the dislocation overlap is negligible, and which are thought to correspond to the regions on the micrographs in which the dislocations can be resolved. The measurements were repeated for several areas of a specimen. Table 3 shows the results; from the spread of values the error appears to be about 25%. In addition there is the possibility of systematic errors. After the specimen is thinned dislocations which are free to move may shorten their lengths by gliding into an orientation such that they traverse the foil along the shortest distance in the slip plane. The magnitude of this effect is difficult to estimate but since most of the dislocations occur in close mesh networks this error is likely to be small. Furthermore, certain dislocations may be invisible (Hirsch *et al.* 1959); the magnitude of this effect depends on orientation and has not yet been studied rigorously; however the error is not likely to exceed 20%. We conclude that the estimates of the densities of visible dislocations are probably accurate to 25% but that they may underestimate the true dislocation densities by about 20%. In spite of these errors the increase in dislocation density with increasing deformation is clearly established.

Attempts were made to estimate the dislocation densities in the dense areas. This is very difficult to do with any precision. However, it appears that for all three deformations the dislocation densities in these areas are about five times the average values.

Electron microscope observations were also carried out on specimens which had recovered but not recrystallized. No significant difference could be detected between the dislocation distributions and densities before and after recovery.

§ 4. Discussion

4.1. *Energy of a Dislocation*

Since the stored energies and dislocation densities are known for comparable specimens, the energy associated with a dislocation can be calculated. Table 4 shows the values of energy per atom plane of dislocation before and after recovery for three different deformations. The differences between the values for different deformations are not significant; the average values are 8·3 ev before and 4·5 ev after recovery. Thus about half the total stored energy is released before recrystallization, apparently without change in the dislocation density.

It is instructive to compare these values with theoretical estimates. The dislocations are found to be arranged in complex networks which are almost certainly not stress free. The energy associated with a dislocation

consists of its self-energy and the energy of interaction with other dislocations. The self-energy (per unit length) is given approximately by

$$E_1 = \frac{G\mathbf{b}^2}{4\pi K} \ln \frac{R}{r_0} + \text{core energy}$$

where G is the shear modulus, $\mathbf{b}$ the Burgers vector, $K = 1$ for a screw, $1 - \nu$ for an edge dislocation, ν Poisson's ratio, R the radius of the volume over which the stress field extends, and r_0 the core radius. A reasonable value for the core energy is $G\mathbf{b}^2/10$ so that we may write

$$E_1 = \frac{G\mathbf{b}^2}{4\pi K}\left(\ln \frac{R}{r_0} + 1\right).$$

The value of R is uncertain; however, a lower limit is given by the length of a dislocation segment in the networks, i.e. about 200 Å, and an upper limit by the size of the cells, i.e. about 1 μ after heavy deformation. The mean of the values for E_1 for edge and screw dislocations, of several values of R are shown in table 5 (r_0 is taken as $\mathbf{b}/2$). Values using the more detailed energy expression due to Schoeck and Seeger (1953) are also shown. These

Table 4. Energy per atom plane of dislocation before and after recovery

Deformation (% extension)	Dislocation density, N (cm/cm^3)	Total stored energy, E_T (cals/g atom)	$L_T = E_T N$ (ev atom plane)	E_R (cals g atom)	$L_R = E_R/N$ (ev/atom plane)
10	$2{\cdot}2 \times 10^{10}$	2·7	$9{\cdot}1 \pm 2{\cdot}5$	1·25	$4{\cdot}2 \pm 1{\cdot}0$
20	$5{\cdot}2 \times 10^{10}$	5·10	$7{\cdot}3 \pm 2{\cdot}5$	2·8	$4{\cdot}0 \pm 1{\cdot}0$
30	$6{\cdot}8 \times 10^{10}$	7·7	$8{\cdot}4 \pm 2{\cdot}5$	4·9	$5{\cdot}3 \pm 1{\cdot}0$

Table 5. The energy per atom plane of dislocations occurring singly, E_1, and in groups of 2, 3, 4 (E_2, E_3 and E_4) whose stress fields extend over a distance R

R (Å)	E_1 (simple formula) (ev/atom plane)	E_1 (Schoeck and Seeger) (ev/atom plane)	E_2 (ev atom plane)	E_3 (ev atom plane)	E_4 (ev/atom plane)
200	2·66	1·90	—	—	—
1000	3·38	2·61	4·1	4·62	5·16
10000	4·4	3·63	6·16	7·7	9·3

are somewhat smaller than the values calculated on the above formulation. Comparison of experimental and theoretical values of dislocation energy shows that the experimental values before recovery are somewhat larger

than the theoretical values of E_1. The energy released during recovery may be due partly to point defects and partly to a reduction of interaction energy accompanying small displacements of the dislocations. This interaction energy is presumably associated with the networks. It is possible for example that the networks contain groups of a few (say 2, 3 or 4) dislocations on the same slip plane, at distances of about 200 Å from each other. The interaction energy for two dislocations at a distance r apart is $(G\mathbf{b}^2/2\pi K)\ln(R/r)$; hence the total energy associated with each dislocation of the pair is

$$E_2 = \frac{G\mathbf{b}^2}{4\pi K}\left(\ln\frac{R}{r_0} + 1 + \ln\frac{R}{r}\right).$$

A similar calculation for three and four dislocations spaced at a distance r gives

$$E_3 = \frac{G\mathbf{b}^2}{4\pi K}\left(\ln\frac{R}{r_0} + 1 + 2\ln\frac{R}{r} - \frac{2}{3}\ln 2\right)$$

and

$$E_4 = \frac{G\mathbf{b}^2}{4\pi K}\left(\ln\frac{R}{r_0} + 1 + 3\ln\frac{R}{r} - \ln 2 - \frac{1}{2}\ln 3\right).$$

Values of E_2, E_3 and E_4 are shown in table 5, for $r_0 = \frac{1}{2}\mathbf{b}$, $r = 200$ Å, and $R = 1000$ Å or 10 000 Å. It is clear from these results that the interaction energy can be accounted for in terms of interactions between groups of only three or four dislocations whose long-range stresses do not cancel and extend over the region of the cells (i.e. $\sim 1\,\mu$). After recovery there may still be some interaction energy but the extent of the long-range stress field must be reduced. The electron microscope observations show no observable difference between the dislocation arrangements before and after recovery. Therefore, if the release in energy during recovery corresponds to a reduction in the interaction energy, this must be brought about by slight movements and re-arrangements of the dislocations in the cell boundaries, for example, by climb, by cutting through other dislocations or by cross-slip.

After recovery the difference between experimental and calculated values of self-energy is hardly significant in view of the experimental errors. It may be concluded that after recovery the experimental value agrees with the theoretical value of the self-energy to within a factor of 2.

Summarizing, it appears that the stored energy values are quite compatible with the observed dislocation distributions, that any long-rauge stresses are at the most of the order of those expected from three or four dislocations piled up in the cell boundaries, and that after recovery the dislocation energy agrees to within a factor 2 with the theoretical value of the self-energy.

4.2. *Comparison of Stored Energy and Flow Stress*

There are at present two main theories which attempt to account for the flow stress of pure metals. In the first, due to Friedel (1955) and Seeger (1957), the flow stress is determined by long-range stresses due to groups of piled-up dislocations; in the second, due to Cottrell (1953), Basinski (1959) and Hirsch (1958), the flow stress is determined by short-range interactions between crossing dislocations.

According to Seeger *et al.* (1957) the temperature-independent part of the flow stress τ_g is given by a relation of the form:

$$\tau_g = \frac{G\mathbf{b}n}{2\pi K} N_G^{1/2}, \qquad \ldots\ldots (1)$$

where N_G is the density of piled-up groups of either edge or screw dislocations. The stored energy per unit volume on this model is essentially the energy of $2N_G$ large dislocations of Burgers vector $n\mathbf{b}$ (the factor 2 taking account of edge and screw dislocations), i.e.

$$E_G = \frac{G(n\mathbf{b})^2}{4\pi K} 2N_G \ln\left(\frac{R}{r_0}\right). \qquad \ldots\ldots (2)$$

Eliminating N_G between eqns. (1) and (2) gives the relationship between E_G and τ_g as:

$$E_G = \frac{2\pi K}{G} \tau_g^2 \ln\left(\frac{R}{r_0}\right).$$

The values of E_G have been calculated from the stress–strain data for the silver used in the stored energy measurements and compared with the experimental values for the stored energy E_T and E_R, before and after

Table 6. Values of the energy stored, E_G, as calculated from a 'pile-up' model compared with the experimental values of the energy stored prior to recovery, E_T, and prior to recrystallization, E_R

Deformation (%)	Flow stress (kg/mm²)	E_G (cals/g atom)	E_T (cals/g atom)	E_R (cals/g atom)
11	6·66	21·2	2·7	1·25
21	8·9	37·0	5·1	2·83
32	10·67	54·0	7·75	3·7
43	11·58	64·0	7·27	4·9

recovery, in table 6. For this calculation R was taken as $1\,\mu$, and the flow stress as one-half of the tensile stress.

It is clear from the large discrepancy between E_G and E_T that the pile-up model cannot account satisfactorily for the flow stress and the stored energy.

It should be emphasized that this conclusion follows directly from the flow stress and stored energy results, and does not depend on any direct microscopic examination of the dislocation structure.

The flow stress and stored energy results might be reconciled by assuming that the pile-ups occur only in certain small regions of the metal, the other regions containing only few dislocations. There is however no evidence at all for such an arrangement. It appears therefore that the simple pile-up or long-range stress theory of flow stress must be abandoned for the case of polycrystalline silver. This conclusion is independent of the number of dislocations in the pile-up; thus any model of flow stress based on a Taylor-type distribution of dislocations throughout the volume of the metal is ruled out.

The significance of the electron microscope observations reported in § 3 will now be appreciated. The dislocations are found to occur in dense networks in bands forming the boundaries of a cell structure, the cells being relatively free of dislocations. On the forest theory the flow stress is determined by the stress required for dislocations to cut through the dense regions of the forest in the boundaries, i.e.

$$\tau_g = \frac{G\mathbf{b}}{2\pi K}\frac{1}{l_f} \qquad \ldots\ldots\ldots \quad (3)$$

where l_f is the spacing between forest dislocations in the boundary. The dislocation density in the boundaries N_f will be $\sim 1/l_f^2$, and observations indicate that $N_f \sim 5N$, where N is the average dislocation density. It is clear at once that on this model the energy will be much smaller for a given flow stress since only part of the volume of the metal is occupied by dislocations.

In fact the energy, E_F, is given by

$$E_F = \frac{NG\mathbf{b}^2}{4\pi K}\ln\frac{R}{r_0}$$

and substituting from eqn. (3) we obtain

$$E_F = \frac{1}{m}\frac{\pi K}{G}\tau_g^2 \ln\frac{R}{r_0}$$

where we have put $N_f = mN$. Putting $m \sim 5$, E_F is $\sim E_G/10$, when $R \sim 1\,\mu$, or somewhat less for smaller values of R. Thus the values of E_F are fairly close to but rather smaller than the experimental values E_T, the remaining discrepancy being possibly due to the presence of some long-range stresses, or due to a contribution to E_T from point defects. The agreement between E_F and E_R is satisfactory.

It is clear then that the essentially non-uniform distribution of dislocations observed can account both for the flow stress in terms of a forest intersection mechanism and for the stored energy.

4.3. *Relation between Flow Stress and Dislocation Density*

Figure 5 shows a plot of the square root of the average dislocation density, N, against the tensile stress. σ. It appears that $\sigma \propto N^{1/2}$; taking

the flow stress τ_g as $\frac{1}{2}\sigma$, from the slope of fig. 5 we find

$$\frac{\tau_g}{N^{1/2}} = 4{\cdot}1 \times 10^3 \text{ dynes/cm.}$$

The significance of this relation is not clear since according to the forest model the flow stress is determined by the local dislocation density in the

Fig. 5

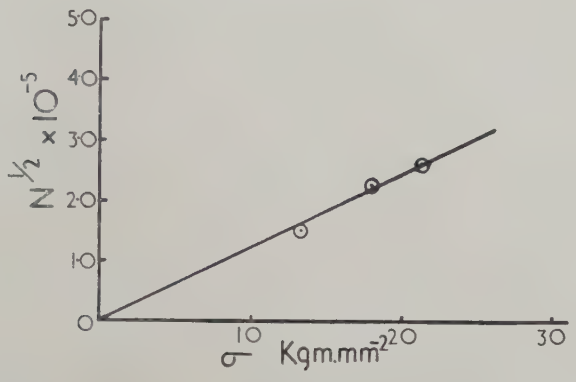

Plot of the square root of the average dislocation density, N, against the tensile stress, σ.

cell boundaries, N_f. Although precise measurements are difficult, it appears that approximately $N_f \sim 5N$ for all deformations examined so that

$$\tau_g \sim 1{\cdot}8 \times 10^3 N_f^{1/2}.$$

This expression should be compared with the approximate theoretical relation for the flow stress on the forest theory, i.e.

$$\tau_g \sim \frac{G\mathbf{b}N_f^{1/2}}{2\pi K} = 1{\cdot}3 \times 10^3 N_f^{1/2}.$$

In view of the inaccuracy in determining the ratio N_f/N, and of the precise form of the theoretical expression for the dislocation intersection mechanism, the agreement between theory and experiment can be considered to be satisfactory.

§ 5. Conclusion

Electron transmission micrographs of deformed polycrystalline silver show that the dislocations are arranged non-uniformly in dense bands forming the boundaries of a cell structure. Only a fraction of the volume of the metal is occupied by dislocations; a reasonable measure of this fraction is N_f/N, i.e. about 20%. The experimental values of flow stress can be accounted for satisfactorily in terms of this arrangement on the assumption that it is determined by the stress required for a dislocation to penetrate the dense forest in the boundaries. Thus, although the flow

stress may be high if the local dislocation density is large, the energy associated with this distribution of dislocations is relatively small since only part of the volume of the metal is occupied by dislocations. In fact, the experimentally measured values of stored energy are compatible with the observed dislocation distribution, provided that the long-range stresses associated with the networks are relatively small (particularly after recovery). The values of flow stress and stored energy are not compatible with each other if the flow stress is attributed to long-range stresses from pile-ups, and no pile-ups are observed on the electron micrographs. During recovery there is a considerable energy release but no observable decrease in dislocation density. It is not yet clear whether this release of energy is due to the relief of long-range stresses or due to the disappearance of point defects. In the latter case it might be expected that the release of stored energy during recovery would be associated with a decrease in the resistivity; it is proposed to carry out such measurements.

Electron microscope observations on the dislocation distributions in cold-worked polycrystalline Ni, Cu, Au, Al (Hirsch 1958) showed that the arrangements are rather similar to those in Ag. There is no reason to doubt that in these metals also the flow stress is determined essentially by the dislocation intersection mechanism at the boundaries. On the other hand, pile-ups are observed in stainless steel (Whelan *et al.* 1957) and α-brass (Hirsch 1958) and in these cases the long-range stresses may be important. Further experiments are needed to clarify this point.

The application of the 'forest theory' to single crystals will be discussed elsewhere.

Acknowledgments

We wish to thank Professor N. F. Mott, F.R.S., and Dr. W. H. Taylor for stimulating discussions, and for constant help and encouragement. Our thanks are also due to Dr. O. Krisement for his help and advice on the problem of calorimetry, to Dr. G. C. Smith and Mr. S. Charter for facilities provided for straining calorimeter specimens, to Messrs. C. K. Jackson and G. Rickards for assistance in electron microscopy, and to other members of the metal physics group for useful discussions. One of us (J. E. Bailey) acknowledges the receipt of a maintenance grant from the Admiralty.

References

Bailey, J. E., 1959, Ph.D. Dissertation, University of Cambridge.

Basinski, Z. S., 1959, *Phil. Mag.*, **4**, 393.

Burke, J. E., and Turnbull, D., 1952, *Progress in Metal Physics*, **3** (London : Pergamon Press).

Cottrell, A. H., 1953, *Dislocations and plastic flow in crystals* (Oxford : Clarendon Press).

Friedel, J., 1955, *Phil. Mag.*, **46**, 1169.

Hirsch, P. B., 1958, *Report on Symposium on Internal Stresses & Fatigue in Metals* (Detroit : General Motor Labs.).

Hirsch, P. B., Horne, R. W., and Whelan, M. J., 1956, *Phil. Mag.*, **1,** 677.
Hirsch, P. B., Howie, A., and Whelan, M. J., 1959, *Phil. Trans.* (in the press).
Jacquet, P. A., 1956, Electrolytic & Chemical Polishing : Metallurgical Reviews, **1,** 2.
Seeger, A., 1957, *Report of Lake Placid Conference on Dislocations & Mechanical Properties of Crystals* (New York : Wiley), p. 243.
Seeger, A., Diehl, J., Mader, S., and Rebstock, H., 1957, *Phil. Mag.*, **2,** 323.
Seeger, A., and Schoek, G., 1953, *Acta Met.*, **1,** 519.
Whelan, M. J., Hirsch, P. B., Horne, R. W., and Bollman, W., 1957, *Proc. roy. Soc.* A, **240,** 524.

Investigation of the Annealing of Nickel Deformed by Compression by X-ray and Stored Energy Measurements†

By D. Michell and E. Lovegrove

Division of Tribophysics,
Commonwealth Scientific and Industrial Research Organization,
University of Melbourne, Australia

[Received December 15, 1959]

Abstract

X-ray diffraction patterns from bulk specimens of nickel deformed by compression have been measured with a Geiger-counter spectrometer. A composite specimen has been used to overcome the effects of preferred orientations.

The results indicate that during the annealing there is no change in the background intensity. No evidence has been found for stacking faults or changes in lattice parameter. The integrated intensities of all lines remain constant up to a temperature of annealing of about 480°c. A large decrease (30–75%) in the integrated intensity of all lines occurs on annealing to 600°c and this is attributed to extinction; an estimate of 2–4 μ is obtained for the size of the 'perfect' regions required to produce this effect.

The diffraction profiles are analysed by a number of methods. The broadening produced by the particle size effect is small. The stored energies derived from the various methods of analysis range from 0·04–2·4 cal/g. Best agreement is obtained between values of stored energy measured using a calorimetric method (0·28 cal/g) and those derived from x-ray measurements if it is assumed that the distribution of strain is Gaussian.

§ 1. Introduction

In the study of the deformation of metals and their subsequent recovery on annealing it is desirable to compare the results of x-ray determinations with measurements of other properties such as stored energy, electrical resistivity, density, etc. Measurements of the latter properties are generally made on bulk specimens, whereas most accurate measurements of the x-ray diffraction patterns have been made on powdered specimens since there is then no complication due to preferred orientations or original grain size. However, it has been shown (Michell and Haig 1957, Clarebrough *et al.* 1955) that the energy stored in nickel deformed by grinding is considerably greater than in bulk specimens of nickel deformed to fracture by torsion. Thus it is evident that if the comparison between various properties is to be meaningful, the measurements should all be made on the one type of specimen.

In the present work the x-ray diffraction patterns from bulk specimens of nickel deformed by compression have been investigated after various

† Communicated by Dr. W. Boas.

stages of annealing, using a Geiger-counter spectrometer. The effects of preferred orientation have been eliminated by using a composite specimen consisting of a number of sections cut in selected orientations from the deformed material. The results have been compared with measurements of the energy stored in similar specimens deformed in the same manner.

§ 2. Material and Deformation

The nickel used in the present experiments was taken from a bar of purity 99·85%, batch *M* of Clarebrough *et al.* (1960). As the grain size (1 mm) of the nickel supplied was too large to produce continuous Debye–Scherrer rings it was refined by annealing the bar for 30 min at 700°C in an atmosphere of nitrogen, deforming it by three successive compressions of 25% perpendicular to each other and then heating it at the rate of 6°C per min to 660°C in an atmosphere of nitrogen. Two such cycles of deformation and annealing produced a final grain size of 30–40 μ.

Fig. 1

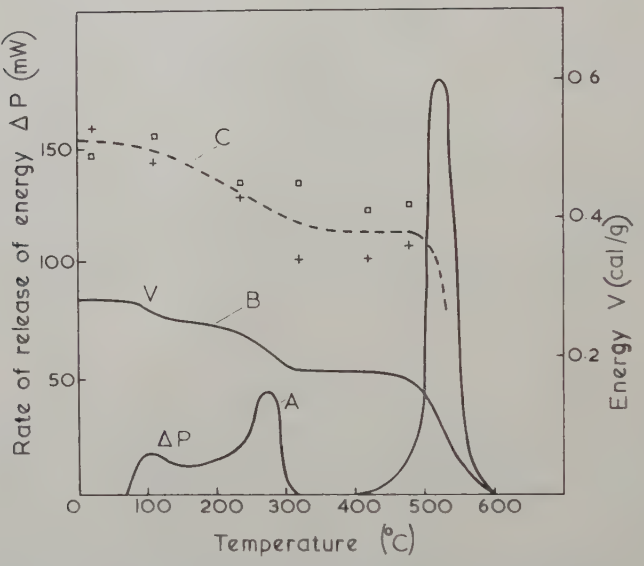

Release of energy from deformed nickel during annealing as a function of temperature.

(A) Rate of release of energy from nickel deformed by 25% cubic compression. (B) Stored energy remaining in the nickel (computed from A). (C) Calculated stored energy from Warren–Averbach analyses assuming Gaussian strain distribution. + For 111 and 222 reflections; □ for 300 and 400 reflections.

After grain refinement the nickel was in the form of rectangular blocks 1 in. × 1 in. × 2 in., the size required for the preparation of stored energy specimens. In order to preserve this shape and at the same time introduce a high degree of deformation with a minimum of preferred orientation, the final deformation also consisted of three compressions, perpendicular to each other, each of 25%.

§ 3. Stored Energy

Specimens of deformed metal were prepared for the determination of stored energy. The technique and apparatus used in making these measurements were as described by Clarebrough *et al.* (1952). The energy stored and the manner of its release are shown in fig. 1.

§ 4. X-ray Measurements

4.1. *Preparation of Specimens for X-ray Work*

Preliminary x-ray measurements made on specimens deformed in the manner described in § 2 showed that the degree of preferred orientation was such that the measurement of one element of length of a Debye–Scherrer ring could not be taken as typical of the whole ring. The following method of preparing specimens was therefore developed to minimise the effect of this preferred orientation.

If a specimen consisting of a sphere of polycrystalline metal is oscillated about its centre in such a way that all directions within the sphere are presented with equal probability to the x-ray beam, then the distribution of intensity around a Debye–Scherrer ring will be uniform and representative of the average intensity diffracted by all grains within the bulk material even if preferred orientations are present. Spherical specimens have been used in x-ray work (e.g. Mitchell and Rowland 1954), but they are undesirable in work involving the measurements of line shapes since they introduce more instrumental broadening than is obtained with flat specimens. An approximation to the use of a sphere which does not introduce additional instrumental broadening, consists of assembling in the one plane a number of flat sections, cut in selected orientations from the bulk material and presenting these with equal probability to the x-ray beam. The number of sections required is dependent on the extent and nature of the preferred orientation present in the deformed bar and the perfection to which the averaging effect is required. In the present case, ten sections were chosen corresponding to the faces of an icosahedron. However, specimens having any number of sections could be prepared by using other methods of selection.

The specimen prepared in this manner is shown in fig. 2. It consists of ten sections cut from a bar of nickel in the planes whose normals are shown in the stereographic projection, fig. 3, where the axes a, b and c represent the directions of the three compressions. It is desirable that no two sections are equivalent even if the resultant texture in the bar has cubic symmetry, or radial symmetry with respect to one of the directions of deformation. To avoid this, the orientation of the icosahedron relative to the axes a, b and c was selected so that when the normals shown in fig. 3 were referred to a unit stereographic triangle, no two were coincident (fig. 4), indicating that no two faces had the same relation to the directions of compression.

The sections were milled from the deformed bar, cut to approximately the required shape and then ground to the final dimensions. At all times the lightest of cuts were taken and copious quantities of coolant used.

Fig. 2

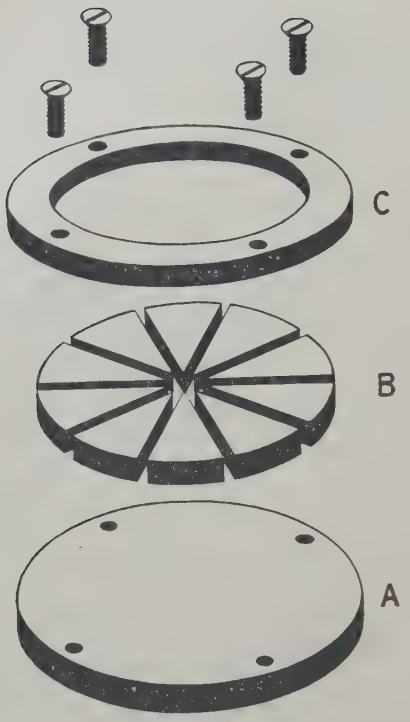

Unassembled components of composite specimen.
(A) Backing plate. (B) The ten sectors from the deformed bar. (C) Annular clamping ring and screws.

Fig. 3

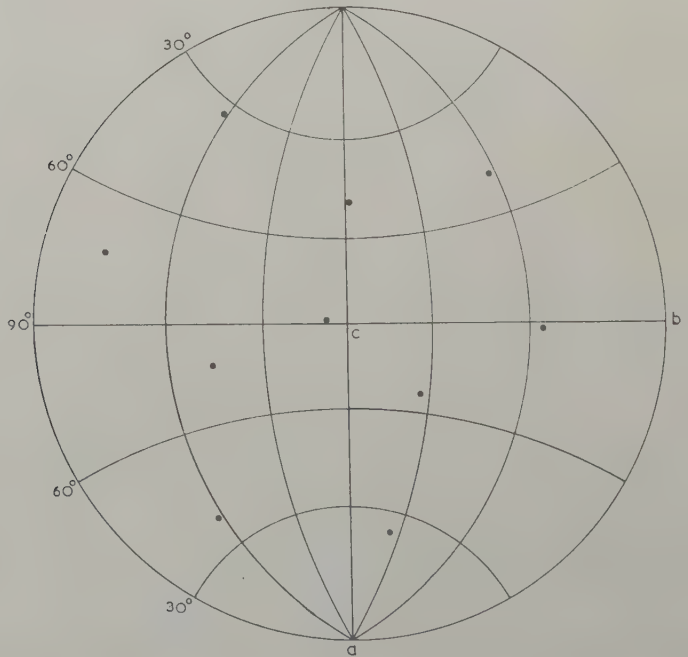

Stereographic projection showing the directions selected for the sections of the composite specimen. The *a*, *b* and *c* axes correspond to the directions of deformation.

An annular ring of wedge-shaped cross section C, together with four screws, was used to clamp the sectors B to a backing plate A (fig. 2). After assembly the complete specimen was again lightly ground, polished on metallographic papers and approximately 10 μ of the surface was removed by electropolishing. Preliminary measurements on a specimen deformed and machined in the same manner established that this treatment did not introduce any measurable change in the diffraction lines, nor did the removal of an additional 100 μ of surface by electropolishing.

Fig. 4

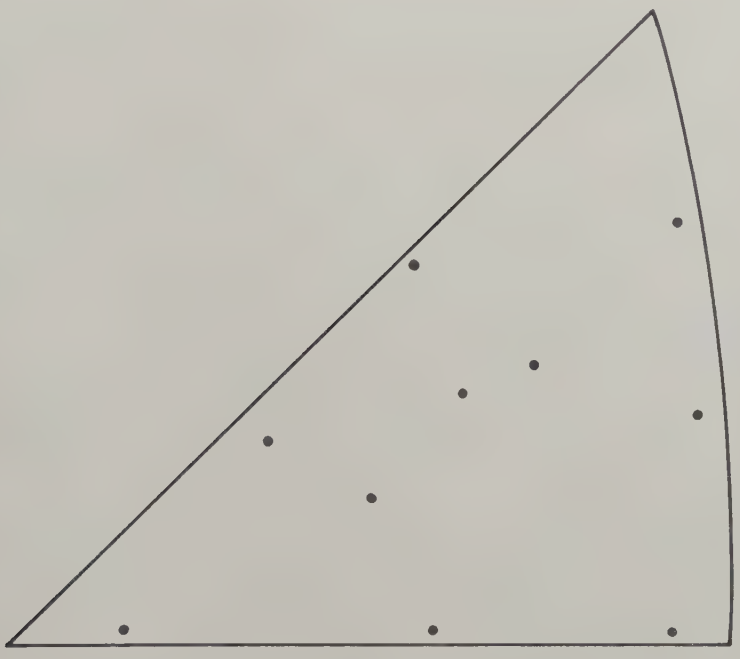

The directions selected for the sections referred to a unit stereographic triangle.

X-ray photographs made by a glancing incidence technique were used to investigate the effect of the preferred orientations in the individual sectors on the resultant Debye–Scherrer rings. Individually, the sectors produced rings whose intensities varied markedly round their peripheries but on rotating the specimen in its own plane, so that the sectors were presented in turn to the incident beam, Debye–Scherrer rings were obtained which showed no variation in intensity around their peripheries. The x-ray patterns obtained for the 111 and 200 reflections are shown in fig. 5 (Pl. 54). The central pattern is that obtained whilst rotating the composite specimen and the outer ten patterns are those obtained from the individual sectors.

4.2. *Experimental Method*

The diffraction pattern for the deformed specimen was measured first. The specimen with a thermocouple attached was then placed in a stainless steel tube and heated in an atmosphere of nitrogen at a rate of 6°C per min to 110°C. The tube was then cooled rapidly with water to room temperature and the diffraction pattern measured. The specimen was then replaced in the stainless steel tube and heated in nitrogen as quickly as possible to 110°C and then at 6°C per min to 235°C. It was then withdrawn, cooled as before and the diffraction pattern measured. This process was repeated for temperatures of 320°C, 420°C, 480°C, 540°C, 600°C and 700°C.

The x-ray diffraction patterns were measured with a Geiger-counter spectrometer using monochromatic Cu Kα radiation obtained by reflection from a crystal of lithium fluoride (Michell and Haig 1957). The 111, 222, 200 and 400 lines were measured in detail. Sufficient counting time was spent on the 311 line to enable graphical resolution of the tail of the 222 line to be made. The 331 line was measured in detail for the specimen in the deformed state, after the anneal to 420°C and in the fully annealed state. The total counting time spent on each pattern was approximately 45 hours and more than half of this was spent in measuring the background intensities and the tail regions to the lines.

Before and after each pattern was measured, the peaks of the 111 and 331 lines of a reference specimen of annealed nickel were scanned so that corrections could be applied for changes in sensitivity of the spectrometer. As the standard deviation of the reference peaks observed during the nine weeks of the experiment was only 1·2%, no corrections have been made for this effect.

All measurements have been corrected for the dead time of the counter (600 μs), for the wave shape of the x-ray output from the monochromator and for the background level of the counter in the absence of x-rays (constant at 45 counts per min).

§ 5. Results of the X-ray Measurements

The diffraction pattern obtained after heating the specimen to 700°C has not been analysed in detail since it was not significantly different from that obtained after heating to 600°C.

5.1. *Background Level*

The background levels of the diffraction patterns were determined by the method employed by Hall and Williamson (1951) and Michell and Haig (1957). At angles of 35°, 64°, 110° and 127° in 2θ there appeared to be no overlapping of the tails of adjoining lines. The intensities at these angles are shown in fig. 6. Since the probable error in each of these intensities is less than one count per min, it is apparent that the intensity at each of these angles is effectively independent of the temperature of annealing and has therefore been taken as the background level at that

Fig. 6

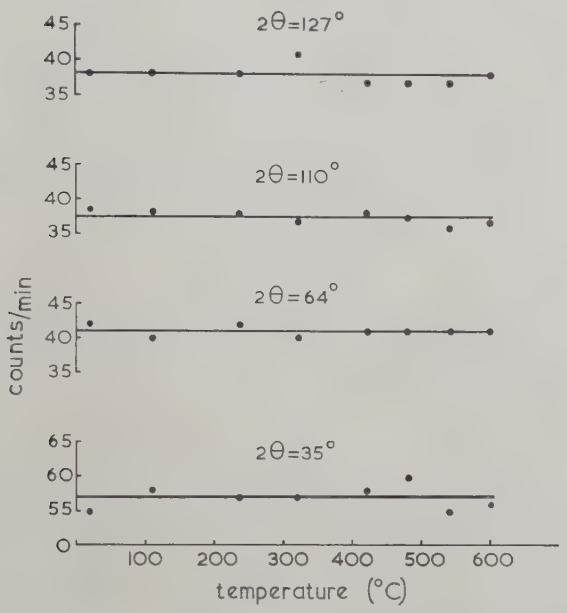

Corrected x-ray intensities at 35°, 64°, 110°, and 127° in 2θ as functions of the temperature of annealing.

Fig. 7

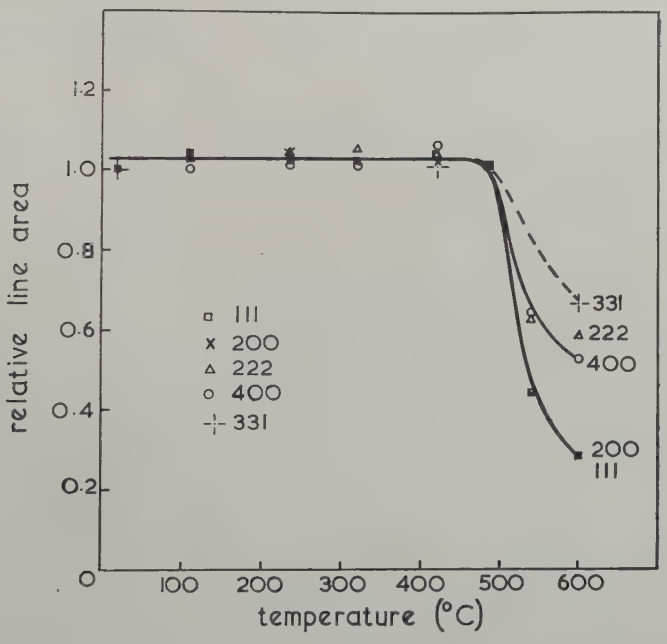

Integrated intensities of the 111, 200, 222, 400, and 331 reflections relative to the integrated intensities from the deformed specimen, as functions of the temperature of annealing.

particular angle. The background level at other angles has been taken to be that found by linear interpolation between these values.

5.2. *Integrated Intensities of the Lines*

The areas of the 111, 200, 222 and 400 lines above the background level have been computed and their variation with the temperature of annealing is shown in fig. 7. In no case does any significant change in area occur at temperatures of annealing below 480°C but in all cases a marked decrease in the areas of all lines occurs on annealing to 600°C.

5.3. *Position of the Maxima of the Diffraction Lines*

Examination of the positions of the peaks of the resolved α_1 components of the measured lines, as a function of temperature of annealing, shows no evidence for stacking faults (Paterson 1952) or change in lattice parameter, within the experimental error of $\pm 0{\cdot}01°$ in 2θ.

5.4. *Shape of the Diffraction Lines*

Inspection of the line profiles when plotted on an extended intensity scale and compressed angular scale shows that in the deformed state the lines have tails which extend for several degrees. Only small changes in the line shapes occur during annealing to 480°C and the maximum change in peak height is approximately 10%. On heating above 480°C, the line shapes change markedly particularly in the central regions. The width of all lines decreases but the peak height does not increase correspondingly since the integrated intensity decreases. In fact, the peak height of the 111 line decreases from 24 000 c.p.m. at 480°C to 8500 c.p.m. at 600°C. The decrease in intensity in the tail regions of the lines, after heating the specimen to 600°C, appears to be much less than the decrease in intensity in the central regions of the lines.

The decrease in integrated intensity cannot be due to a change in texture since x-ray photographs show that the 111 and 200 Debye–Scherrer rings are still uniform. However, the following experiment shows that it can be attributed to extinction.

The annealed specimen was lightly ground on 600 carborundum paper to reduce the perfection of the crystals at the surface and thus reduce any extinction. After this treatment the integrated intensities of the lines were found to have increased to about the values obtained for the deformed specimens and the peak height of the 111 line was approximately 27 000 c.p.m. The breadth of the 331 line was only slightly greater than that from the annealed specimen, indicating that the strains introduced by the grinding were less than 1% of those introduced by the original deformation. The surface layer was then removed in stages by electropolishing and measurements of the peak heights of the lines and the breadth of the 331 line made at each stage. At first, the peak heights of the lines increased and the breadth of the 331 line decreased, but after the removal of 10–20 μ of surface the peak heights began to decrease until after the

removal of approximately 100 μ of surface the peak of the 111 line was 9900 c.p.m. The initial increase in peak height is probably due to a decrease in line breadth following the removal of the more severely deformed surface layer. However, the removal of additional surface material exposes more perfect grains and, although the line breadth continues to decrease, the rapid decrease in integrated intensity substantially reduces the peak height. It may therefore be concluded that the decrease in intensity on annealing to 600°C is due to extinction.

§ 6. Analysis of the Diffraction Patterns

6.1. *Extinction*

It is difficult to calculate the integrated intensity from a crystal when its state of perfection is unknown. However, equations for the two extreme cases (i.e. the ideally perfect and the ideally imperfect mosaic) have been derived (James 1948).

Some idea of the extent of perfection in the grains of the nickel specimen may be gained by comparing the ratio of the theoretical integrated intensities of the ideally imperfect crystal (ρ_{mosaic}) and the ideally perfect crystal (ρ_{perfect}) with the ratio of the areas of the lines after deformation (A_{deformed}) and after heating to 600°C (A_{annealed}). These ratios are listed in table 1.

Table 1. Comparison of the Theoretical and Measured Relative Intensities from 'Perfect' and 'Imperfect' Nickel

Line	$\frac{\rho_{\text{mosaic}}}{\rho_{\text{perfect}}}$ Theoretical	$\frac{A_{\text{deformed}}}{A_{\text{annealed}}}$ Measured
111	8·8	3·6
200	7·9	3·6
222	5·5	1·8
400	4·6	1·9
331	4·3	1·5

The integrated intensities in the deformed state are probably given by the equation relating to the ideal mosaic and the results indicate that in the annealed state, although the perfection of the grains has increased, either the size or the degree of perfection of the perfect regions is less than that assumed in the derivation of the equation for intensity reflected by an ideally perfect crystal.

The decrease in the integrated intensity from crystals more perfect than the ideal mosaic may be due to either primary or secondary extinction. The application of a number of formulae for extinction (Williamson and Smallman 1955) to the results for the nickel failed to produce conclusive

evidence for the type of extinction present. It seems reasonable to assume, however, that on annealing to 600°C, regions of high perfection were produced and that considerable primary extinction was present. That the decrease in intensity for bulk specimens was considerably greater than the corresponding change in intensity previously observed from nickel powder (Michell and Haig 1957) may be attributed to the fact that the grain size of the powder after recrystallization was 2-3 μ compared with 30-40 μ for the bulk material. This larger grain size, together with the higher purity of the nickel (99·85%) used in the present experiments, would probably lead to the production of regions of greater perfection in the annealed state than those produced in the powder of lower purity (99·6%).

If the whole decrease in integrated intensity is attributed to primary extinction, an estimate of 2–4 μ for the size of the perfect regions is obtained from the classical Darwin formula. In order to ascertain whether a substructure of this dimension was present, the specimen was examined with an optical microscope and an x-ray micro-beam technique capable of resolving misorientations of the order of 20 min of arc. No substructure was detected either in the fully annealed state, after lightly grinding the surface, or during various stages of the removal of the surface layer by electropolishing. Although the results of these experiments were negative, the possibility of a substructure cannot be excluded since misorientations of only 20–30 sec between subgrains would be sufficient to produce a mosaic as detected by x-rays.

6.2. *Integral Line Breadths*

The integral breadths have been calculated for all the measured lines. For a line from a deformed specimen the integral breadth is usually corrected for instrumental broadening by subtracting the integral breadth of the corresponding line from an annealed specimen. However, in this work extinction rendered the integral breadths of the lines in the annealed state unsuitable since it appears to reduce the intensity of the central region of the lines far more than the extremities; neither could the line shapes measured after lightly grinding the surface of the annealed specimen be used, since the grinding broadened the lines by a measurable amount. Similarly, the lines from annealed powder specimens were unsuitable since, in some cases, they were broader than the corresponding lines from the solid specimen after surface deformation by grinding. This effect is probably due to the lower density of the powder specimens which results in greater penetration of the x-rays into the surface.

The integral breadths finally used as corrections for instrumental broadening were obtained in the following way. In the absence of extinction, the general equation of a line profile of a particular reflection was assumed to vary throughout the annealing treatment only by scale factors. Therefore, the ratio of breadth at half height to integral breadth, for the reflection, should be independent of the state of annealing. This constant

was evaluated from the ratio in the deformed states and applied to the breadth at half height in the annealed state. As the grinding experiments indicated that the breadth at half height was affected much less by extinction than the integral breadth, there resulted an estimate of the integral breadth which would have occurred, but for extinction, in the annealed state.

The derived value for the 111 line was 10% lower than that obtained from the measured profile, but in the case of the high angle lines which were least affected by extinction, there was good agreement between the calculated and observed integral breadths.

Fig. 8

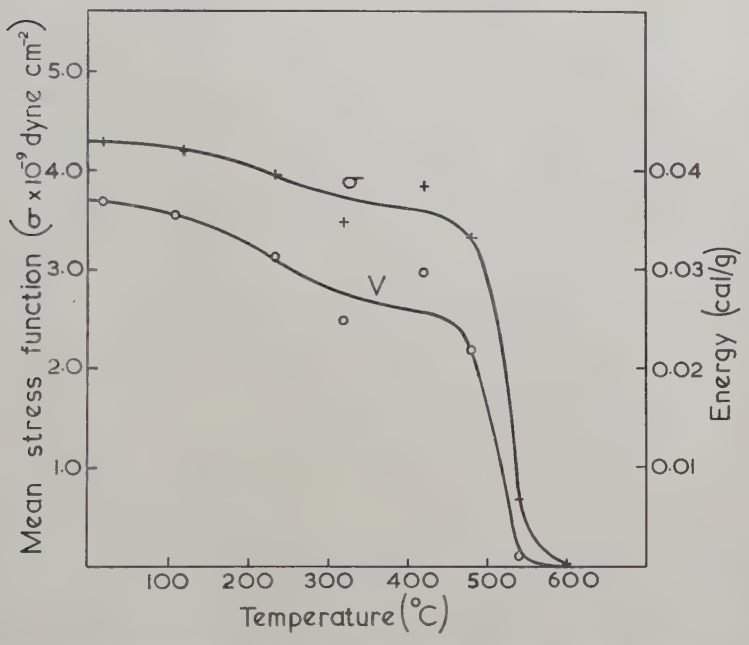

Results of the analysis of the line breadths. Mean stress function, σ, and calculated stored energy, V, as functions of the temperature of annealing.

The integral breadths β of the lines after correction for instrumental broadening were investigated by the method proposed by Hall (1949) and Mazur (1949) and used by Michell and Haig (1957) to give values of 'apparent particle size' t and mean stress function σ. The results indicated that particle size broadening was small. Although no significance could be attached to the variation of particle size with annealing temperature, a minimum estimate of particle size in the deformed state was 10^4 Å. The 'mean stress functions' are shown in fig. 8 as a function of annealing temperature. The r.m.s. stress, $\sigma_{\text{r.m.s.}}$, will depend on the actual stress distribution but, as this distribution is unknown, we assume that $\sigma_{\text{r.m.s.}}$ is equal to the 'mean stress function'. Values of stored energy V have

then been computed from the equation $V = 3\sigma_{\text{r.m.s.}}{}^2/2E$, where E is an average value of Young's modulus: (see Stibitz (1936), Faulkner (1960)), and are plotted as a function of temperature in fig. 8.

6.3. *Fourier Analyses of the Line Profiles*

The Fourier coefficients $A_n (n = 1$ corresponds to the repeat distance a_3 of the unit cell) for the low angle halves of the resolved α_1 components of the measured lines were determined directly with an electronic computer (CSIRAC) and were corrected for instrumental broadening by the method of Stokes (1948). In this correction a knowledge of the line shapes obtained from the annealed material in the absence of extinction is required. As these line shapes could not be measured directly they were approximated in the following way. The peak heights were calculated from the integral breadths derived in § 6.2 and the integrated intensities in the deformed state. The region over which the intensities remained substantially unaffected by extinction was determined from the grinding experiments. Between this region and the peak, the measured ordinates were adjusted by a factor which varied linearly with 2θ, decreasing from the value, calculated peak height/measured peak height, at the peak of the line to unity at the region unaffected by extinction. This method of adjustment for extinction was the most satisfactory of several which were tried as it gave the best agreement with the line shapes measured on surface ground specimens.

Fig. 9

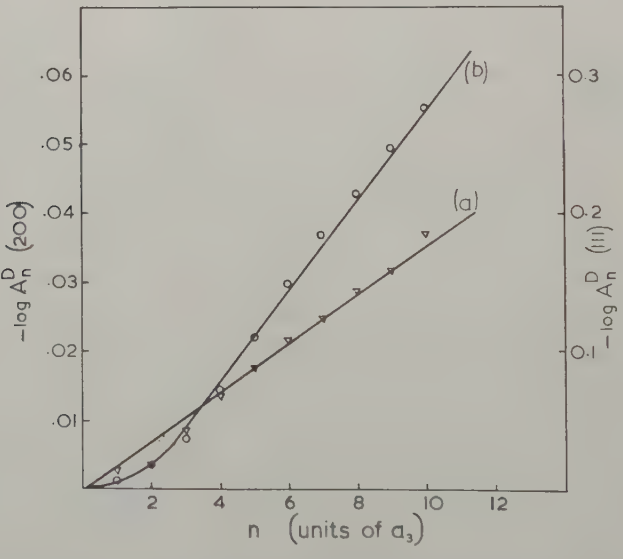

Logarithm of the Fourier coefficients of the strain broadening, $\log A_n{}^D$, after separation of the particle size effects by method 1 (*a*), as a function of the order n of the coefficients; (*a*) 111 and 222 reflections, and (*b*) 200 and 400 reflections.

Fig. 10

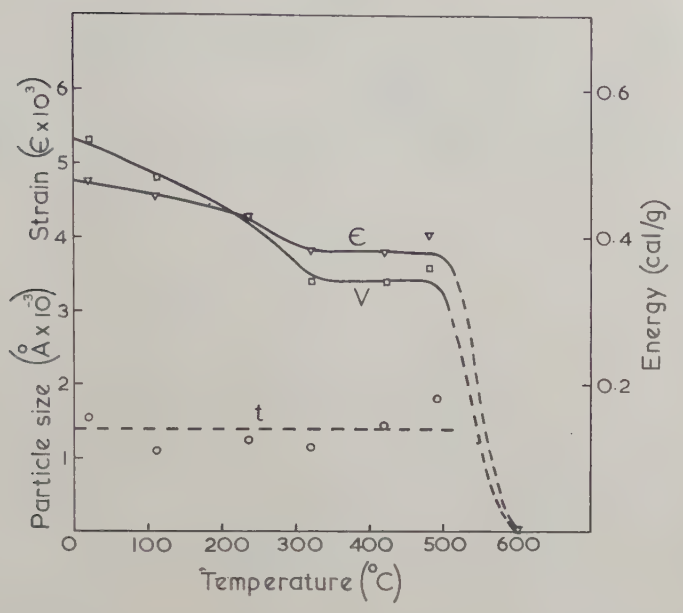

(*a*)

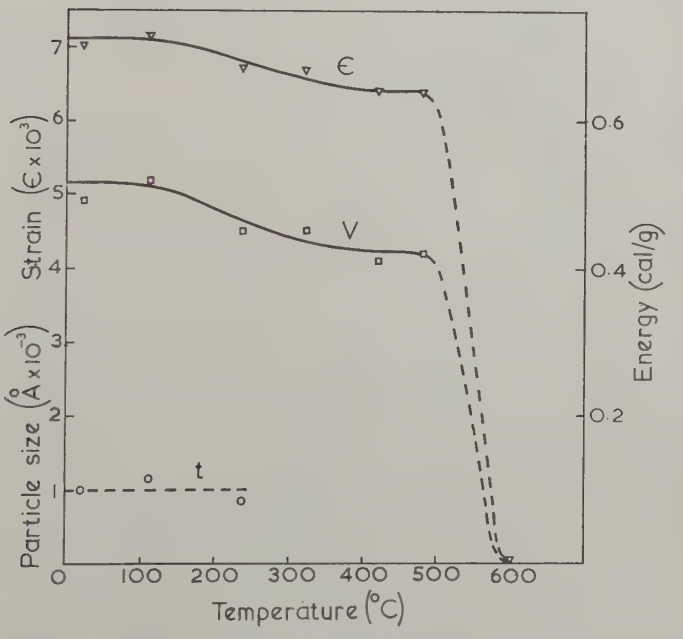

(*b*)

Results of the Fourier analysis (Gaussian distribution of strain). Apparent particle size, t, root mean square strain ϵ, and stored energy, V, as functions of the temperature of annealing: (*a*) for the 111 and 222 reflections, and (*b*) for the 200 and 400 reflections. No reliable estimate of t could be made for temperatures above 235°C for case (*b*).

Table 2. Summary of Results of Analyses

(*a*) 111–222 reflections

Annealing temperature (°C)	Analysis 1 *a* Gaussian strain distribution. Broadening due to strain and particle size			Analysis 1 *b* Gaussian strain distribution. Broadening due to strain only		Analysis 2 *a* Cauchy strain distribution. Broadening due to strain and particle size			Analysis 2 *b* Cauchy strain distribution. Broadening due to strain only	
	r.m.s. strain ($\times 10^3$)	Stored energy (cal/g)	Particle size (Å)	r.m.s. strain ($\times 10^3$)	Stored energy (cal/g)	r.m.s. strain ($\times 10^3$)	Stored energy (cal/g)	Particle size (Å)	r.m.s. strain ($\times 10^3$)	Stored energy (cal/g)
20	4·75	0·53	1540	5·37	0·68	9·0	1·92		8·4	1·66
110	4·52	0·48	1100	5·37	0·68	8·6	1·75		8·4	1·66
235	4·28	0·43	1280	5·06	0·61	8·1	1·55	No	7·9	1·48
320	3·80	0·34	1160	4·80	0·55	7·2	1·22	real	7·5	1·33
420	3·80	0·34	1440	4·80	0·55	7·2	1·22	values	7·5	1·33
480	3·92	0·36	1800	4·72	0·53	7·4	1·30	obtainable	7·4	1·30

(*b*) 200–400 reflections

Annealing temperature (°c)	Analysis 1 *a* Gaussian strain distribution Broadening due to strain and particle size			Analysis 1 *b* Gaussian strain distribution Broadening due to strain only		Analysis 2 *a* Cauchy strain distribution Broadening due to strain and particle size			Analysis 2 *b* Cauchy strain distribution Broadening due to strain only	
	r.m.s. strain ($\times 10^3$)	Stored energy (cal/g)	Particle size (Å)	r.m.s. strain ($\times 10^3$)	Stored energy (cal/g)	r.m.s. strain ($\times 10^3$)	Stored energy (cal/g)	Particle size (Å)	r.m.s. strain ($\times 10^3$)	Stored energy (cal/g)
20	7·0	0·49	1000	7·3	0·53	15·2	2·30		13·0	1·69
110	7·2	0·52	1160	7·4	0·55	15·6	2·44	No	13·2	1·74
235	6·7	0·45	840	6·9	0·48	14·5	2·10	real	12·3	1·51
320	6·7	0·45	—	7·2	0·52	14·5	2·10	values	12·8	1·64
420	6·4	0·41	—	7·1	0·50	13·9	1·92	obtainable	12·6	1·59
480	6·5	0·42	—	7·15	0·51	14·1	1·98		12·6	1·59

(*c*) 331 reflection

Annealing temperature (°c)		Analysis 1 *b* Gaussian strain distribution Broadening due to strain only			Analysis 2 *b* Cauchy strain distribution Broadening due to strain only	
		r.m.s. strain ($\times 10^3$)	Stored energy (cal/g)		r.m.s. strain ($\times 10^3$)	Stored energy (cal/g)
20		4·1	0·32		11·3	2·4
420		4·1	0·32		11·3	2·4

The derived coefficients of the lines, from the nickel when annealed to various temperatures up to 600°C, were analysed by the following methods:

1. The methods of Warren and Averbach (1949, 1950, 1952) for strain distributions which are Gaussian.

(*a*) The broadening was attributed to the simultaneous effects of small particle size and strain, and values of the strain coefficients A_n^D and the particle size coefficients A_n^P were deduced. As shown in fig. 9, $\log A_n^D$ is a linear function of n over the range $n=2$ to $n=10$, and for the coefficients derived from the 111 and 222 lines a reasonable line of fit can be drawn through the origin (curve (*a*)). This indicates that for the range of n considered here the profile for these reflections may be represented by a Cauchy function. Williamson and Smallman (1954) have pointed out that an incorrect choice of background level or inaccurate measurements in the tail regions may cause the plot of $-\log A_n^D$ against n for a Cauchy profile to be of the form shown in fig. 9, curve (*b*), and that the linear section is approximately parallel to the straight line through the origin representing the same Cauchy profile without tail or background errors. The broadening profile we derived from the coefficients A_n^D for the 200 and 400 lines was a reasonable approximation to a Cauchy profile of the same breadth which had been analysed with an assumed background level too high by $1-2\%$ (i.e. $1-2$ counts per min). As such an error in assumed background level was within the experimental accuracy, the values of $\log A_n^D$ for $n=1$ were derived from the slopes of the linear sections of the curves.

Using this method, the coefficients of the 111 and 222, and 200 and 400 reflections were analysed. The results are shown in fig. 10 and also in table 2.

(*b*) All the broadening was attributed to strain and values of strain were obtained from the coefficients to the 222, 400, and 331 reflections.

2. The methods suggested by Williamson and Smallman (1954), based on the assumption that the strain distribution was a Cauchy function.

(*a*) The broadening was attributed to the simultaneous effects of small particle size and strain. Separation of these effects by a plot of $\log A_n$ against $l_0=\sqrt{(h^2+k^2+l^2)}$ where h, k, l are the usual indices of reflection, resulted in nonsensical values of particle size ($A_n^P>1$) for the 111 and 222, and 200 and 400 reflections and therefore the derived values of strain are also doubtful.

(*b*) The 222, 400, and 331 coefficients were analysed, attributing all broadening to strain. The r.m.s. strain ϵ was calculated for a cut-off strain of 0·2.

In calculating stored energy from strain, Stibitz's equation has not been used since Faulkner (1960) using the same assumptions has shown it to be incorrect. Faulkner obtains the equation:

Energy stored in an isotropic material

$$V=\frac{15E}{2(3-4\nu+8\nu^2)}\overline{\left(\frac{\Delta D}{D}\right)^2},$$

where E is an average value of Young's modulus, ν is Poisson's ratio and $\overline{(\Delta D/D)^2}$ is the mean square value of the strain. This equation leads to energies of 2–3 times those obtained from Stibitz's equation. Since nickel is anisotropic only approximate values of energy have been obtained from the derived strains using the value of Young's modulus E_{hkl} appropriate to the direction of the strains.

The results of all the Fourier analyses are summarized in table 2.

§ 7. Discussion

7.1. *Stored Energy*

The rate of release of energy ΔP as a function of temperature (fig. 1, curve A) is very similar to that obtained for specimens deformed by unidirectional compression. According to Clarebrough *et al.* (1960) the evolution of energy between 420 and 590°c is associated with the removal of dislocations during recrystallization, whereas the peak in the ΔP curve at 250°c is associated with the removal of vacancies. However, the ΔP curves for nickel of this purity (99·85% Ni) differ from those obtained for nickel of lower purity (99·6% Ni) used in previous work (Clarebrough *et al.* 1955, Michell and Haig 1957) in that the plateau region associated with the re-arrangement and annihilation of dislocations is absent. It is considered that in the higher purity nickel used here re-arrangement and annihilation of dislocations is complete by 300°c.

7.2. *X-ray Measurements*

The measurements made on bulk specimens of nickel indicate that any change in the background level is less than the experimental error, and that there is no detectable change in the position of the lines, which might be attributed either to variations in lattice parameter or to changes in stacking fault density. In these respects the results are in agreement with those of Michell and Haig (1957) from powdered nickel.

The large decrease of 30–75% in integrated intensity which occurred in all lines when the specimen was heated to temperatures above 480°c is attributed to extinction. Precise treatment of this phenomenon is difficult since the separation of extinction into two simple types is probably unjustified. However, the observed decrease in intensity may be explained qualitatively in terms of primary extinction. If the imperfections in the grains are due to dislocations, then an average spacing of 3μ between dislocations would produce misorientated blocks of the requisite size and result in a minimum dislocation density of 10^7 lines per cm^2 which is of the order of that expected for annealed specimens.

The decrease in intensity of the central portion of the lines without a corresponding decrease in the tails observed after heating above 480°c suggests that even in the annealed state there are some regions within the grains which are more perfect than others. Since the tails are produced

by the less perfect regions, it seems reasonable to deduce that they are less affected by extinction than the central portion of the lines which is more dependent on the perfect regions.

The assumptions made in correcting the integral breadths for instrumental broadening in the line broadening analyses (§ 6.2) are not serious, but those made in approximating to the line profiles (§ 6·3) in the annealed state are of greater consequence. The approximations made should not introduce an error greater than 10% in the values of stored energy shown in table 2 but may introduce a considerable error in the value of the 'apparent particle size'. Since the broadening due to the 'particle size' effect is small anyway, too much reliance should not be placed on these values. The various methods of analysis give qualitatively similar results indicating that there is a small decrease in lattice strain on annealing below 480°C and then a sharp decrease on annealing above 480°C. This is in general agreement with the measured release of stored energy.

Quantitatively, however, the various methods give different values of lattice strain and energy. The energies derived from the line broadening analyses (§ 6.2) are an order of magnitude too small, but from the line shape analysis (§ 6.3), assuming a Cauchy strain distribution, the energies are 5–10 times greater than the measured values. The results from the Warren and Averbach treatment (fig. 1 C) are almost twice the measured values of stored energy (fig. 1 B) but suggest that in the present work a Gaussian distribution of strain is the most reasonable approximation to that present in the metal.

The disagreement between the measured and calculated energies is disappointing but it should be remembered that the value of strain derived from the Warren and Averbach type of analysis is dependent on the distance L over which the strain is calculated. If the high strain in the immediate neighbourhood of a dislocation is to be included, this distance should be small and it seems likely that energies calculated from

$$\frac{\langle \Delta L^2 \rangle^{1/2}}{L} \quad \text{for} \quad L \to 0$$

will include almost all the energy associated with isolated dislocations, low angle boundaries, etc. In practice, it is difficult to determine accurately values of

$$\frac{\langle \Delta L^2 \rangle^{1/2}}{L} \quad \text{for} \quad L \to 0$$

due to the difficulties in measuring the tails of the line profiles and it is necessary to choose some finite value of L over which the displacements are averaged. In the present work, this distance has been selected as a_3 ($6-7$ Å for the 111 and 200 reflections and 15 Å for the 331 reflection) and values of $\langle \Delta L^2 \rangle^{1/2}$, $(L = a_3)$ have been obtained by assuming that $-\log A_n{}^D$ (or ΔL^2) is proportional to L. Although this assumption is within the experimental accuracy, it seems unlikely that it is correct since it leads to

$$\frac{\langle \Delta L^2 \rangle^{1/2}}{L} \to \infty \quad \text{for} \quad L \to 0.$$

This assumption almost certainly leads to values of

$$\frac{\langle \Delta L^2 \rangle^{1/2}}{L}, \quad \text{for} \quad L = a_3,$$

which are too high.

Values of strain derived from a Cauchy strain distribution cut off at a strain of 0·2 lead to energies considerably in excess of those measured directly and it seems that for bulk specimens of nickel this distribution is too extreme. Michell and Haig (1957) postulated a strain distribution based on the Gay, Hirsch and Kelly model for a deformed metal. It was suggested that the distribution may be a weighted sum of two simple distributions, one for the comparatively low strain regions within the particles and another for the highly strained boundary regions. For powder where the volumes of the two regions are of comparable magnitude, the resulting strain distribution probably has large tails due to the highly strained boundary regions. For the bulk specimens of nickel, the 'particle size' is considerably larger than for the powder and, since the strain is lower, the contribution of the boundary regions to the composite strain distribution is probably much less than that from the particles themselves. The resultant distribution thus approximates to the simple one representing the particles alone. It appears from this work that a Gaussian function is a reasonable approximation to the strain distribution in bulk specimens of nickel.

Acknowledgments

We wish to thank Dr. Boas for his continued interest and encouragement. The stored energy measurements were made by L. M. Clarebrough, M. E. Hargreaves and G. W. West, and the authors are particularly grateful for this cooperation. We should also like to thank J. F. Nicholas for many helpful discussions, G. J. Ogilvie for a number of valuable suggestions concerning specimen preparation, and D. L. Grubb who constructed the specimens with care and patience.

References

Clarebrough, L. M., Hargreaves, M. E., Loretto, M. H., and West, G. W., 1960, *Acta Met.* (in press).

Clarebrough, L. M., Hargreaves, M. E., Michell, D., and West, G. W., 1952, *Proc. roy. Soc.* A, **215,** 507.

Clarebrough, L. M., Hargreaves, M. E., and West, G. W., 1955, *Proc. roy. Soc.* A, **232,** 252.

Faulkner, E. A., 1960, *Phil. Mag.*, **5,** 519.

Gay, P., Hirsch, P. B., and Kelly, A., 1954, *Acta Cryst.*, **7,** 41.

Hall, W. H., 1949, *Proc. phys. Soc. Lond.* A, **62,** 741.

Hall, W. H., and Williamson, G. K., 1951, *Proc. phys. Soc. Lond.* B, **64,** 937, 946.

James, R. W., 1948, *The Optical Principles of the Diffraction of X-rays. The Crystalline State*, Vol. II (London : G. Bell and Sons), p. 269.

Mazur, J., 1949, *Nature, Lond.*, **164,** 358.

Michell, D., and Haig, F. D., 1957, *Phil. Mag.*, **2,** 15.
Mitchell, C. M., and Rowland, J. F., 1954, *Acta Met.*, **2,** 559.
Paterson, M. S., 1952, *J. appl. Phys.*, **23,** 805.
Stibitz, G. R., 1936, *Phys. Rev.*, **49,** 862.
Stokes, A. R., 1948, *Proc. phys. Soc. Lond.*, **61,** 382.
Warren, B. E., and Averbach, B. L., 1949, *J. appl. Phys.*, **20,** 1066 ; 1950, *Ibid.*, **21,** 595 ; 1952, *Ibid.*, **23,** 497.
Williamson, G. K., and Smallman, R. E., 1954, *Acta Cryst.*, **7,** 574 ; 1955, *Proc. phys. Soc. Lond.*, **68,** 577.

Calculation of Stored Energy from Broadening of X-ray Diffraction Lines†

By E. A. Faulkner
Division of Tribophysics, Commonwealth Scientific and Industrial Research Organization, University of Melbourne

[Received February 16, 1960]

Abstract

A new calculation is made of the stored energy in a deformed isotropic material, in terms of the mean-square lattice strain. An isotropic stress distribution is assumed.

From the broadening of x-ray reflections in deformed metals it is possible to deduce $\overline{(\Delta d/d)^2}$, the mean-square variation in the separation d of the lattice planes contributing to the reflection. From this a calculation may be made of the energy stored in the material, if assumptions are made about the distribution of the stress components in the specimen. In this note this calculation will be carried out for an isotropic material, with assumptions leading to an isotropic stress distribution. An equation due to Stibitz (1937), which is based on the same assumptions and which has been widely quoted, will be shown to be incorrect.

The stress at any point in a crystal may be specified by the directions of the principal stress axes (x', y', z') and the magnitudes of the principal stresses $(f_{x'x'}, f_{y'y'}, f_{z'z'})$. We may define a mean-square principal stress f^2, and a stress correlation constant C, by the relations

$$\left.\begin{aligned} \overline{f^2_{x'x'}}+\overline{f^2_{y'y'}}+\overline{f^2_{z'z'}}&=3f^2, \\ \overline{f_{x'x'}f_{y'y'}}+\overline{f_{y'y'}f_{z'z'}}+\overline{f_{z'z'}f_{x'x'}}&=3Cf^2. \end{aligned}\right\} \quad . \; . \; . \quad (1)$$

The corresponding principal strains are given by expressions like

$$e_{z'z'}=(f_{z'z'}-\nu f_{x'x'}-\nu f_{y'y'})/E, \quad . \; . \; . \; . \; . \quad (2)$$

where E is Young's modulus and ν is Poisson's ratio.

The quantity $\Delta d/d$ is equal to the strain component $e_{z''z''}$ where the z'' axis is the direction of the normal to the planes concerned in the reflection. If (l, m, n) are the direction cosines of the z'' axis relative to the principal stress axes at any point, we have for the mean-square value of $\Delta d/d$ over all parts of the crystal

$$\overline{\left(\frac{\Delta d}{d}\right)^2}=\overline{e^2_{z''z''}}=\overline{(n^2e_{z'z'}+l^2e_{x'x'}+m^2e_{y'y'})^2}. \quad . \; . \; . \; . \quad (3)$$

† Communicated by Dr. W. Boas.

We now assume that there is no correlation between the magnitudes of the principal stress components and the direction cosines of their axes, and, furthermore, that the axes are isotropically distributed; this implies an isotropic distribution of both stress and strain. Combining eqns. (1), (2), and (3), and using this assumption, we obtain

$$\overline{\left(\frac{\Delta d}{d}\right)^2} = \frac{f^2}{5E^2}[3-4\nu+8\nu^2+2C(1-8\nu+6\nu^2)]. \quad . \quad . \quad (4)$$

The stored energy is given by

$$V=\tfrac{1}{2}(\overline{f_{x'x'}e_{x'x'}}+\overline{f_{y'y'}e_{y'y'}}+\overline{f_{z'z'}e_{z'z'}})=\frac{3f^2}{2E}(1-2C\nu), \quad . \quad . \quad (5)$$

so the resulting expression for the stored energy in terms of the mean-square variation in the separation of the lattice planes is

$$V=\frac{15E}{2}\frac{1-2C\nu}{3-4\nu+8\nu^2+2C(1-8\nu+6\nu^2)}\overline{\left(\frac{\Delta d}{d}\right)^2}. \quad . \quad . \quad . \quad (6)$$

It is now necessary to make a further assumption about the strain distribution in the crystal, in order to assign a value to the constant C. There are several relatively simple assumptions which may be made, of which two will be discussed here:

(a) The three principal stress components are independently distributed, so that the mean value of products such as $f_{x'x'}f_{y'y'}$ is zero. This is the assumption that was made by Stibitz (1937) and corresponds to $C=0$. Equation (6) becomes

$$V=\frac{15E}{2(3-4\nu+8\nu^2)}\overline{\left(\frac{\Delta d}{d}\right)^2}=2{\cdot}93E\overline{\left(\frac{\Delta d}{d}\right)^2} \quad . \quad . \quad . \quad (6a)$$

where the expression has been evaluated for the typical case of $\nu=\frac{1}{3}$ in order to facilitate comparison with other results.

(b) Only shear stresses are present in the material, so that at every point the hydrostatic component $(f_{x'x'}+f_{y'y'}+f_{z'z'})$ is zero. This gives $C=-\frac{1}{2}$ and

$$V=\frac{15E}{4(1+\nu)}\overline{\left(\frac{\Delta d}{d}\right)^2}=2{\cdot}81E\overline{\left(\frac{\Delta d}{d}\right)^2}. \quad . \quad . \quad . \quad . \quad (6b)$$

A consideration of the strain field of an isolated dislocation in isotropic material shows that assumption (b) is probably the more realistic one; however, for $\nu=\frac{1}{3}$ the numerical coefficients are so similar that it is immaterial which of the two is adopted.

It will be seen that eqn. ($6a$) is different from the result

$$V=\frac{3E}{2(1+2\nu^2)}\overline{\left(\frac{\Delta d}{d}\right)^2}$$

which was obtained by Stibitz (1937) using the same assumptions and which, for $\nu=\frac{1}{3}$ gives

$$V=1{\cdot}23E\overline{\left(\frac{\Delta d}{d}\right)^2}.$$

In his approach to the problem, Stibitz treated the principal strains like the components of a vector, so his calculation leads to the result $\overline{e^2_{z''z''}} = \overline{e^2_{z'z'}}$ because in this case all sets of axes are equivalent. In fact, the principal axes (x', y', z') are not equivalent to any other set of axes because they are chosen so as to make $e_{x'y'} = e_{y'z'} = e_{z'x'} = 0$; the quantity $(e^2_{xx} + e^2_{yy} + e^2_{zz} + \frac{1}{2}e^2_{xy} + \frac{1}{2}e^2_{yz} + \frac{1}{2}e^2_{zx})$ is invariant under a rotation of axes, so that the value of $\overline{e^2_{z''z''}}$, where the z'' axis has no particular relation to the principal axes, must always be less than $\overline{e^2_{z'z'}}$.

There has been very little work in which a direct comparison has been made between calorimetrically measured values of stored energy and values calculated from x-ray line broadening. However, Michell and Haig (1957) made x-ray and calorimetric measurements on nickel which had been deformed by grinding, and calculated values of stored energy from the x-ray observations. On the assumption that the strain distribution function was of the Cauchy type with strain cut-off values of 0·2, and using Stibitz' equation with $\nu = 0{\cdot}3$, they obtained values of V which were lower than the calorimetrically measured values by a factor of about 2·5. The use of the corrected expression (6*b*) would raise the calculated values by a factor of 2·3 and so give a much better agreement between the two figures.

References

Michell, D., and Haig, F. D., 1957, *Phil. Mag.*, **2**, 15.
Stibitz, G. R., 1937, *Phys. Rev.*, **52**, 619.

CORRESPONDENCE

Statistical Methods in Rock Magnetism

By S. K. Runcorn
King's College, Newcastle upon Tyne

[Received February 18, 1960]

Research workers in palaeomagnetism have hitherto found it useful in their assessment of the precision of a set of directions of magnetization determined from a geological formation to use the statistical method introduced by Fisher (1953). Fisher takes as a standard frequency distribution function $f(\theta)$ the following:

$$f(\theta) = \frac{1}{2 \sinh K} \exp(K \cos\theta) \quad . \quad . \quad . \quad . \quad . \quad . \quad (1)$$

where K is a statistic of precision and θ the angle with the true direction. Fisher shows that the maximum likelihood estimate of the true direction is the vector mean direction and of K is $N-1/N-R$ where R is the length of the vector sum of the N directions, each represented by unit vectors.

Fisher further shows how an angle of confidence, α, may be calculated such that the mean direction makes an angle less than the true direction with a probability of 95%.

Wilson (1959) objects to this usage on the ground that all distributions of directions of magnetizations may not follow this law and that, in consequence, the angle of confidence calculated above may "contain falsely implied precision". He proposes instead that workers in this subject should use the following mean cosine. which is the analogue of the variance in Gaussian statistics:

$$1 - \tfrac{1}{2}\delta^2 = \overline{\cos\delta} = \frac{S \cos\delta_i}{N} \quad . \quad . \quad . \quad . \quad . \quad . \quad (2)$$

where δ_i is the angular deviation of a single reading from the vector mean, and the following expression to correspond to the standard error of the mean of Gaussian statistics:

$$\epsilon = \frac{\delta}{\sqrt{N}} = \sqrt{\left\{\frac{\overline{\cos\delta}}{N}\right\}}. \quad . \quad . \quad . \quad . \quad . \quad . \quad (3)$$

In this way Wilson believes that the assumption of law (1) has been avoided. This view is wrong. It is, of course, possible to define a quantity from the sample of directions determined by eqn. (2) without assuming it is a sample drawn from an infinite population described by (1), just as it is possible to define a standard deviation in statistics of a single variation,

without assuming the sample to have been drawn randomly from a population following the normal law. But while both these quantities are dependent on the scatter of the measurements, their real significance depends on the probability distribution law, for one can think of such laws which would have only one per cent or as many as ninety-nine per cent of the observations lying outside the 'standard deviation' defined in this way!

We use the statistical methods based on the Gaussian law in the case of one variate and on law (1) in the case of dispersion on a spherical surface because, in physics and geophysics, scatter is usually due to a number of unrelated causes. Where one has good reason to believe the scatter is due to a single cause, such as the varying amounts of magnetization along the present field sometimes superposed on the original direction of magnetization of a rock, common sense prevents use of the statistical methods in the straightforward form described above.

References

Fisher, R. A., 1953, *Proc. roy. Soc.* A, **217,** 295.
Wilson, R. L., 1959, *Phil. Mag.*, **4,** 750.

The K Emission Spectrum of Metallic Lithium

By R. S. Crisp and S. E. Williams
University of Western Australia, Nedlands, Western Australia

[Received March 17, 1960]

Several authors have published lithium K spectra obtained from solid and evaporated targets. Although it has been well established that the maximum intensity does not occur at the high-energy edge as in sodium, it has also been concluded that Li does not exhibit the high-energy edge which, as a conductor, it should possess (Catterall and Trotter 1959).

We have previously published (Fisher *et al.* 1958) a K spectrum taken from a solid target of Li which indicates the existence of such an edge, though the resolution in this case was only 0·23 ev, the vacuum conditions not very good, the target energy 24 w, and the target temperature unknown. The width of the edge from 5% to about 80% of the maximum intensity is 0·47 ev, including the instrumental width.

Technical improvements made since this spectrum was obtained have enabled us to record the Li K spectrum in the third order of a 1 m glass grating under improved vacuum conditions in which there was virtually no target contamination and for which the Li, an evaporated layer on a copper target, was essentially at the cooling water temperature. The target energy was 4 w. The spectrum as directly recorded (one of several) is shown in fig. 1. The resolution of 0·9 A is calculated according to the criteria of Fisher (1954), the slit widths being 40 μ and the 1 m grating having 576 grooves per millimetre. This is equivalent to an energy resolution of 0·07 ev using the third order of Li K.

The spectrum clearly shows a high-energy edge, characteristic of an unfilled band, which extends to 75% of the maximum intensity where a discontinuity of slope can be seen. From this point to the maximum there occurs the ' roll over ' which has been attributed to the anisotropy of the Fermi surface. The first order spectrum also shows an edge extending to the same proportion of the maximum intensity. The width of the edge, including the instrumental window, is 0·30 ev. Our spectrum agrees with that of Skinner (1940) who found that at 300°K the edge width of Li K was 0·3 ev.

The spectrum obtained by Catterall and Trotter (1959) shows an edge width (to 75% of maximum intensity) of 0·55 ev, their resolution being given as 0·2 ev. The spectrum of Bedo and Tomboulian (1958), which has been plotted as a density of states curve, shows about the same width, though the instrumental window is given as 0·06 ev. A spectrum obtained by Bedo and published by Tomboulian (1957) suggests the presence of an edge.

Fig. 1

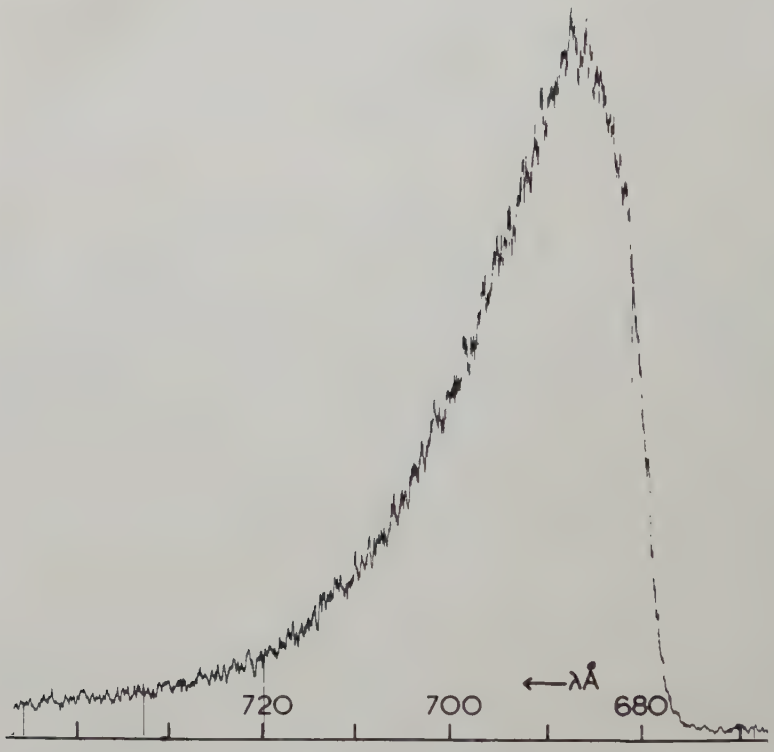

Recorder trace of Li K; 3rd order, target current 1 mA. volts 4000, target chamber pressure 10^{-6} mm, maximum count rate 640 per sec. Resolution 0·9 A. Scanning speed 8 A per min.

Fig. 2

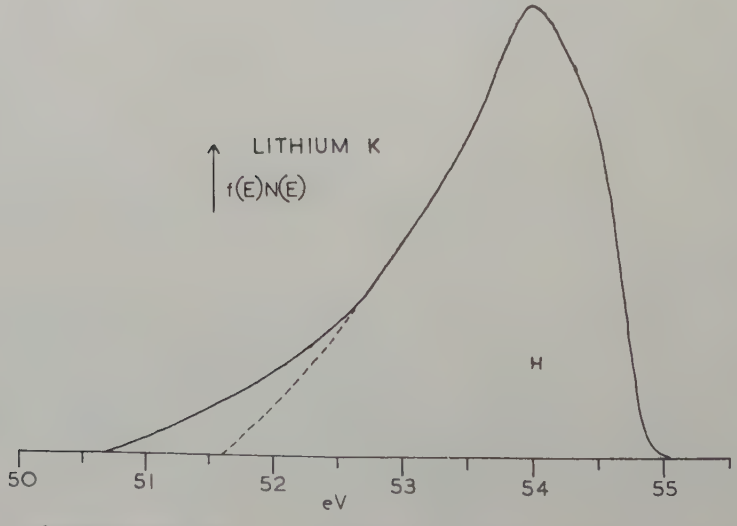

Density of states curve for Li K reduced from fig. 1, using $f(E)N(E)=\lambda^3 I(\lambda)$ (Crisp 1958). Width of the instrumental window is indicated.

The excess 'edge width' appearing in some of the published spectra would require the target temperature to be well over 700°K if temperature effects are to be invoked. The high-energy edge side of our spectrum shows a change of slope at 75% of maximum intensity and a marked lack of symmetry about the axis of half maximum intensity. These features can hardly arise from insufficient resolving power which would smooth the curve to a symmetrical form in which the presence of a true edge would be less apparent.

It would therefore appear unnecessary to seek a theoretical explanation for the non-appearance of a high energy edge in Li as some authors have done.

Figure 2 shows the density of states curve reduced from the intensity curve according to the formula $f(E)N(E)=\lambda^3 I(\lambda)$ which is accurate in the case of an instrument counting photons passing through a 'window' of fixed width (Crisp 1958).

Measurements on first-order spectra of sodium L (resolution 0·065 ev) and potassium M (resolution 0·024 ev) show edge widths of 0·21 ev and 0·19 ev respectively for evaporated layers on a copper target cooled to about 15°C. The relevant spectra will be published at a later date.

References

Bedo, D. E., and Tomboulian, D. H., 1958, *Phys. Rev.*, **109,** 35.
Catterall, J. A., and Trotter, J., 1959, *Phil. Mag.*, **4,** 1164.
Crisp, R. S., 1958, *Aust. J. Phys.*, **11,** 449.
Fisher, P., 1954, *J. opt. Soc. Amer.*, **44,** 665.
Fisher, P., Crisp, R. S., and Williams, S. E., 1958, *Opt. Acta*, **5,** 31.
Skinner, H. W. B., 1940, *Phil. Trans. roy. Soc.*, **239,** 95.
Tomboulian, D. H., 1957, *Handb. Phys.*, **30,** 246.

Diamagnetic Shielding of Nuclei in Metals

By T. P. Das†
Department of Chemistry, Columbia University, New York

and E. H. Sondheimer
Department of Mathematics, Queen Mary College, London

[Received April 7, 1960]

Nuclei in metals are generally found to have a larger Larmor frequency at a given magnetic field than in ions in solution or in non-metallic solids (Knight 1949). This paramagnetic Knight shift is usually explained as arising from the alinement of conduction electron spins in a magnetic field, which also gives rise to the Pauli spin paramagnetic susceptibility χ_p. The purpose of the present note is to point out that, in addition to their contribution to the paramagnetic shift through their spins, the conduction electrons may also produce an appreciable diamagnetic shift due to their orbital motion in a magnetic field. This orbital motion is known to produce the Landau diamagnetic contribution χ_d to the susceptibility (Landau 1930).

We have calculated the diamagnetic contribution to the nuclear resonance shift, for the case of free electrons, by an adaptation of the methods used by Sondheimer and Wilson (1951) and Hebborn and Sondheimer (1959) to calculate the diamagnetic susceptibility. We use perturbation theory to calculate the partition function $Tr\exp(-\mathscr{H}/kT)$ for an electron gas in the presence of the dipole field of a nucleus of magnetic moment μ_N (considered as fixed in direction) and a uniform applied magnetic field H. Plane waves are chosen as basis functions and all magnetic field terms in the electronic Hamiltonian $\mathscr{H}$ are treated as small, so that the partition function (and hence the free energy) is obtained as a series in ascending powers of μ_N and H. Then, if F' is the term in the free energy which is proportional to $\mu_N H$, we obtain the shielding constant σ_d as $-\mu_N^{-1}\partial F'/\partial H$. A lengthy but straightforward calculation gives, for a degenerate Fermi gas,

$$\sigma_d = -\frac{4\pi n\mu_0^2}{3\zeta}, \quad \ldots\ldots\ldots \quad (1)$$

where n is the electron density, μ_0 is the Bohr magneton and ζ is the Fermi level. Comparing this with the expression for the paramagnetic shielding constant

$$\sigma_p = \frac{8\pi}{3}\chi_p\langle|\psi_F(0)|^2\rangle\Delta, \quad \ldots\ldots\ldots \quad (2)$$

† Supported by the U.S. Atomic Energy Commission Contract AT(30–1)–2498 with Columbia University, New York.

where Δ is the atomic volume and $\langle|\psi_F(0)|^2\rangle$ is the average value of the wave-function density at the nucleus for electrons at the Fermi surface (Townes *et al.* 1950), we have, since $\chi_d = -n\mu_0^2/2\zeta$ for free electrons,

$$\frac{\sigma_d}{\sigma_p} = \frac{\chi_d}{\chi_p \langle|\psi_F(0)|^2\rangle \Delta}. \qquad (3)$$

This ratio has the value $-\frac{1}{3}$ for free electrons, since $\langle|\psi_F(0)|^2\rangle = 1/\Delta$ and $\chi_d = -\frac{1}{3}\chi_p$ in this case. The equality of σ_d/σ_p and χ_d/χ_p for free electrons is a consequence of the fact (pointed out to us by Dr. A. B. Pippard) that, when the electron density is constant, the part of the field at a nucleus contributed by the electrons within the Lorentz sphere is simply

$$(8\pi/3)(\chi_p + \chi_d)H,$$

so that the frequency shift is a pure susceptibility effect.

For Bloch electrons in an actual metal this conclusion is no longer valid, and the treatment given above must be generalized to include the periodic lattice potential in $\mathscr{H}$; Bloch wave functions must then be used to evaluate the matrix elements required in the calculation of the partition function. This problem will be discussed in a later paper. It is usually assumed that σ_d is always negligibly small compared with σ_p, since in real metals $\langle|\psi_F(0)|^2\rangle\Delta$ is in general large compared with unity. However, if we assume, for an order-of-magnitude estimate, that eqn. (3) still applies and that the dominant contribution to χ_d comes from the usual Landau-Peierls expression (Peierls 1933) evaluated for electrons with an effective mass m^*, we obtain

$$\frac{\sigma_d}{\sigma_p} = -\frac{1}{3}\frac{(m/m^*)^2}{\langle|\psi_F(0)|^2\rangle\Delta}. \qquad (4)$$

This suggests that σ_d may be comparable in magnitude with σ_p whenever m^* is small, as is frequently the case in multivalent metals in which high-curvature portions of the Fermi surface lie close to a zone boundary. For the case of beryllium metal, as an example, the observed Knight shift $\sigma = \sigma_d + \sigma_p$ is practically zero, while the theoretical value of σ_p is predicted to be 0·01%. Assuming that $\sigma_d = -\sigma_p$ and taking $\Delta = 7{\cdot}8 \times 10^{-24}\,\mathrm{cm}^3$ and $\langle|\psi_F(0)|^2\rangle = 1{\cdot}03a_0^{-3}$, where a_0 is the Bohr radius (Pomerantz and Das 1960), we obtain from eqn. (4) $m^* \approx 0{\cdot}08\,m$, which agrees in order of magnitude with estimates obtained from the de Haas–van Alphen effect (Shoenberg 1957).

We have so far regarded the applied magnetic field as so small that only the non-oscillatory part of χ_d need be considered. If we assume that eqn. (3) remains valid for all values of H and substitute the complete expression for χ in the effective mass approximation (Sondheimer and Wilson 1951) we obtain

$$\sigma = \frac{64\pi^2 m^{*3/2}}{9h^3}\mu_0^{*2}(2\zeta)^{1/2}\left[3\frac{m^{*2}}{m^2}\langle|\psi_F(0)|^2\rangle\Delta - 1\right.$$
$$\left. - \frac{3\pi kT}{\mu_0^* H}\left(\frac{\zeta}{\mu_0^* H}\right)^{1/2}\sum_{r=1}^{\infty}\frac{(-1)^{r+1}\cos\left(\frac{r\pi m^*}{m}\right)\sin\left(\frac{1}{4}\pi - \frac{r\pi\zeta}{\mu_0^* H}\right)}{r^{1/2}\sinh(r\pi^2 kT/\mu_0^* H)}\right], \qquad (5)$$

where $\mu_0^* = e\hbar/2m^*c$. Whilst this equation cannot be expected to be in any way quantitatively reliable, it suggests that there may be oscillations in σ as a function of $1/H$ when $\pi^2 kT/\mu_0^* H$ is of order unity. These oscillations, like the de Haas–van Alphen oscillations in the magnetic suceptibility, are due to the quasi-periodic character of the density of states function for a degenerate Fermi gas in a magnetic field, and should be observable under conditions similar to those required to observe the de Haas–van Alphen effect (see Shoenberg 1957). The field stability and homogeneity necessary for this purpose should be readily obtainable with the magnets currently available for nuclear magnetic resonance experiments. The amplitude of the oscillations in σ is estimated to be of the same order as $\sigma_{//}$, that is about 10^{-4}, for metallic beryllium at 4°K in a field of the order of 20 kG. One would also expect oscillations in the shielding of ^{25}Mg, ^{67}Zn and ^{199,201}Hg nuclei in the metals and for ^{1}°C in graphite since the effective masses in all these cases are small.

Acknowledgments

The authors are grateful to Professor M. Bloom and Professor R. Barrie for helpful discussions about the oscillations in shielding at high fields and low temperatures.

References

Hebborn, J. E., and Sondheimer, E. H., 1959, *Phys. Rev. Letters*, **2,** 150.
Knight, W. D., 1949, *Phys. Rev.*, **76,** 1259.
Landau, L., 1930, *Z. Phys.*, **64,** 629.
Peierls, R., 1933, *Z. Phys.*, **80,** 763.
Pomerantz, M., and Das, T. P., 1960, *Phys. Rev.* (in the press).
Shoenberg, D., 1957, *Progress in Low Temperature Physics*, **2,** 226.
Sondheimer, E. H., and Wilson, A. H., 1951, *Proc. Roy. Soc.* A, **210,** 173.
Townes, C. H., Herring, C., and Knight, W. D., 1950, *Phys. Rev.*, **77,** 852.

Direct Evidence for the Presence of Quarter-dislocations in Talc Monocrystals

By S. Amelinckx and P. Delavignette
S.C.K. Mol-Donk, Belgium

[Received January 26, 1960]

Quarter dislocations have been postulated first, on a geometrical basis, by Kronberg (1957) to account for the plastic behaviour of sapphire. Evidence for the existence of half-dislocations, so called Shockley partials, in stainless steel has been presented by Whelan (1958) who also discussed their interactions.

We present here direct evidence that quarter-disolocations exist in talc, and probably in the related clay minerals.

Thin cleavage foils of talc monocrystals were examined in transmission electron microscopy using the technique developed by Hirsch and Whelan (1959) for metal foils. The cleavage plane in talc is also the glide-plane; the crystals are extremely soft as a consequence of glide on this plane.

An examination of the talc structure (Wells 1950) indicates that glide takes place between the two successive oxygen sheets, which have the ring structure shown in fig. 1. These oxygen layers establish the contact between electrically neutral multilayers; their bonding is therefore very weak. Glide between these planes requires dislocations with a Burgers vector AA_1, AA_2 or AA_3 as shown in fig. 1. Dislocations with a Burgers vector AA_1 are not stable according to the 'square of the Burgers vectors' criterium; they will split into four partials with 'Burgers' vectors $A\alpha$, $\alpha\beta$, $\beta\gamma$, γA_1 as indicated in the same fig. 1. Between the four partial dislocations ribbons of stacking faults are present. They are of a different kind but have probably very nearly the same stacking fault energy. The configuration of partials is therefore mainly determined by their elastic interaction. All successive partials repel, the equilibrium separation is therefore given approximately by fig. 2.

All the characteristics of the described dislocation ribbons were actually observed as shown in fig. 3 (*a*), (*b*), (*c*) and (*d*) (Pls. 55 and 56). These figures refer to the same area, but show a different contrast, due to a different inclination of the foil. Figure 3 (*a*) reveals only two of the partial dislocations, whilst fig. 3 (*b*) shows in one area three of them and in another area all four. In fig. 3(*c*) on the other hand the contrast is such as to reveal the stacking faults between 1 and 2 and between 3 and 4. Whilst finally fig. 3 (*d*) shows the stacking fault ribbons between the three pairs of dislocations, with a slightly darker contrast between partials 2 and 3. Since the plane of the stacking fault is exactly parallel to the foil surfaces only a uniform contrast is observed in the cases here considered.

Fig. 1

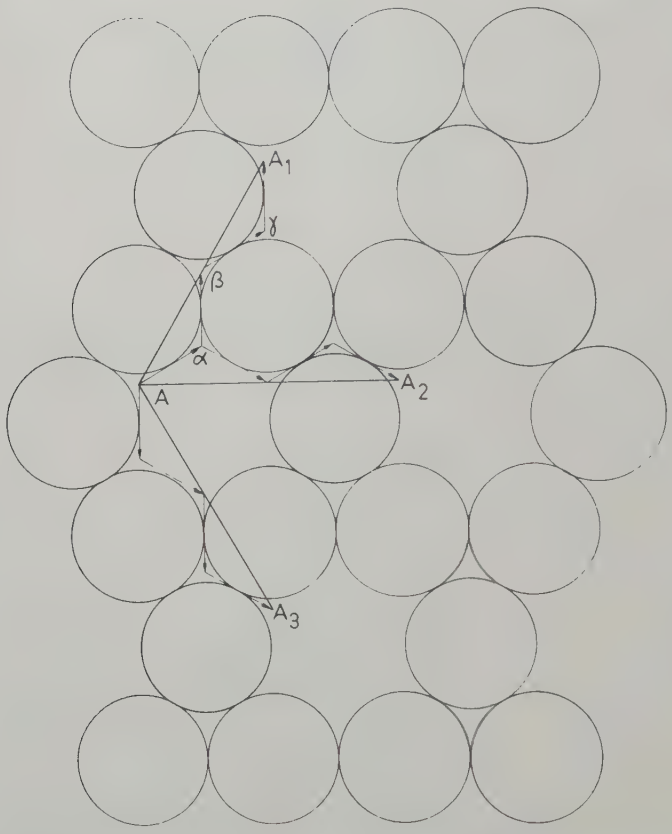

Ring structure of oxygen layers in the talc structure. glide occurs between two such layers. Possible Burgers vectors are AA_1, AA_2 and AA_3: AA_1 which is not stable splits into four partial dislocations.

Fig. 2

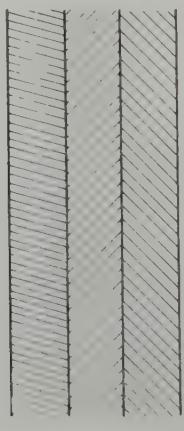

Schematic representation of the configuration of partials and stacking faults in a fourfold dislocation ribbon.

The fact that stacking fault contrast of the expected kind is observed between the individual lines is an indication that we have very probably to do with the real effect and not, e.g., with the formation of a double image as described by Hirsch and Whelan (1959). Further evidence follows from a consideration of the particular kinds of nodes which are observed.

A more detailed account of these observations will be published elsewhere.

Acknowledgments

We are indebted to Mr. Goens, Director of the C.E.N. Mol, for permission to publish this paper. We also wish to thank Mr. Nicasy for his skilful preparation of specimens and Mr. Beyens for careful photographic work.

References

Hirsch, P. B., and Whelan, M. J., 1959, *J. Inst. Met.*, **87,** 392, 406.
Kronberg, M. L., 1957, *Acta Met.*, **5,** 507.
Wells, A. F., 1950, *Structural Inorganic Chemistry* (Oxford: University Press), p. 580.
Whelan, M. J., 1958, *Proc. roy. Soc.* A, **249,** 114.

[*The Editors do not hold themselves responsible for the views expressed by their correspondents.*]

Fig. 5

(*a*)

(*b*)

Etch pits on specimen driven at $\epsilon = 2{\cdot}7 \times 10^{-4}$, showing dislocations produced by the vibration. In (*b*) the dislocations seem to originate from a sub-grain boundary. Stress direction horizontal. Mag. $\times 180$.

Fig. 1

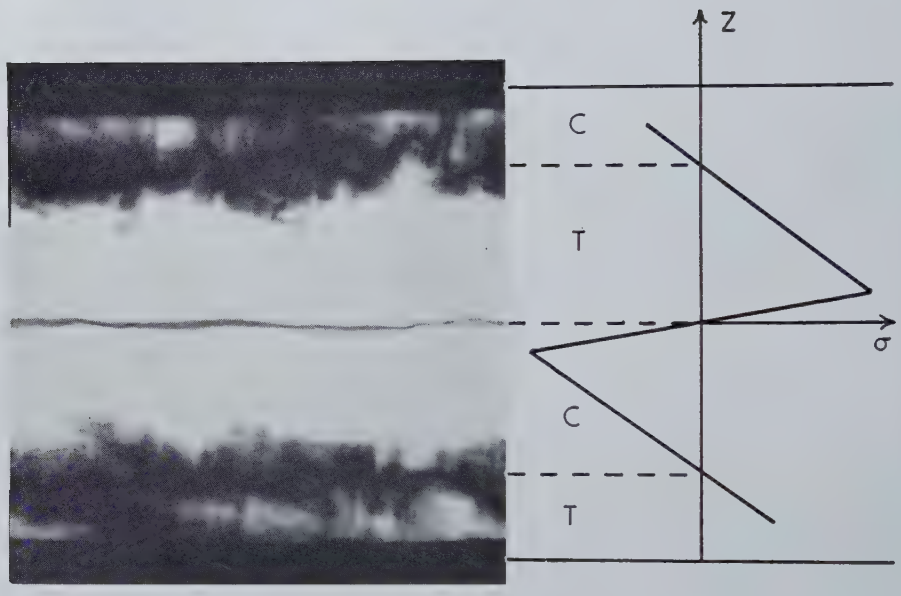

Figs. 1–5

Successive stages in the reverse bending of a singly-bent bar (external couples still applied). T = tension, C = compression. Photographs taken with crossed nicols at 45° to the extinction directions.

Fig. 2

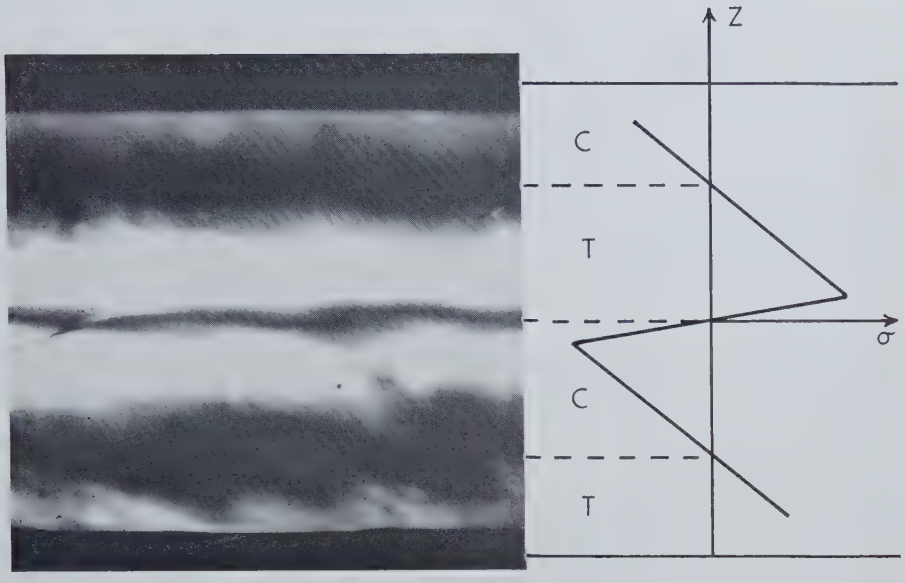

Fig. 3

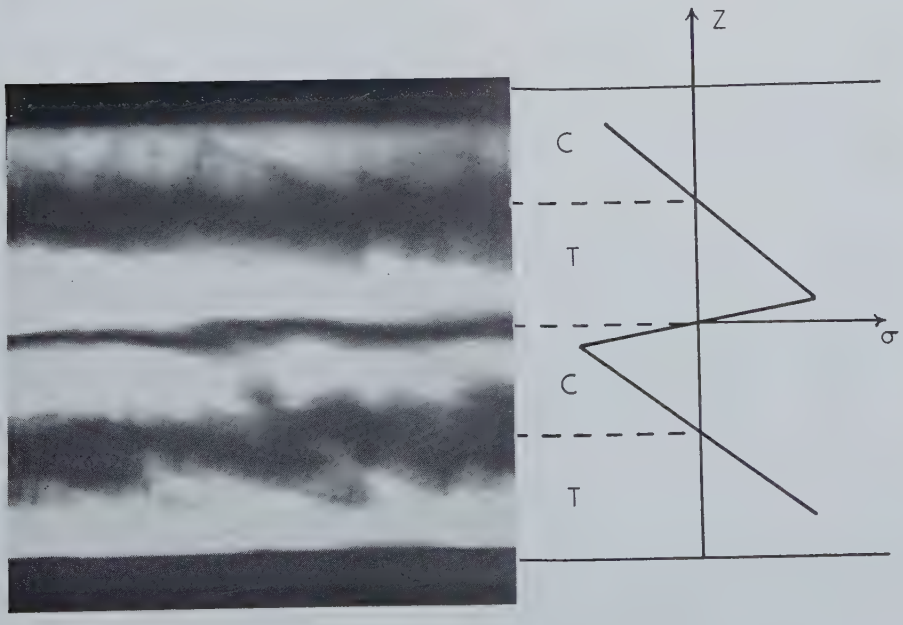

Fig. 4

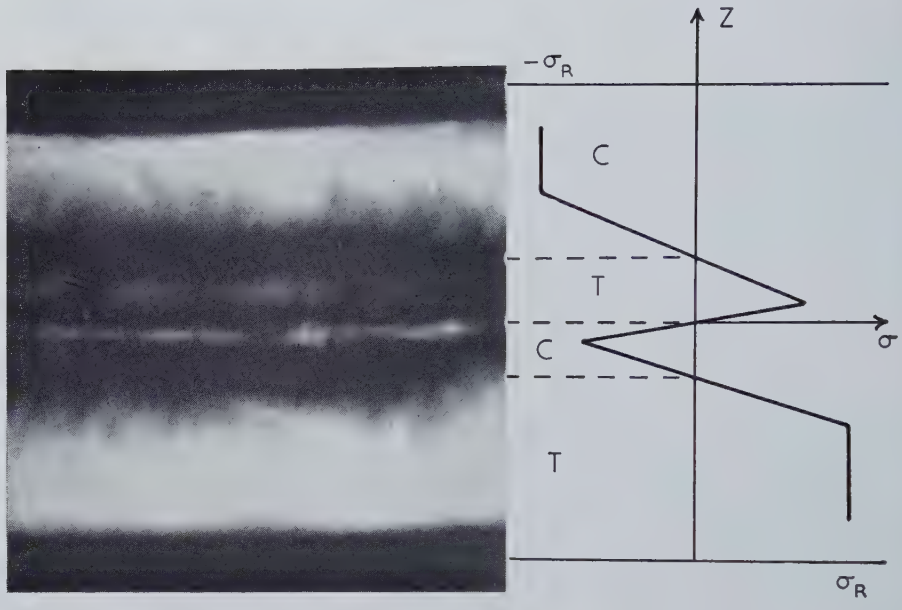

Fig. 5

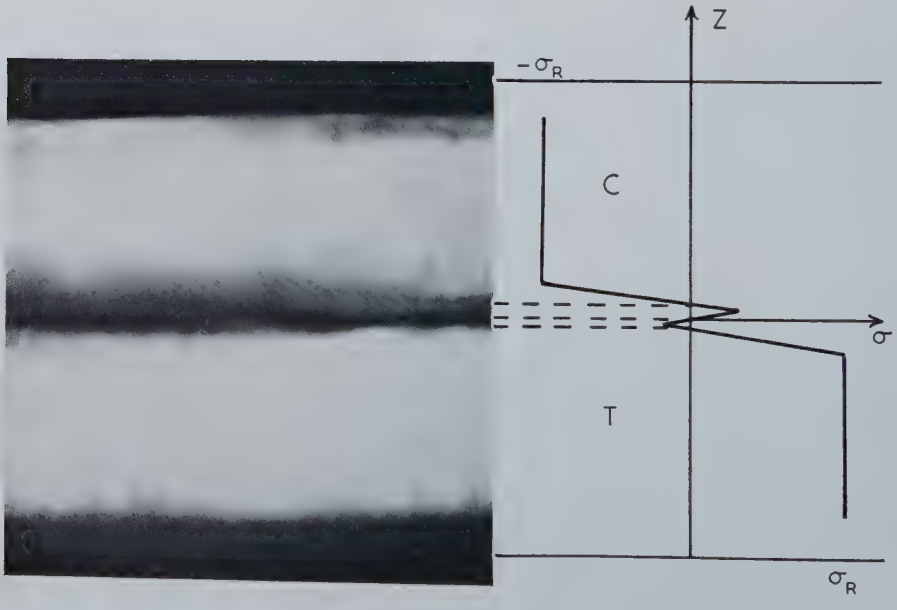

Fig. 1

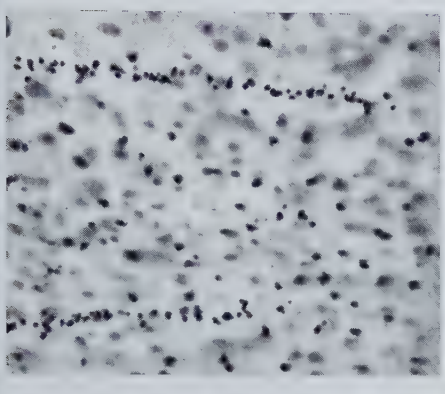

(*a*) Monatomic terraces on the surface of a crystal of silver bromide, associated with dislocation loops and decorated by the separation of particles of silver. ×1050.

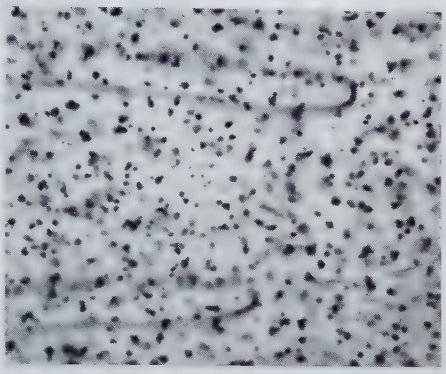

(*b*) Segments of the loops where the dislocations are in the screw orientation and define the ends of the surface terraces. 3 microns below figure 1 (*a*). ×1050.

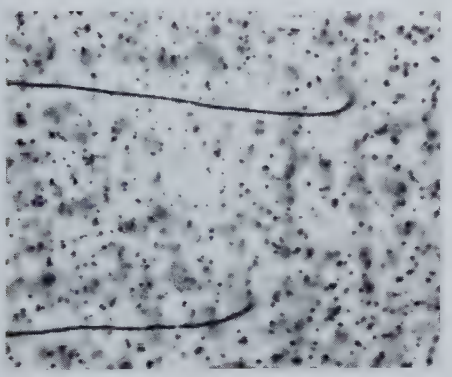

(*c*) Segments of the loops where the dislocations are in the edge orientation and are parallel to the corresponding surface terraces. 6 microns below fig. 1 (*a*). ×1050.

Fig. 3

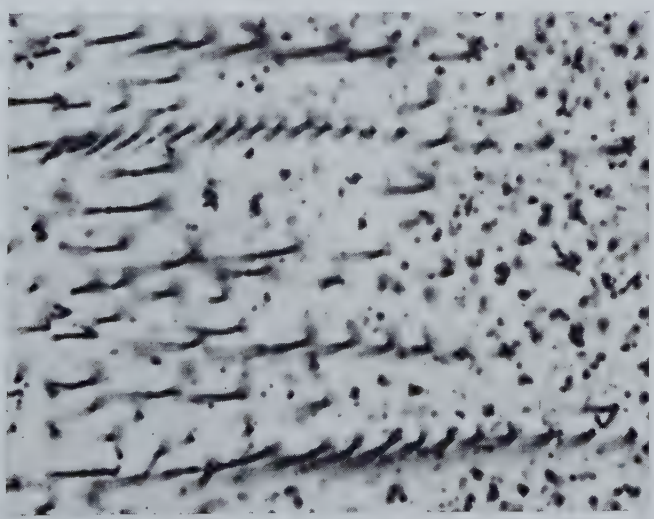

Successions of dislocation loops meeting the surface in the edge orientation and tending to lie on (110) glide planes. There are no surface terraces to be decorated and the loops are only very faintly visible where they are in the screw orientation below the surface. ×1425.

Fig. 2

Cadmium crystals on a quartz fibre after 75 min of growth at $\sigma \simeq 0{\cdot}7$. $\times 28$.

Fig. 3

Random distribution of whiskers and platelets 5 min after beginning of growth, when σ_{max} was $\sim 1{\cdot}4$. $\times 46$.

Fig. 4

Platelet growth when σ_{max} was ~ 3. $\times 11$.

Fig. 5

High density of hexagonal plates after one day of growth when σ_{max} was ~ 8. $\times 100$.

Fig. 6

Dendritic growth at $\sigma_{max} \sim 110$ and $T \sim 180°C$. $\times 28$.

Fig. 7

A cadmium ' snowflake '. $\times 45$.

Fig. 3

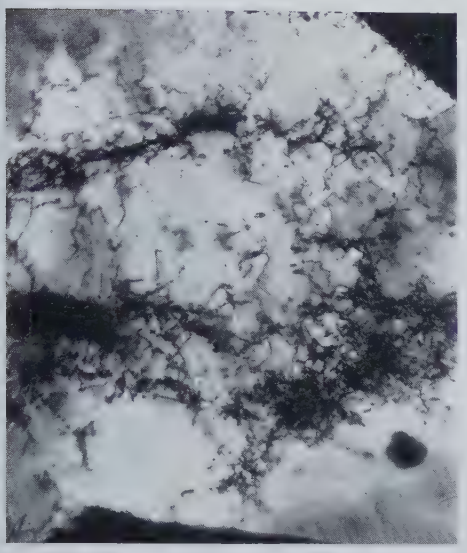

1 μ (*a*)

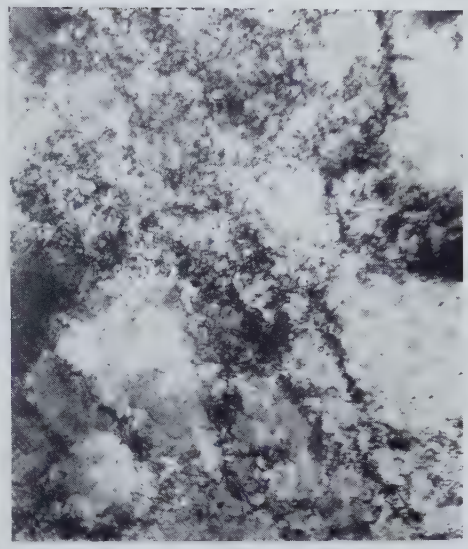

1 μ (*b*)

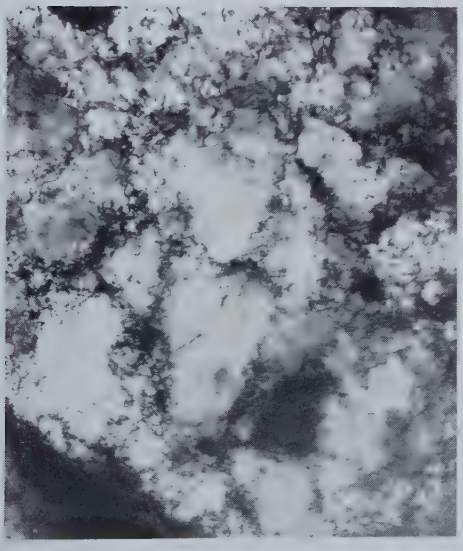

1 μ (*c*)

(*d*)

(*a*) Micrograph of polycrystalline silver deformed 10% in tension (×20 000).
(*b*) Micrograph of polycrystalline silver deformed 20% in tension (×20 000).
(*c*) Micrograph of polycrystalline silver deformed 30% in tension (×20 000).
(*d*) Electron diffraction pattern from an area $\frac{4}{3}$ μ diameter, of silver deformed 30% in tension.

Fig. 4

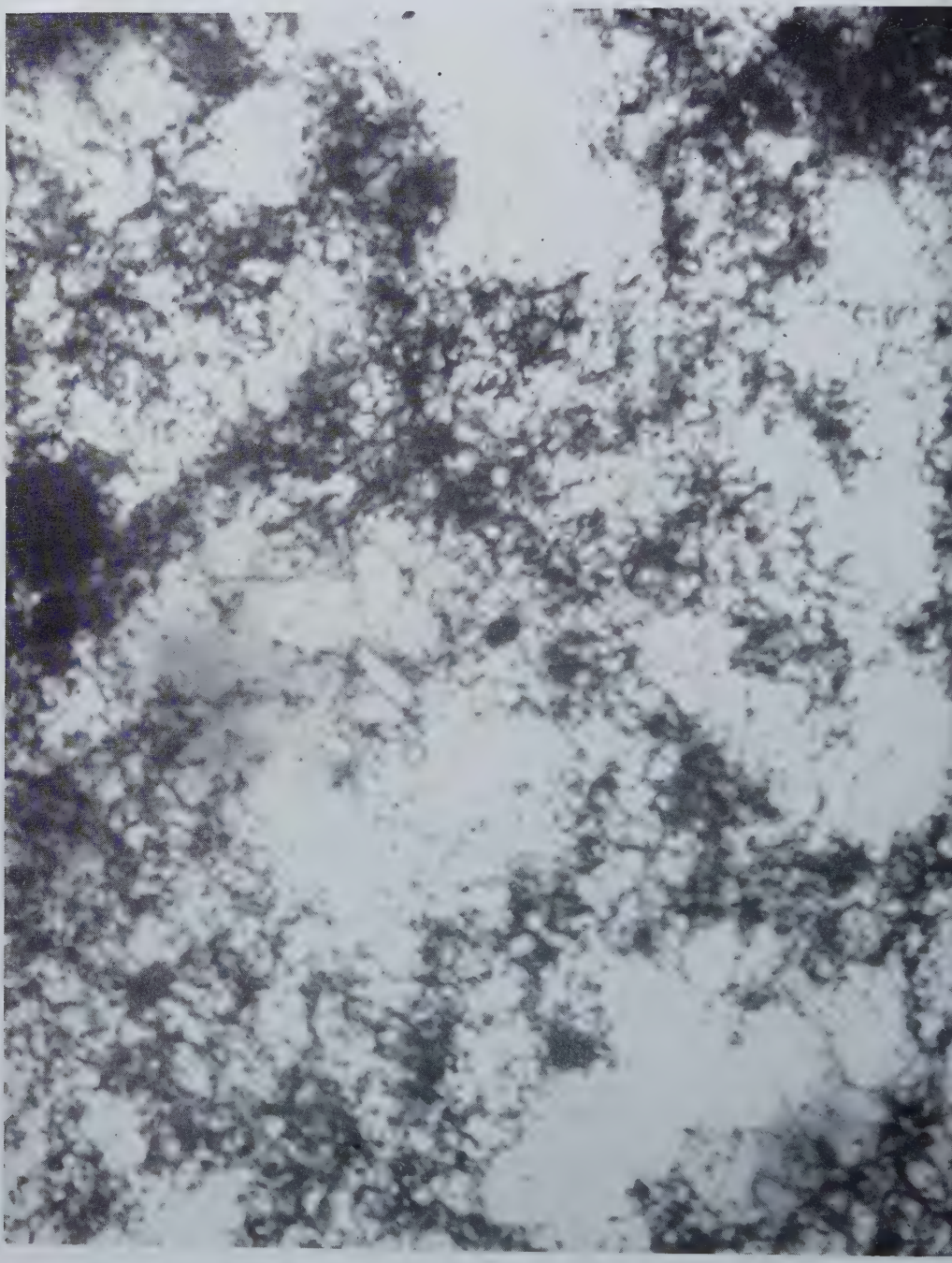

Micrograph of polycrystalline silver deformed 25% in tension, showing the complex networks in the cell boundaries (×80 000).

Fig. 5

The x-ray patterns obtained for the 111 and 200 reflections from the nickel composite specimen. The central pattern is that obtained by rotating the specimen, and the outer ten patterns are those obtained from the individual sectors.

Fig. 3

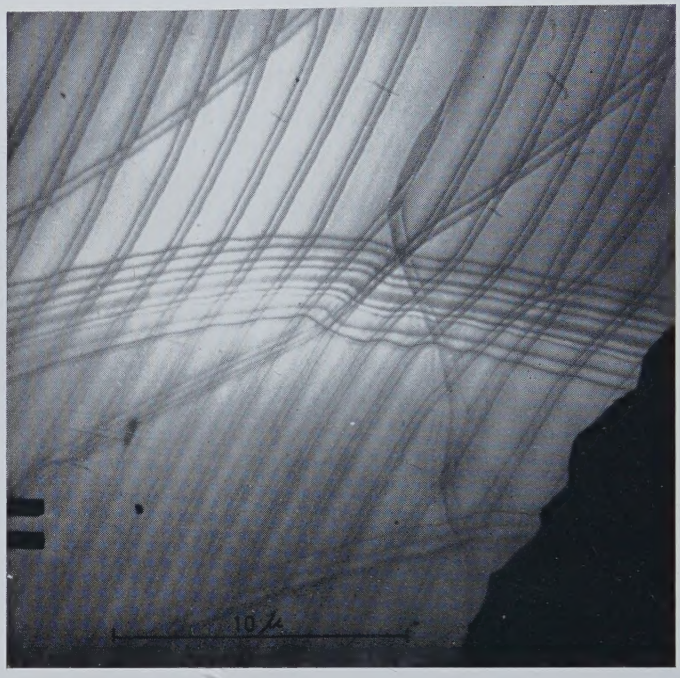

(*a*)

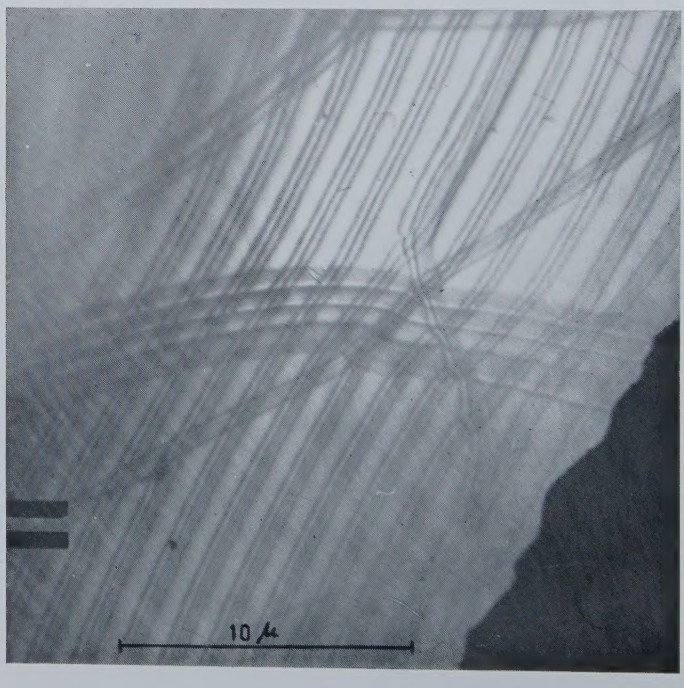

(*b*)

Two images of the same area, showing different features :

(*a*) Two partials are visible from the main family of dislocations.
(*b*) Three partials are visible in one area, all four are visible in a second area.

(Fig. 3 *continued*)

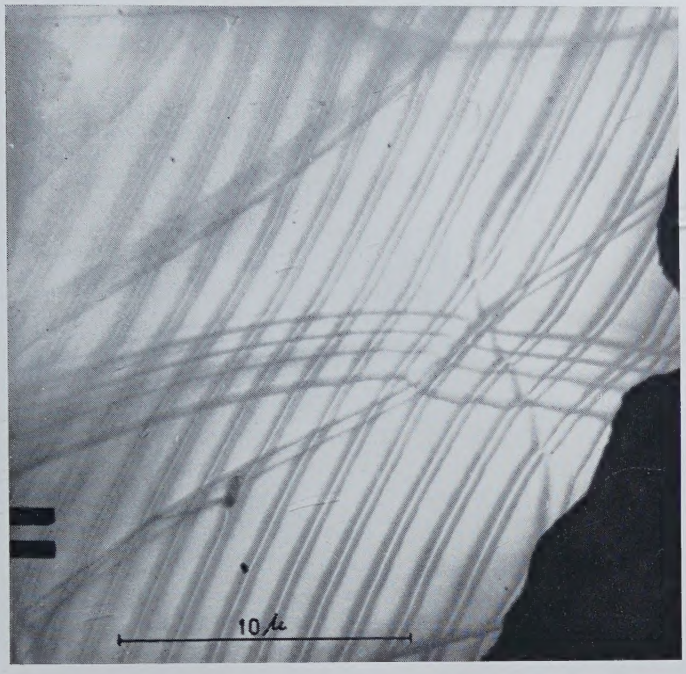

(*c*)

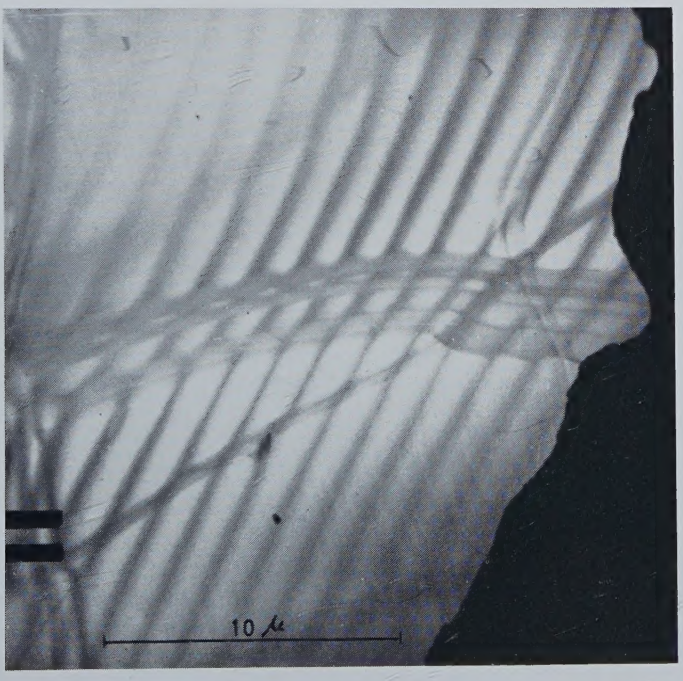

(*d*)

Two images of the same area, showing different features :

(*c*) The two external stacking fault ribbons have dark contrast.

(*d*) The central stacking fault ribbon has dark contrast; the two external ribbons have a somewhat lighter shade.